METABOLIC AND RESPIRATORY PATHWAYS CONTROLLING *VIBRIO CHOLERAE* COLONIZATION

By

Andrew John Van Alst

A DISSERTATION

Submitted to
Michigan State University
in partial fulfillment of the requirements
for the degree of

Microbiology and Molecular Genetics – Doctor of Philosophy

2021

ABSTRACT

METABOLIC AND RESPIRATORY PATHWAYS CONTROLLING *VIBRIO CHOLERAE* COLONIZATION

By

Andrew John Van Alst

Vibrio cholerae is an enteric pathogen of the human small intestine that proliferates to high cell density during human infection. Although not typically classified as a virulence factor, metabolism is a cornerstone for fitness in the host environment. In this work, I explore the essential role of aerobic metabolism, including oxidative respiration, for successful colonization of *V. cholerae* in the infant mouse model. Oxidative respiration is the most efficient energy generating metabolic pathway in living organisms and supports the rapid proliferation of *V. cholerae* in the small intestinal environment. Despite knowledge that oxygen diffuses from the host epithelium into the gut lumen, the role of oxygen in supporting colonization and proliferation of *V. cholerae* had not been explored prior to the work presented here in Chapters 2 and 3.

In Chapter 2, by targeting the pyruvate dehydrogenase (PDH) complex, an enzyme required to convert pyruvate to acetyl-CoA under aerobic conditions, I show that aerobic metabolism through the PDH complex is required for population expansion in the infant mouse. As the gut was predominantly considered anaerobic and exists in a state of low oxygen tension, I also examined the contribution of anaerobic metabolism to infant mouse colonization. By targeting cognate pyruvate formate-lyase (PFL) that similarly converts pyruvate to acetyl-CoA, but only under anaerobic conditions, I determined that anaerobic respiration is dispensable for colonization. In Chapter 3, I directly test the

importance of aerobic and anaerobic respiration by targeting the complete set of terminal oxidases and terminal reductases encoded by *V. cholerae*. Using a modified Multiplex Genome Editing by Natural Transformation (MuGENT) approach, I generated strains denoted Aero7 and Ana4. Aero7 is a functionally strict anaerobe derivative of *V. cholerae*, lacking all four terminal oxidases (*cbb*$_3$*, bd*-I*, bd*-II*,* and *bd*-III), whereas Ana4 lacked functionality in each of the four terminal reductase complexes (fumarate, trimethylamine-*N*-oxide, nitrate, and biotin sulfoxide reductases). Disruption in the oxidase complexes in strain Aero7 severely attenuated *V. cholerae* colonization in the infant mouse, however, no attenuation was observed for Ana4. These data supported our findings in Chapter 2 that aerobic, but not anaerobic metabolism was critical for *V. cholerae* growth in the infant mouse. Furthermore, I determined that the *bd*-I oxidase, and to a lesser extent the *cbb*$_3$ oxidase, support oxidative respiration during infection with *bd*-II and *bd*-III oxidases being dispensable for colonization.

In summation, aerobic metabolism through the PDH complex and the terminal reduction of oxygen by the *bd*-I oxidase are essential to *V. cholerae* colonization of the infant mouse. Through this work, I uncovered a role for oxidative metabolism for *V. cholerae* colonization. These findings expand our knowledge of *V. cholerae* biology and pathogenicity in the gastrointestinal tract and implicate oxygen as a critical electron acceptor that shapes the progression of enteric infections.

To my family:

My mother Julie,
my father Ed,
my sisters Kassie and Lizzie,
my grandparents, aunts, uncles, and cousins.

ACKNOWLEDGEMENTS

First and foremost I would like to thank Victor DiRita, Ph.D. for providing me the opportunity to carry out research in his lab and for supporting my growth as a researcher and an individual as member of his lab family. Through every step, Vic was provided unwavering support and guidance, and for that I will be forever grateful. I would also like to thank my guidance committee, Christopher Waters, Ph.D., Shannon Manning, Ph.D., and Lee Kroos, Ph.D. The path to a Ph.D. is hardly ever linear and I am thankful for their guidance through the ups, downs, and turns that my project had taken to reach the finish line. It is not uncommon to pick up tendencies of those we hold in high esteem and I am thankful I was able to experience the kindness and joy each of these researchers brought to their labs each and every day. This has without a doubt imprinted upon me the type of mentor I wish to be one day.

To all the members of the DiRita lab family, both past and present, for making the lab a home. First off, I would like to thank Rhia who was there at the start and now at the end of my journey. Rhia was a stalwart of stability throughout my Ph.D. and a reliable source of amazing baked goods I am sure to miss. Jeremiah Johnson, for dealing with me as a green, aspiring, microbiologist and giving guidance in the early stages of my project. Natalia Martin, for her passion and imparting on me the importance of saying “yes” to the things we care about and “no” when we can no longer give what we care most about our all. Ritam Sinha, for showing me that it is okay to slow down, take your time, and that life is not always a race. Lucas Demey, for his seemingly endless excitement and curiosity for science and for his contribution of the TcpA Westerns in Chapter 3 that

were his bread and butter. Beth Ottosen, for her like-mindedness both in kindness and introversion, keeping me sane, especially through the pandemic, for her help in pig mucin extraction, and for her willingness to get food whenever the situation called for it. I'd also like to thank my undergraduate mentee, Shaun Dunyak, who stuck it out through a trial period of my lab mentoring allowing me to develop as a mentor. Lastly from the lab, I also want to thank all the other undergraduates and visiting students who made the lab a fun place to be.

I would also like to thank the Michigan State University Microbiology and Molecular Genetics Department. Working alongside such amazing people was an absolute pleasure during my time at MSU. The folks at the MSU Meat Lab were also wonderful people I had the pleasure of getting to know on mucus collection days, trading baked goods for pig intestines was always the bargain. I also appreciate the kindness from the folks at the MSU Histology Research Core, helping me despite my absolute chasm of histology research knowledge.

To all of my friends who have been immeasurably important to my success – Thank you! This journey would not have been possible and not nearly as fun without you.

Lastly, I want to thank my family. My parents Ed and Julie Van Alst who have always supported me in anything I have done. Who knew I would finally be leaving MSU nearly 9 years after you helped me move in that first day of undergrad. My sisters Kassie and Lizzie, for always being there and bringing joy to my life. And to my grandparents who

have always looked upon my successes with bright eyes and wonder. The love and support I have had throughout my life is what made this Ph.D. possible.

TABLE OF CONTENTS

LIST OF TABLES

LIST OF FIGURES

KEY TO ABBREVIATIONS

ACS-1 ..... Acetyl-CoA Synthase-1

AKGDH ..... Alpha-Ketoglutarate Dehydrogenase

ANCOVA ..... Analysis of Covariance

ATP ..... Adenosine Triphosphate

BSO ..... Biotin Sulfoxide

CI ..... Competitive Index

CIP ..... Calf Intestine Phosphatase

CoMPAS ..... Comparative Multiplex PCR Amplicon Sequencing Coupled with Pulsed Amperometric Detection

CT ..... Cholera Toxin

DMSO ..... Dimethyl Sulfoxide

EAEC ..... Enteroaggregative *Escherichia coli*

EHEC ..... Enterohemorrhagic *Escherichia coli*

ETC ..... Electron Transport Chain

FbFP ..... Flavin-Binding Fluorescent Protein

Fnr ..... Fumarate and Nitrate Regulatory Protein

FRET ..... Förster Resonance Energy Transfer

GCV ..... Glycine Cleavage Multienzyme

GlcNAc ..... *N*-Acetylglucosamine

HIF-1 ..... Hypoxia Inducible Factor

HPAEC-PAD ..... High-Performance Anion-Exchange Chromatography

IBD ..... Irritable Bowel Disease

IP.....Inoculum Pool

Ipa..... Invasion Plasmid Antigen

IPTG.....Isopropyl β-D-1-Thiogalactopyranoside

LAP .....Listeria Adhesion Protein

LEE .....Locus of Enterocyte Effacement

LLO .....Listeriolysin O

LOD.....Limit of Detection

MASC-PCR ..... Multiplex Allele-Specific Polymerase Chain Reaction

MDHHS.....Michigan Department of Health and Human Services

MiGS .....Microbial Genome Sequencing Center

MP..... Mouse Pool

MuGENT ..... Multiplex Genome Editing by Natural Transformation

NAC..... N-Acetyl-L-Cysteine

PCR.....Polymerase Chain Reaction

PDH.....Pyruvate Dehydrogenase

PFL..... Pyruvate Formate-Lyase

PMNs ..... Polymorphonuclear Neutrophils

PPAR-γ..... Peroxisome Proliferator-Activated Receptor γ

PSIM ..... Porcine Small Intestinal Mucin

Q .....Quinone

ROS ..... Reactive Oxygen Species

SCFA..... Short Chain Fatty Acid

SDS.....Sodium Dodecyl Sulfate

STEC..... Shiga Toxin-Producing *Escherichia coli*

Stx..... Shiga Toxin

T3SS..... Type III Secretion System

T6SS.....Type VI Secretion System

TCP..... Toxin-Coregulated Pilus

TMAO.....Trimethylamine-*N*-Oxide

TMPD..... $N_1N_1N'_1N'$-Tetramethyl-*p*-Phenylene-Diamine Dihydrochloride

WT..... Wild Type

YFP.....Yellow Fluorescent Protein

Chapter 1 – Introduction – Oxygen and Enteric Bacterial Infections

1.1 – Abstract

Oxygen is critical in shaping the human intestinal ecosystem. Under homeostasis, the gut is in a state of physiological hypoxia that is maintained through a complex symbiosis between host cells and the microbiota. For enteric pathogens, oxygen plays a role in many facets of pathogenesis and disease progression. All enteric pathogens interact with gut oxygen, and many have evolved mechanisms to both exploit molecular oxygen for growth and subvert damage from reactive oxygen species. Periods of dysbiosis brought on by bacterial infection and other means further drive oxygen into the lumen of the intestine. Here I review oxygen as a key molecule influencing enteric bacterial pathogenesis and disease.

1.2 – Introduction

The evolution of ancient microorganisms that led to the use of oxygen in metabolism marked a significant milestone in evolutionary history (1). Oxygen became expansively abundant in Earth's atmosphere during the great oxidation event where ancient photosynthetic cyanobacteria began converting CO_2 to O_2 (2). Present day organisms have been evolutionarily shaped by oxygen, accruing strategies to benefit from its high energy bonds and mitigate damage from harmful oxygen radicals.

Within the intestinal tract, oxygen plays a major role in shaping the intestinal microbial landscape (3). During homeostasis, resident bacterial communities are composed of diverse taxa that maintain a healthy gut ecosystem through multilayered symbioses between gut microbes and the host (4). Facultative anaerobes of the gut maintain a relatively anaerobic lumen by scavenging oxygen that diffuses from host epithelium,

allowing for the growth of obligate anaerobes within the gut community (5). These obligate anaerobes produce short-chain fatty acids that support barrier function of the host epithelium, and influence host cell metabolism, which limits diffusion of oxygen into the gut lumen from host tissue (6).

Gut oxygen is also critical during periods of dysbiosis brought on by enteric infections. Oxygen is one of many environmental signals for pathogens that drives efficient colonization and virulence trait expression. During enteric-induced dysbiosis, the inherent balance of oxygen between the microbiota and host shifts as resident populations are displaced and host cell metabolism changes to anaerobic glycolysis leaving unused oxygen to permeate into the gut lumen (7). The influx of oxygen and host responses that generate reactive oxygen species become transient factors that pathogens either exploit or subvert in disease progression. Pathogens capable of exploiting oxygen in the intestinal tract do so through reduction of molecular oxygen by terminal oxidase complexes that support aerobic respiration, a highly efficient energy generating metabolic pathway. Terminal oxidases that support aerobic respiration also aid detoxification of reactive oxygen species alongside other ROS defenses such as catalases, peroxidases, and superoxide dismutases.

The role of oxygen during enteric infection is an emerging area of intense exploration. Here we review current knowledge of how oxygen functions as a signal for bacterial pathogenesis and how it impacts pathogen growth and fitness during infection. We also discuss the function and relevance of terminal oxidases and their role in the

pathogenesis for several enteric pathogens. Lastly, we review technologies, recent advancements, and practical limitations in the measurement of oxygen during infection that are critical to our understanding of oxygen during disease.

1.3 – Oxygen During Homeostasis

1.3.1 – Maintaining Oxygen Levels in the Intestinal Tract

Mucosal oxygenation in the human body depends on blood flow anatomy and local tissue metabolism. Within the gut, the concentration of molecular oxygen varies both radially and longitudinally throughout the length of the intestinal tract (Figure 1.1) (3, 8). Diffusion of oxygen from the capillaries of the highly vascularized intestine leads to a steep oxygen gradient extending from the epithelial crypts to the hypoxic gut lumen (9). This condition of relatively low oxygen in the intestine is referred to as “physiological hypoxia” and is required for maintaining a healthy epithelium (8). Within intestinal villi, oxygen release into the lumen is influenced by villus host cell maturation. In the small intestine, villi extend as finger-like projections into the intestinal lumen and are essential for nutrient and water absorption; they also contain replenishing stem cells at the base of the villus crypt. In the large intestine, elongated crypts are present with stem cells at the base, however, no protruding villi are present. Within both the small and large intestine, epithelial cells are replaced and replenished every four to five days with stem cells giving rise to early transient-proliferated cells that differentiate and mature as they ascend the small intestinal villi or large intestine elongated crypt (10). Epithelial cell turnover is essential for maintaining gut homeostasis and physiological hypoxia.

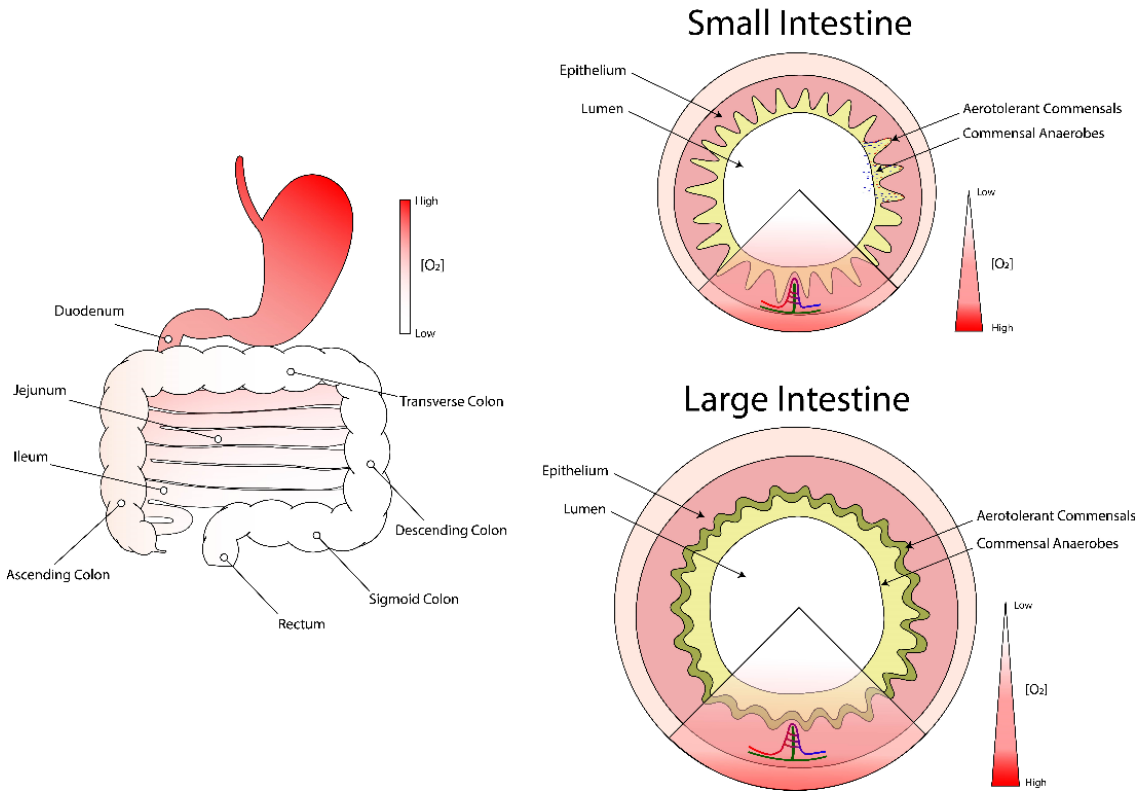

Figure 1.1. Longitudinal and transverse oxygen gradients in the human intestinal tract. Oxygen concentrations decrease throughout the length of the intestine from the upper to lower gastrointestinal tract. In both the small and large intestine, oxygen emanates from the epithelium and decreases to anoxia in the gut lumen. Aerotolerant commensal microorganisms colonize nearer to the epithelium whereas commensal anaerobes are present in the lumen associated with host mucus. Oxygenation of the epithelial tissue is influenced by blood flow to the intestine which can fluctuate as blood flow markedly increases following food consumption to aid in digestion. A blood vessel and lymph node are depicted near the bottom of the intestinal cross sections where highly oxygenated blood is delivered to the intestine in red and exits in blue following delivery of oxygen to the tissue.

In healthy adults, undifferentiated proliferating colonoyctes metabolize glucose to lactate via oxygen-independent anaerobic glycolysis and fermentation, whereas mature colonocytes present further up the crypt preferentially metabolize short chain fatty acids via oxygen-dependent β-oxidation (11). This differential metabolism of villus colonocytes leads to greater oxygenation of the crypt base compared to the ascended crypt environment. This oxygen gradient shapes the microbiota as more aerotolerant

microbes in the phyla Proteobacteria and Actinobacteria are associated with the intestinal mucosa, whereas phyla Bacteroidetes and Firmicutes, comprised mainly of anaerobic microbes, are associated with the mucus layer away from the epithelial tissue (3, 5). The diffusive oxygen from the epithelial tissue is readily consumed by facultative anaerobes, facilitating growth of obligate anaerobes by maintaining a hypoxic gut lumen (5). This intestinal balance of oxygen promotes complementary aerobic and anaerobic metabolisms among the microbiota and maintains a healthy gut community (12).

In addition to microbial-driven luminal oxygen depletion, oxygen is also depleted through the oxidation of host cell lipids. Germ-free mice were observed to maintain a deoxygenated gut lumen comparable to that of conventional mice despite the absence of residential microbial populations. However, lipid oxidation appeared to play a secondary role as oxygen depletion occurred at a much slower rate in germ-free mice compared to conventional mice with an intact microbiota (5).

1.3.2 – Microbe-Host Metabolic Crosstalk and Oxygen Regulation

Just as microbial populations contribute to a gut oxygen balance, so too do microbe-host cell interactions (Figure 1.2). The maintenance of oxygen abundance in the gut is influenced by microbiota signaling within the intestinal tract, where most of our understanding comes from large bowel microbe-host relationships. In the large bowel, the primary mechanism by which oxygen levels are regulated to maintain physiological hypoxia is through metabolite exchange between the bacteria of the gut and host cells (8). Obligate anaerobes of the intestine, primarily the Firmicutes and Bacteroidetes, produce short chain fatty acids such as butyrate (6, 13), which induces β-oxidation

metabolism by activation of the sensor peroxisome proliferator-activated receptor γ (PPAR-γ) in colonocytes (14). This oxidative metabolism consumes oxygen being delivered through the vasculature, preventing large influxes of oxygen from reaching the lumen of the intestine. Furthermore, a recent study revealed that microbiota-derived butyrate maintained the stability of transcription factor HIF-1 (hypoxia inducible factor) through β-oxidation metabolism, which aids epithelial barrier function (15). It is well established that HIF-1 directly regulates production of mucins, antimicrobial peptides (β -Defensin-1), and the tight junction protein claudin-1, which provides protection against several pathogenic organisms (15).

Comparatively less work has explored the metabolic coordination between the microbiota and epithelial cells in the small intestine (16). Phyla that produce short chain fatty acids are present, particularly in the distal ileum which is a more anaerobic environment than the duodenum and jejunum (17). In small intestinal enteroids, addition of butyrate promoted intestinal barrier function, supporting the presence of similar metabolic crosstalk as exhibited in the large intestine (18). More work, however, is required to understand how the dynamically shifting microbiota of the small intestine, which is more unstable than the large intestine, impacts host cell metabolism, community structure, and ultimately oxygen availability (19).

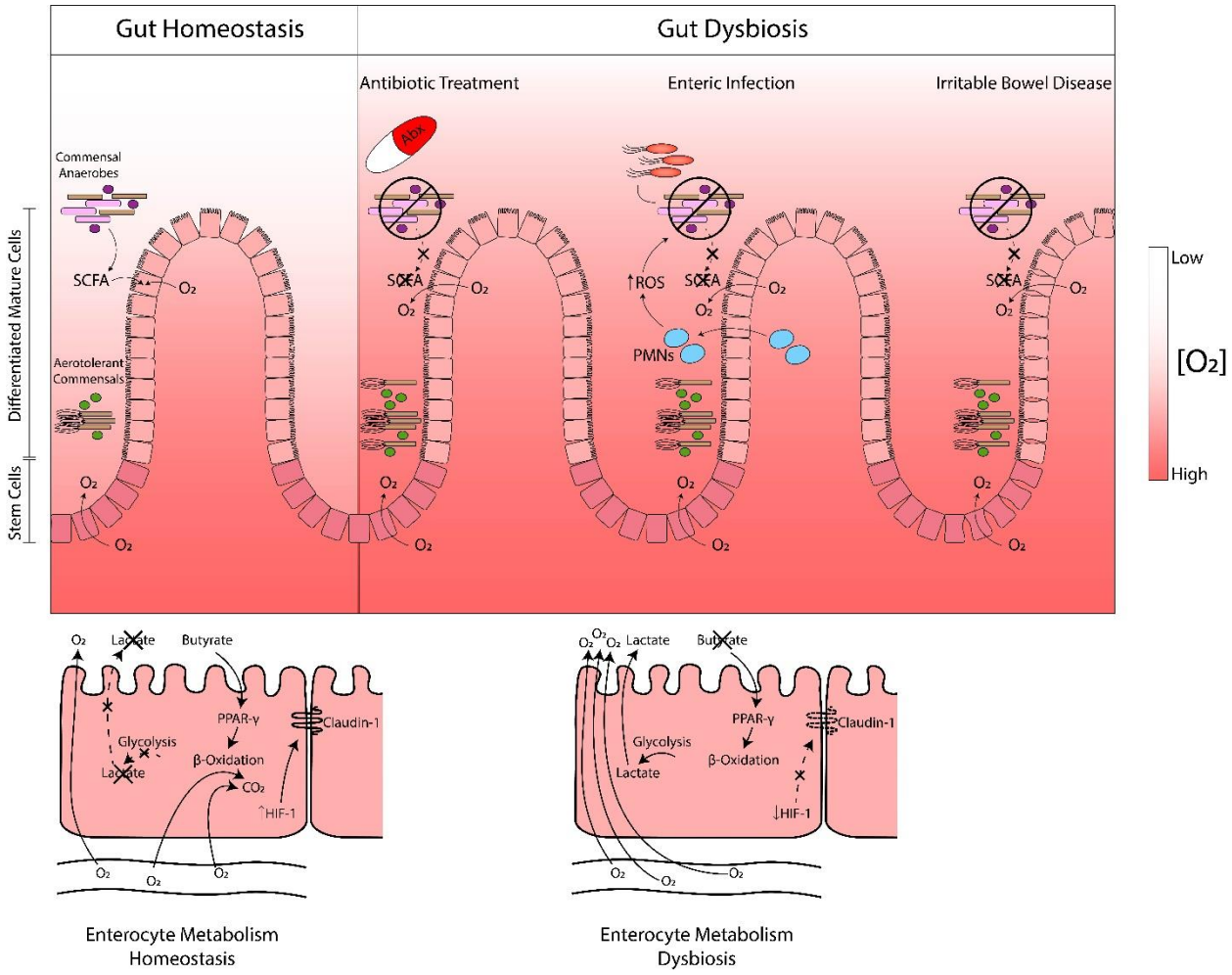

Figure 1.2. Oxygen dynamics in the gut during homeostasis and dysbiosis. Under gut homeostasis commensal anaerobes produce short chain fatty acids (SCFAs) such as butyrate that are consumed by the host epithelium through oxygen-dependent β-oxidation. Cellular hypoxia induces HIF-1 which supports epithelial barrier function through induction of proteins such as tight junction protein claudin-1. Crypt stem cell metabolism is predominantly anaerobic glycolysis allowing for oxygen to diffuse into the crypt space where oxygen becomes most available in the gut generating an oxygen gradient extending to the anoxic gut lumen. During periods of dysbiosis brought on by antibiotic treatment, enteric infection, or irritable bowel diseases, commensal anaerobe populations are reduced, decreasing SCFA production in the gut. This leads differentiated mature cells of the intestine to shift metabolism away from β-oxidation to anaerobic glycolysis, resulting in excess oxygen diffusion into the gut. Excess oxygen leads to the outgrowth of aerotolerant microorganisms as oxygen supports growth and further displaces commensal anaerobe populations. The loss of cellular hypoxia reduces HIF-1 activity and subsequent weakening of epithelial barrier by reducing production of protective proteins such as tight junction protein claudin-1.

1.4 – Oxygen During Dysbiosis

During dysbiosis, the balance of oxygen typically associated with homeostatic conditions becomes disrupted. Dysbiotic events can lead to dramatic fluctuations in oxygen abundance through disturbances to the precise oxygen control ecosystem of the gut. In some events, dysbiosis can lead to a positive feedback loop that perpetuates oxygen dysregulation, slowing gut remediation. Oxygen can become increasingly abundant in the intestine during periods of dysbiosis brought on by antibiotic treatment (20), enteric infection (21), inflammation (22, 23), and other factors that disrupt the resident microbiota of the intestinal tract (Figure 1.2).

Within the intestines, the dominant microbial phyla are Bacteroidetes, Firmicutes, Proteobacteria, Actinobacteria, Fusobacteria, and Verrucomicrobia (24). Bacteroidetes and Firmicutes comprise approximately 90% of the intestinal community with Proteobacteria, Actinobacteria, Fusobacteria, and Verrucomicrobia being less represented overall (25, 26). The Proteobacteria and Actinobacteria are widely classified as facultative anaerobes, and expansion of the Enterobacteriaceae family of the Proteobacteria phyla is assumed to be linked to increases in environmental oxygen availability. This was evident in ileostomy patients whose oxygen-exposed intestines had increased abundance of aerotolerant Lactobacilli and Enterobacteria which returned to normal community structure upon closure of the ileostomy (27). The shift in oxygen availability that leads to expansion of aerotolerant microorganisms coincides with the decrease in aerosensitive microorganisms. These latter microbes include obligate anaerobes responsible for producing the short chain fatty acid, butyrate, which

is consumed by intestinal epithelial cells. Human intestinal tissues lacking butyrate shift metabolism to anaerobic glycolysis, a process that does not consume oxygen (28). This leads to accumulation of oxygen in the epithelium and heightened oxygen levels diffusing into the gut lumen. To compound these effects, depletion of butyrate producing cells reduces epithelial signaling through PPAR-γ which typically limits the bioavailability of luminal oxygen in coordination with T_{reg} proinflammatory regulation (14). Without this activation signal, oxygen dissemination into the gut becomes dysregulated, exacerbating gut dysbiosis.

1.4.1 – Antibiotic-Altered Microbiota Boosts an Oxygenated Gut

Antibiotic treatment is one condition that leads to disturbance of resident gut microbiota. In mice treated with a cocktail of antibiotics, the redox potential of the gut, measured by microelectrode, increased after 24 hours and subsequently returned to baseline over an additional 24h time period, indicating transient fluctuations in oxygen availability in response to antibiotic treatment (29). This effect was also observed in human patients treated with ciprofloxacin where gut taxonomic richness, diversity, and evenness decreased but returned to near pre-ciprofloxacin treatment after 4 weeks (30). In another human case study, antibiotic treatment with amoxicillin-clavulanic acid causing antibiotic-associated diarrhea led to complete loss of clostridial cluster XIVa, reduction in clostridial cluster IV, and reduction in a *Bacteroidetes fragilis* cluster (31) which constituted the majority of butyrate-producing species (32). The loss of butyrate production in the gut due to antibiotic treatment was also observed in mice after being fed multiple antibiotics in drinking water followed by an oral dose of clindamycin which coincided with a change in the intestinal microbiota (33). The loss of SCFA producing

microorganisms results in elevated oxygen levels in the gut and decreased intestinal barrier function.

However, not all antibiotics are created equal. Antibiotics can target small subsets of bacteria or have broad-spectrum bactericidal properties which can differentially alter microbial gut composition. Doxycycline and clarithromycin decreased specific bacterial populations in the gut whereas phenoxymethylpenicillin, nitrofurantoin, and amoxicillin had very little impact on the gut microbiome composition (34). These summarized findings suggest that not all antibiotic treatment affect gut composition and oxygen availability in the same way.

1.4.2 – Enteric-Altered Microbiota Boosts an Oxygenated Gut

Disturbances in microbiota caused by enteric infection are similar to those from antibiotic driven shifts in microbiota that affect oxygen levels of the gut (35). Among infections from multiple enteric pathogens (*Escherichia coli* STEC O157 and non-O157, *Salmonella* spp., *Shigella* spp., and *Campylobacter* spp.) infected individuals showed expansion of Proteobacteria populations and decreases in Bacteroidetes and Firmicutes, which recovered after alleviation of infection (36).

In the case of *Salmonella enterica* serovar Typhimurium infection, infected mice colonized with a humanized microbiota had increases in Enterobacteriaceae and a decreases in the relative abundance of Bacteroidetes and Firmicutes (37, 38). This is driven in part by virulence factors deployed by *Salmonella* Typhimurium during infection. Specifically, through the action of the Salmonella type III secretion system (T3SS), large

depletions in *Clostridia* class microorganisms in the gut were observed (7). Type III secretion system-1 effector proteins and flagellar motility of *Salmonella* Typhimurium increases the respiratory burst of human neutrophils which would lead to more oxygen species in the gut altering gut community composition (39). The antimicrobial elastase activity of host neutrophils, which flood the intestine during infection, kill susceptible bacteria of the gut; a shift not seen in concomitant control neutrophil depletion infections (40). Indeed, displacement of butyrate-producing bacteria would be beneficial to *S.* Typhimurium as butyrate limits its pathogenicity (7, 41). Host inflammatory responses and displacement of resident microbiota subsequently leads to increased oxygenation of the gut. For the bacterial pathogens *Citrobacter rodentium* and *S.* Typhimurium*,* an inflamed gut leads to aerobic expansion of these pathogens, furthering disease progression (7, 38, 42). *Vibrio cholerae*, a pathogen of the small intestine, also appears to elicit oxygen accumulation in the gut. Through the action of cholera toxin, during infection, *V. cholerae* shows signatures of increased TCA cycle expression and elicits an accumulation of luminal L-lactate, both indicators that host epithelial cells have shifted to anaerobic glycolysis, resulting in oxygen accumulation in the gut (43).

Direct microbe-microbe interactions between pathogenic bacteria and members of the microbiome can also disrupt bacterial community composition and affect oxygen dynamics in the host. One example of a microbe-microbe interaction that affects community structure involves Type VI secretion system (T6SS) dependent killing (44). The T6SS of *V. cholerae* supported colonization in both the infant mouse and infant rabbit through T6SS-dependent killing of commensal populations for niche

establishment (45, 46). T6SS are not just limited to *V. cholerae* as they exist in *Campylobacter jejuni, Shigella flexneri, Citrobacter rodentium,* and *S.* Typhimurium (47–49). The T6SS of *C. rodentium*, a mouse enteropathogen model for human enteropathogenic and enterohemorrhagic *E. coli* infections (50), supports competition with non-pathogenic *E. coli in vitro* (50, 51). *Salmonella* Typhimurium also competes with bacteria of the gut using a T6SS, but only targets specific members of the microbiota in order to invade the gastrointestinal tract (52). Deeper understanding of how T6SSs influence pathogen biology is emerging, but how they change oxygen availability through interbacterial competition remains to be thoroughly investigated.

1.4.3 – Host Inflammation Boosts an Oxygenated Gut

Host inflammation is associated with overgrowth of Enterobacteriaceae, a correlate of increased oxygen in the gut (53). In mice treated with dextran sodium sulfate, a model of colitis, non-pathogenic E. coli proliferate by formate oxidation to expand in the inflamed gut (54). Changes in gut composition are prevalent in the intestines of patients with irritable bowel disease (IBD) such as ulcerative colitis and Crohn's disease, for whom periods of intestinal inflammation are common. Crohn's disease results in depletion of butyrate producing bacteria (55). Ulcerative colitis reduces overall diversity and is tied to increases in Proteobacteria populations (56). These gut composition changes resulted in a shift toward Enterobacteriaceae and away from commensal anaerobic populations (57, 58). Commonly associated with intestinal dysbiosis in IBD patients, oxygen is hypothesized to perpetuate lasting problems in these patients as facultative anaerobes dominate and prolong disease (59).

1.5 – Oxygen as a Signal for Pathogens in the Host Environment

Oxygen levels serve as a signal for intestinal microorganisms (Figure 1.3) (3). The same is true for pathogens as they progress through infection (60). Oxygen is detected by enteric pathogens through oxygen sensitive regulators that respond to intracellular redox potential to control bacterial responses that promote pathogenicity and fitness during infection (61).

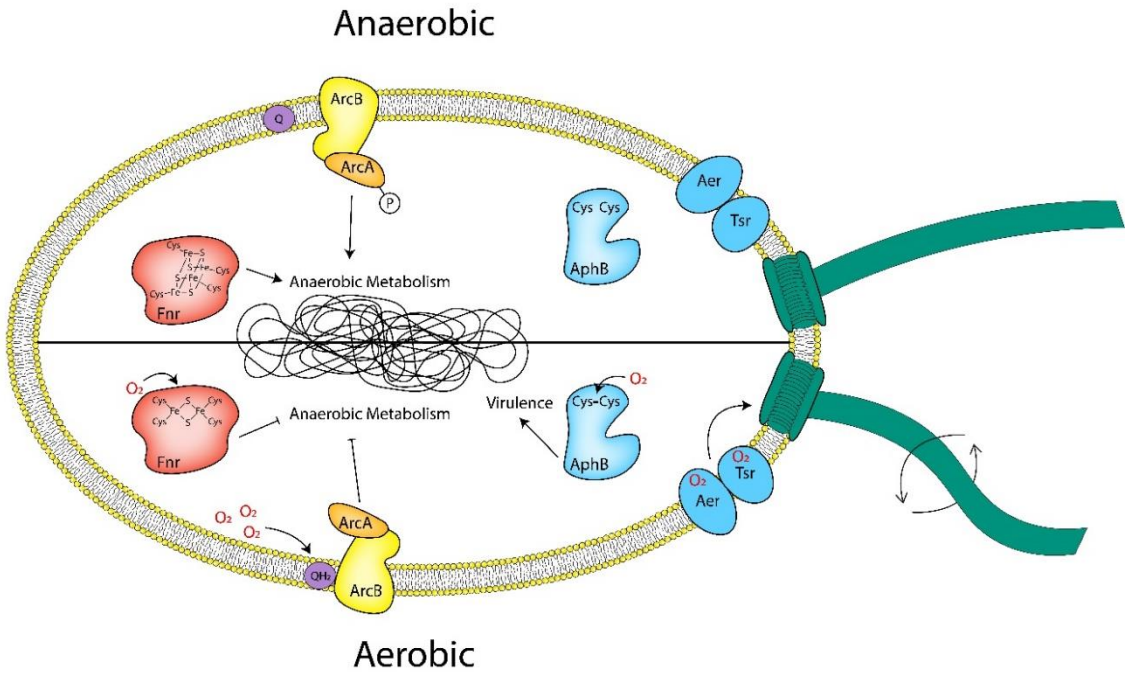

Figure 1.3. Oxygen responsive signaling in bacteria. Iron-sulfur containing proteins, such as Fnr, respond to oxygen through the oxidation of Fe-S clusters. Fnr responds to the presence of oxygen affecting gene expression for anaerobic metabolism. Anaerobic metabolism genes are induced in anaerobiosis and repressed in aerobiosis. Two component regulators such as ArcAB respond to oxygen through indirect energy sensing through the quinone pool. Quinones (Q) are electron carriers in the electron transport chain. In anaerobiosis, through kinase activity, ArcB phosphorylates the response regulator ArcA which induces genes involved in anaerobic metabolism. In aerobiosis, electron carrying quinones (QH_2) interact with ArcB which changes from a kinase to a phosphatase, dephosphorylating ArcA, which no longer induces genes involved in anaerobic metabolism. AphB responds to oxygen by formation of disulfide bridges following oxidation of coordinating cysteines. In

aerobiosis, disulfide bridge formation activates AphB to induce virulence gene expression. In anaerobiosis, no disulfide linkages are formed, so no virulence genes are activated. Aer and Tsr are oxygen transducers that support aerotaxis in some bacterial cells. In the presence of oxygen, Aer and Tsr drive flagellar motility in a chemotactic response whereas in the absence of oxygen, Aer and Tsr do not affect cell motility.

1.5.1 – Direct Oxygen Sensor Response Complexes

Iron-sulfur clusters are one class of oxygen responsive molecular switches that react to the presence of oxygen (62). Many types of iron-sulfur clusters exist that can collectively respond to redox potentials ranging from +500mV to -500mV, a wide range in redox response that can affect a function in oxygen sensing, electron transfer, and enzyme activities (63, 64). A prominent iron-sulfur cluster-containing regulator in pathogenic and nonpathogenic *E. coli* as well as other prominent bacterial pathogens, is the fumarate and nitrate regulatory (Fnr) protein that responds to the presence of oxygen (65, 66). The iron-sulfur cluster in Fnr becomes oxidized in the presence of oxygen, causing release of the protein from its DNA-bound dimeric conformation. This leads to de-repression of >100 genes in *E. coli* (67) and modifies >300 genes in *S.* Typhimurium, including genes involved in virulence (68). In fact, Fnr modulates expression of virulence genes in several pathogens (69). In *S. flexneri*, Fnr is important for both early and later stages of infection. Oxygen mediated Fnr de-repression directs activation of the T3SS Ipa (invasion plasmid antigen) secretion into host cells upon reaching the relatively oxygenated intestinal crypts which promotes epithelium intracellular invasion (70). Oxygen consumption for luminal *S. flexneri* occurs through *cydAB* bd oxidase which is required for intracellular survival (71), which leads to further tissue colonization

as foci of hypoxia develop and Fnr signaling in a now oxygen-limited environment activates anaerobic metabolic pathways to support further proliferation (72, 73).

Thiol-based molecular switches are another mechanism for oxygen and redox sensing within the host environment. Thiol-based switches respond to the presence of reactive oxygen species as cysteine thiolates readily react with ROS species to form or break disulfide linkages resulting in a change of conformation to direct regulatory responses (74, 75). In *V. cholerae*, oxygen sensing by thiol molecular switches is proposed to be important for spatiotemporal regulation of virulence gene expression (76, 77). Virulence expression under differential oxygen conditions is controlled by thiol-switch virulence regulators, AphB and OhrR, in which homodimerization through oxygen responsive cysteine residues occurs under low oxygen conditions and leads to the expression of the toxin-coregulated pilus (TCP) (Figure 1.4) (78, 79). This oxygen response leads to early production of TCP during infection, priming *V. cholerae* cells for microcolony formation upon reaching intestinal crypt spaces.

1.5.2 – Indirect Oxygen Sensor Response Complexes

Two component regulatory systems also sense and respond to oxygen availability. One prominent example is the ArcAB two component system most thoroughly studied in *E. coli* and *Salmonella* (80, 81). Upon oxidation of redox-active cysteine residues by quinone electron carriers in aerobic conditions, ArcB becomes a phosphatase leading to ArcA dephosphorylation and inactivation (82). Oxidation through the quinone electron carriers can be considered an indirect barometer of oxygen availability as quinones readily obtain electrons during oxidative respiration that then relays this oxygen

availability signal to response proteins such as ArcB. ArcB itself is insensitive to molecular oxygen and reactive oxygen species, making indirect oxidized quinones the sole pathway for oxygen sensing (82). Oxygen sensing through ArcAB promotes fitness of *E. coli* and *S.* Typhimurium by modulating expression of genes necessary for resistance to reactive oxygen stress, a trait that is critical for *Salmonella* intracellular survival (83, 84). In *V. cholerae*, active ArcA (anaerobic conditions) in Classical biotypes induces expression of the master virulence regulator *toxT* while expression of downstream *tcpA-F*, encoding the toxin-coregulated pilus, is initially expressed in the more anaerobic lumen of the gut to initiate epithelial attachment (85). However, not all ArcAB response networks are necessary for colonization as *arcA* deletion in *Salmonella enterica* serovar Enteriditis was not compromised for virulence in mice (86). Another example of an oxygen responsive two component system is RacRS in the microaerophile *Campylobacter jejuni*, which responds to low oxygen concentrations to optimize *C. jejuni* growth in the presence of alternative electron acceptors nitrate and trimethylamine-N-oxide (TMAO) (87).

Oxygen sensing transducers can also influence bacterial cell signaling in response to oxygen availability and increasing energy gradients. Aerotaxis is a form of chemotaxis in which bacterial cells sense energy levels through their electron transport chain (88). In *E. coli*, Aer and the serine chemoreceptor Tsr sense oxygen indirectly through respiratory chain electron transport and adjust *E. coli* cell behavior to move in the direction of a higher energy environment, typically toward higher oxygen concentrations (89, 90). Aer and Tsr proteins are highly conserved in enterohemorrhagic O157:H7 *E.*

coli and may play an important role in pathogen colonization in directing bacterial cells to the epithelium with higher relative concentrations of oxygen, although this has yet to be investigated. *V. cholerae* also maintains aerotactic chemoreceptors Aer1 (AerB) (91) and Aer2 (92), although the direct contribution of each chemoreceptor during colonization is unknown. Likely, aerotaxis through Aer1 and Aer2 is not required for colonization as nonchemotactic *V. cholerae* outcompete wild type cells in the infant mouse, indicating that chemotaxis may not be required *in vivo* for a pathogen of the small intestine (93). For *Salmonella*, aerotaxis is also present and was found to benefit fitness during infection, directing bacteria towards high energy electron acceptors such as oxygen, nitrate, and tetrathionate (94, 95). Aerotaxis may also benefit *C. jejuni* as it is predicted to contain two aerotaxis responsive chemoreceptors, although the current role for these receptors during infection is unknown (96, 97).

1.5.3 – Spatiotemporal Oxygen Signaling Benefitting Pathogenicity

Oxygen is also involved in the spatiotemporal regulation of virulence gene expression in enteric pathogens during infection (Figure 1.4). Enterohemorrhagic *E. coli* (EHEC) colonization potential is enhanced under microaerobic conditions as adherence, T3SS expression, and translocation activity were considerably elevated compared to aerobic and anaerobic conditions (98). This suggests that producing virulence factors near the microaerobic epithelium optimizes colonization and pathogenicity. In addition to the above mentioned oxygen sensing complexes of ArcAB and Fnr that drive differential gene expression, EHEC strains also have four copies of the gene encoding a small RNA, DicF, which senses low oxygen environments, three copies more than commensal *E. coli* (99). In low oxygen environments, such as the intestine, DicF

releases from the ribosome binding site allowing for the translation of PchA protein which in turn promotes expression of the T3SS (99). The elevated copies of *dicF* may support more sensitive and nuanced oxygen regulatory control in pathogenic *E. coli* than is needed in non-pathogenic strains. Oxygen availability also affects Shiga toxin (Stx) production in EHEC given that microaerobic environments lead to the highest levels of Stx production (100). Suppressing virulence expression in the anaerobic lumen and driving production near the epithelium is a fitness strategy that increases the likelihood of disease progression. Enteroaggregative *E. coli* (EAEC) also responds to high concentrations of oxygen, in coordination with host cell contact which induces virulence expression (101). However, virulence expression was highest in aerobic conditions for EAEC even though the transition from the anaerobic lumen to the microaerobic epithelium would still be expected to play a role in signal timing and pathogenesis.

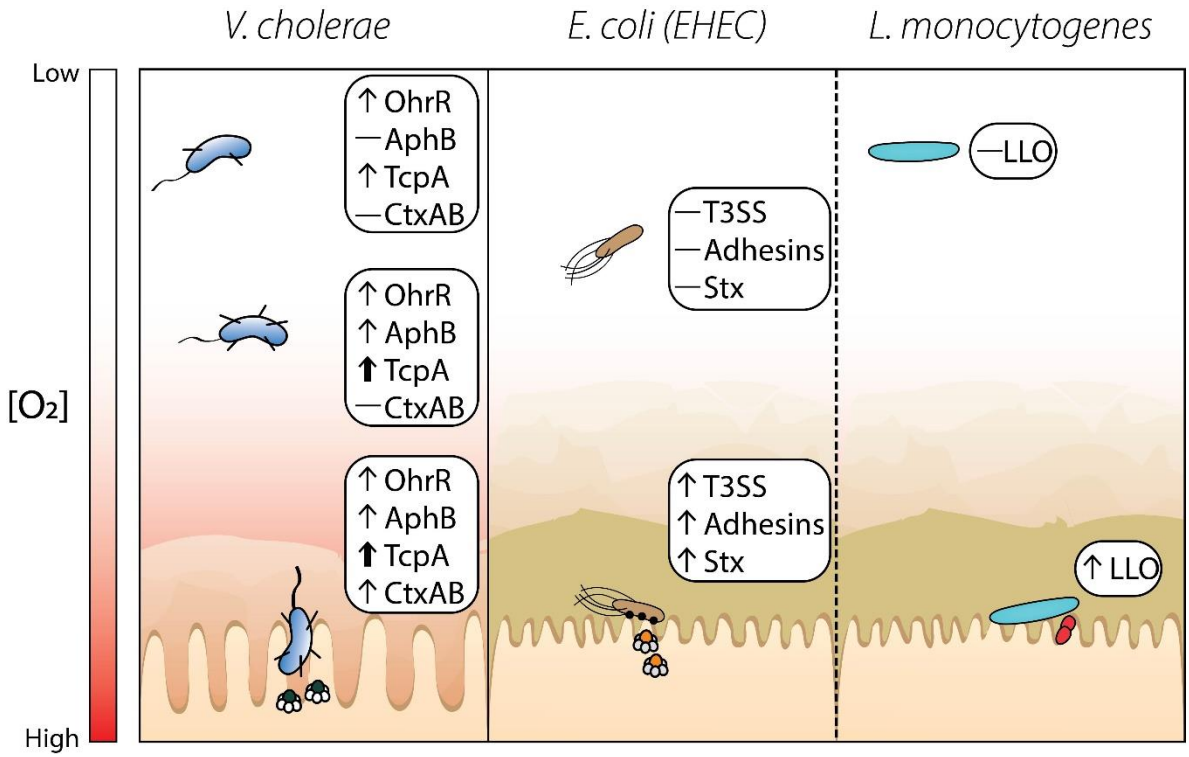

Figure 1.4. Oxygen responsive spatiotemporal gene regulation in bacterial pathogens. *Vibrio cholerae* responds to low oxygen conditions, initially activating OhrR which induces early toxin-coregulated pilus (TCP) production. In higher oxygen concentrations, AphB becomes activated to further induce TCP production. At the host epithelium where oxygen is in greatest abundance, cholera toxin (CT) production is induced to elicit disease. Enterohemorrhagic *Escherichia coli* does not produce virulence factors in the low oxygen environment of the intestinal lumen. As oxygen levels increase near the host epithelium, oxygen responsive gene regulation leads to the production of the type 3 secretion system (T3SS), adhesion proteins, and Shiga toxins (Stx). *Listeria monocytogenes* does not produce Listeriolysin O (LLO) in the anaerobic gut lumen, however, oxygen levels near the epithelium induce initial production of the LLO hemolysin that aids in host cell uptake via phagocytosis.

V. cholerae also responds to spatial localization within the intestine through oxygen sensing. AphB and OhrR thiol-switches and the ArcAB two component system in the anaerobic lumen coordinate early expression of TCP which is proposed to prime microcolony formation and adherence (78, 79). Expression of *tcpA*, encoding the major TCP pilin subunit, is upregulated biphasically during infection in both early and later stages of infection, presumably in an initial luminal population followed by further

induction in the intestinal crypt (76). *ctxAB*, which is coregulated with *tcpA* by ToxT, however, is not expressed biphasically and is only expressed in coordination with *tcpA* in the later stage infection (76). In the Classical *V. cholerae* biotype, H-NS proteins appear to prevent cholera toxin (CT) production in anaerobic, but not aerobic conditions (102). Functionally, this would translate to lack of CT production in the anaerobic lumen and CT production near the host epithelium where diffusive oxygen alleviates H-NS repression. Of note, however, is that CT is produced in anaerobic virulence factor inducing conditions by El Tor *V. cholerae*, indicating differential regulation between the biotypes *in vitro* that may affect *in vivo* spatiotemporal expression (103).

Listeria monocytogenes is an intracellular pathogen of the intestine, colonizing the host cell cytosol, which enables its cell to cell spread (104). In the absence of oxygen, virulence factors including the Listeria adhesion protein (LAP) were highly expressed (105), mirroring early-infection expression of adhesion proteins in EHEC and *V. cholerae* (106). For Listeriolysin O (LLO), the primary toxin of *L. monocytogenes,* gene expression, but not toxin production per se, was enhanced in anaerobic conditions, particularly in the presence of short chain fatty acids (SCFAs) (106, 107). This primed expression may occur in the lumen of the intestine where SCFAs are produced by the commensal microbiota, and when exposed to low levels of SCFAs in the presence of oxygen, LLO production and activity was enhanced (107). This coordinated regulation of transcription and translation of LLO may facilitate *L. monocytogenes* infectivity as it comes into proximity with the host epithelium, an area typically devoid of SCFA-producing commensal bacteria in the large intestine and with relatively higher oxygen

concentrations (107). Stimulated extracellular LLO production might then lead to perforation of host cells to stimulate internalization by the host epithelium (108). This LLO priming may also benefit the bacteria after internalization to ensure rapid lysis of the phagosomal membrane, limiting time within the compartment to gain quick access to the host cytosol (109).

1.6 – The Influence of Oxygen on Pathogen Growth and Survival

1.6.1 – Gut Oxygen in Anaerobic and Aerobic Metabolism of Pathogens

Varying oxygen concentrations in the gut likely influences the metabolism of all gut microbes, both resident and transient. Anaerobic metabolism predominantly occurs in the hypoxic lumen, away from the more oxygenated host epithelium where oxidative respiration supports growth of facultative anaerobes. Oxidative respiration is the most efficient energy-generating metabolic pathway, supporting cellular processes for growth and proliferation. Bacterial pathogens capable of oxidative respiration therefore benefit from the presence of oxygen during infection, particularly near the epithelium where oxygen is most abundant.

V. cholerae is one such pathogen that benefits from both anaerobic and aerobic metabolism during infection, using oxygen as a growth factor promoting proliferation. Given the separate microenvironments of the intestine between the more anaerobic lumen and more oxygenated epithelium, maintaining both anaerobic and aerobic metabolic pathways would be beneficial for pathogen fitness *in vivo*. *V. cholerae* benefits from anaerobic nitrate respiration, especially when coordinated with fermentation in a streptomycin-treated adult mouse model (110, 111). Aerobic

respiration, on the other hand, was determined to be essential for *V. cholerae* colonization in the infant mouse where colonization was severely attenuated in the small intestine, the primary site for *V. cholerae* infection in the human body (103). A much more severe colonization deficiency was observed when aerobic metabolism was disrupted than when anaerobic respiration was disrupted.

For both pathogenic and non-pathogenic *E. coli*, anaerobic respiration is important for growth and persistence in the gut, likely in the anaerobic mucus layer (112). Additionally, pathogenic and non-pathogenic strains also require aerobic respiration for colonization of the mouse, as mutant strains defective for oxidative respiration are displaced in competition with co-respiring cells (54, 113). When comparing aerobic and anaerobic metabolisms, defects in oxidative respiration through the cytochrome *bd* oxidase were more attenuated for competition colonization in mice compared to nitrate or fumarate reductase deletion strains, indicating aerobic metabolism is more important to *E. coli* replicative success in the gut of mice (112). As the human intestine is larger than the mouse gut, there is a greater volume of anaerobic space in the human colon, which may increase the relative importance of anaerobic metabolism for *E. coli* colonization.

S. Typhimurium also benefits from both anaerobic and aerobic metabolism to proliferate in the mouse gut (7). In genetically resistant mice that do not become moribund after *S.* Typhimurium infection, *Clostridia* spp. were reduced, and aerobic respiration was required for optimal colonization (7). In the same study, anaerobic nitrate respiration

was also necessary for optimal colonization of the mouse gut, suggesting the dual proliferative functions of both metabolic pathways (7). Anaerobic respiration of ethanolamine was also shown to be an important driver of *S.* Typhimurium growth as tetrathionate becomes readily available in the gut following the respiratory burst of PMNs during disease (114, 115).

C. rodentium influences its own aerobic expansion in the gut through cryptic hyperplasia via the T3SS, which influences expansion of undifferentiated proliferating (Ki67-positive) colonic epithelial cells (42). Undifferentiated Ki67 epithelial cells are incapable of butyrate oxidation and are therefore likely to lead to higher levels of oxygen in the gut. Ki67 expansion may not be the only host change that affects oxygen availability as a *C. rodentium espO* (hyperplasia-inducing factor) mutant had reduced Ki67 counts yet demonstrated similar levels of shedding compared to WT (116). Nonetheless, the effects of *C. rodentium* infection change host cell metabolism in the infection microenvironment to one of anaerobic glycolysis and lactate efflux in mice alongside reduced uptake of microbiota-derived butyrate which promotes lumen oxygenation (117). For *C. rodentium*, aerobic expansion is considered to be important for colonization as strains lacking a functional *cydAB bd* oxidase were attenuated for colonization of the adult mouse (42).

For the microaerophile *C. jejuni*, oxygen is required for a class I ribonucleotide reductase for DNA synthesis (118). Oxygen is therefore necessary to support DNA replication and cell division. However, too much oxygen is detrimental to *C. jejuni* as it is

non-viable at atmospheric oxygen levels. In a unique form of regulatory metabolism, formate is highly metabolized by aerobic respiration in *C. jejuni*, but as it is used, reduces oxidase activity resulting in expression of proteins needed for alternative electron acceptor anaerobic respiration (119). Thus *C. jejuni* fine tunes its response to oxygen to maintain DNA replication while also consuming excess oxygen to maintain cell viability.

Clostridioides difficile, an obligate anaerobe, is particularly susceptible to oxidative damage (120). *C. difficile* employs specialized strategies to detoxify molecular oxygen that enters the cell. One enzyme produced to limit oxygen within the cell is cysteine desulfurase (*IscS2*), which plays a currently undefined role in oxygen resistance (121). Additionally, two flavodiiron proteins (FdpA and FdpF) and two reverse rubrerythrins (revRbr1 and revRbr2) detoxify oxygen and function additively in oxygen tolerance to maintain cell viability (122, 123). In addition to oxygen tolerance, reverse rubrerythrins also have peroxide reductase activity, further protecting *C. difficile* from this reactive oxygen species (123). Reactive oxygen species are particularly harmful to *C. difficile* as it lacks canonical ROS defense proteins. To address this, *C. difficile* employs a specialized strategy to prevent oxidative stress by sensing and capturing host heme during gastroenteritis for protection against redox stressors (124). Cells lacking the heme capture system *hsmRA* were attenuated for mouse colonization, indicating an essential role for this novel defense strategy (124). Oxygen and ROS defenses are critical for *C. difficile* as oxygen becomes prevalent during antibiotic treatment,

predisposing the host to infection, and during pathogen-induced gastroenteritis, which increases oxygen and ROS presence in the gut.

1.6.2 – Reactive Oxygen Species in Bacterial Growth and Death

An important host defense is production of reactive oxygen species, which can affect enteric pathogen survival (125). Host polymorphonuclear neutrophils (PMNs) generate reactive oxygen species by activating NADPH oxidase to limit pathogen survival (126). Superoxide (O_2^-), hydrogen peroxide (H_2O_2), hydroxyl radicals ($OH\cdot$), and hypochlorous acid (HOCl) are reactive oxygen species made by PMNs and macrophages that arrest the growth of bacterial pathogens (127, 128). And pathogens have evolved multiple mechanisms to adequately survive this stress during infection. These involve production of catalase, superoxide dismutase, and peroxidase which neutralize the reactive agents (129, 130). Gene expression to resist ROS is controlled through oxygen sensors such as Fnr (131) and ArcAB (83) and, in the case of *response to* hypochlorite, the transcription factor YjiE (132). These resistance mechanisms, however, do not completely protect bacteria, as at high levels of ROS cells will succumb to irreparable cellular damage (133). Even after ROS stressors are removed prior to cell death, once the threshold level is met *E. coli* cells will progress to cell death (134).

Bacteria also have the capacity to exploit subinhibitory ROS levels to their advantage. In non-pathogenic *E. coli*, catalases *katE* and *katG* covert H_2O_2 into molecular oxygen that is respired through the secondary *bd*-II oxidase *appBCX* (*cyxAB*) conferring a growth advantage in the inflamed gut (135). As this has been observed in non-pathogenic *E. coli*, it is of interest to investigate the potential for pathogenic *E. coli* species and other

facultative anaerobic pathogens to capture and use ROS for enhanced oxidative respiration.

1.7 – The Terminal Oxidases of Bacterial Pathogens

Bacterial pathogens that respire oxygen encode terminal oxidase complexes for oxygen reduction (Figure 1.5). These terminal oxidases can be of the heme-copper oxidase (HCO) superfamily, which is subdivided into A, B, and C-type (136), or of the quinol oxidase family (137). In the final step of the electron transport chain (ETC), these terminal oxidase complexes catalyze the reduction of molecular oxygen to water [O_2 + $4H^+$ + $4e^-$ → $2H_2O$] which generates an electrochemical proton gradient across the cytoplasmic membrane as four positively charged protons are consumed in this reaction (138). This step is consistent among all terminal oxidase complexes, however, additional electron transfer steps in the ETC and proton translocation efficiencies based on HCO-type vary among bacterial respiratory chains and contribute to the generation of a proton gradient (138). Generally, HCO terminal reduction is coupled to proton translocation which translates to higher energy production compared to *bd* oxidases (138). *bd* oxidases are not coupled to proton translocation, and are further characterized by typically having high affinities for oxygen, being composed of two subunits, and are subdivided into either short or long Q-loop categories base on the connecting loop between transmembrane helices 6 and 7 in subunit I (137). The electrochemical proton gradient generated through the ETC is important for the functionality of ATP synthase which generates high energy ATP for supporting cellular processes and growth (139).

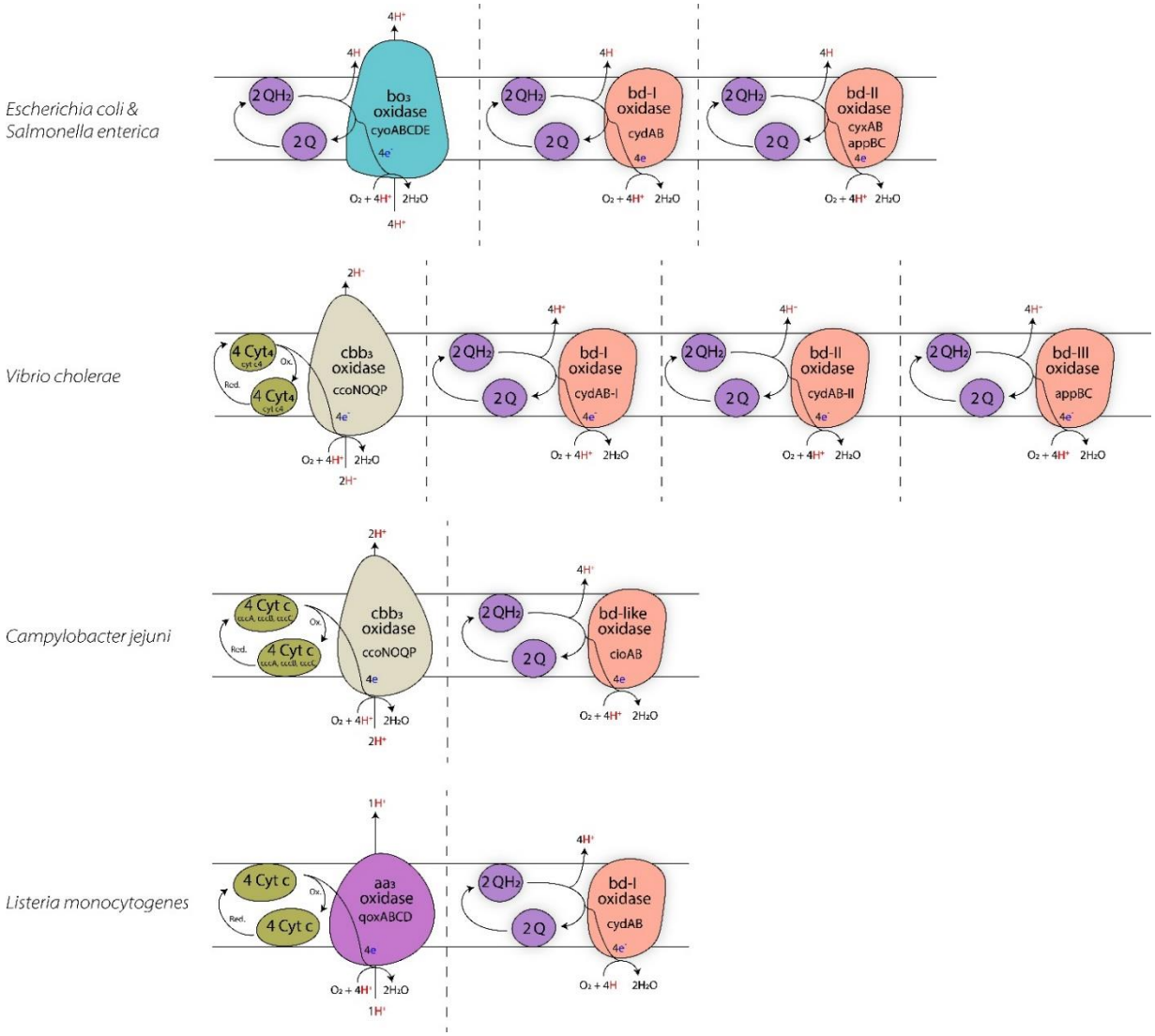

Figure 1.5. Terminal oxidase complexes of enteric pathogens. *Escherichia coli* and *Salmonella enterica* both maintain a single *bo*$_3$ oxidase complex, *cyoABCDE*, alongside two *bd* oxidases *cydAB* and *appBC* (*cyxAB*). Each of these complexes acquires electrons from the quinone pool. *Vibrio cholerae* maintains a single *cbb*$_3$ oxidase, *ccoNOQP*, and three *bd* oxidases, *cydAB*-I, *cydAB*-II, and *appBC*. The *cbb*$_3$ complex receives electrons from cytochrome c$_4$ whereas the *bd* oxidases receive electrons from the quinone pool. *Campylobacter jejuni* maintains a *cbb*$_3$ oxidase, *ccoNOQP*, and a *bd*-like oxidase, *cioAB*. The *cbb*$_3$ complex receives electrons from one of three cytochrome c's, *cccA*, *cccB*, or *cccC* whereas the *bd*-like oxidase receives electrons from the quinone pool. *Listeria monocytogenes* maintains an *aa*$_3$ oxidase, *qoxABCD*, and a *bd* oxidase, *cydAB*. The *aa*$_3$ oxidase receives electrons from a cytochrome c and the *bd* oxidase receives electrons from the quinone pool. All terminal oxidase complexes perform the terminal reduction of oxygen to water [$O_2 + 4H^+ + 4e^- \rightarrow 2H_2O$].

Broadly, bacteria possess multiple terminal oxidase complexes as part of a branched respiratory pathway repertoire (138). Enteric pathogens and their associated terminal oxidase complexes are listed in Table 1. Maintaining functionally redundant terminal oxidase complexes may be attributed to the diversity of environments enteric pathogens inhabit (140). For example, *E. coli* contains three terminal oxidase complexes, the HCO bo_3 (*cyoABCDE*), and two *bd*-type oxidases, *bd*-I (*cydAB*) and *bd*-II (*cyxAB*). The oxidases are differentially expressed, with the bo_3 complex maximally expressed in highly oxygenated environments, and the *bd*-type oxidases maximally expressed in microaerobiosis (141). In microaerobic conditions, a combined signaling response between the ArcAB/FNR systems leads to expression of *cydAB* as opposed to *cyoABCDE* (142). This coordinated regulation leads to *cydAB* expression in low oxygen environments, such as the gut, while restricting *cyoABCDE* expression. This is particularly beneficial as *bd* oxidases have relatively high affinities for oxygen compared to the low affinity bo_3 oxidase, which is preferable in low oxygen microenvironments of the intestine (143, 144). Indeed, the *bd*-I terminal oxidase has been shown to be necessary for non-pathogenic *E. coli* expansion during inflammation (54) and the *bd*-II supports aerobic respiration for *E. coli* following ROS detoxification by catalase enzymes (135). The *bd*-I oxidase was also shown to be important for pathogenic EHEC host colonization as a *cydAB* deletion strain is readily outcompeted by the wild type strain (113).

Table 1.1. Enteric pathogens and terminal oxidase complexes.

Pathogen	*Terminal Oxidase Complexes*	*Reference*
Escherichia coli	*bo*$_3$ (*cyoABCDE*) *bd*-I (*cydAB*) *bd*-II (*cyxAB* / *appBC*)	(145, 146)
Salmonella enterica serovar Typhimurium	*bo*$_3$ (*cyoABCDE*) *bd* (*cydAB*) *bd* (*cyxAB*)	(7)
Vibrio cholerae	*cbb*$_3$ (*ccoNOQP*) *bd* (*cydAB*-I) *bd* (*cydAB*-II) *bd* (*appBC*)	(147)
Listeria monocytogenes	*aa*$_3$ (*qoxABCD*) *bd* (*cydAB*)	(148)
Campylobacter jejuni	*cbb*$_3$ (*ccoNOQP*) *bd* (*cioAB*)	(149)
Clostridium difficile	-	(123)

bd-type oxidases provide additional protective functions for bacterial cells during infection. The *bd* oxidase of *E. coli* displays high catalase activity and protects the cells from hydrogen peroxide stress (150). Additionally, compared to the *bo*$_3$ oxidase, *bd* oxidases are less sensitive to nitric oxide, another host produced defense molecule, making the *bd* oxidase better suited for use in the intestinal environment (151). Finally, the *bd* oxidases are insensitive to sulfide, a host and microbiota produced oxidase inhibitor, allowing for growth in the intestinal environment (152).

Aside from *E. coli*, terminal oxidases are also important in the pathogenesis of *S.* Typhimurium, *S. flexneri*, *C. jejuni*, *L. monocytogenes*, and *V. cholerae*. In *S.* Typhimurium infection, *cydAB* was determined to be important in host tissue, whereas *cyxAB* was important in gut colonization (7). However, a separate study also found *cydAB* to be important in the gut by fecal sample analysis (38). Cytochrome *bd* was

required for expansion of *S. flexneri* by generating hypoxic foci that promote proliferation during later stages of infection (71). In *C. jejuni* CioAB, a low-affinity *bd*-like oxidase, is needed for optimal microaerobic growth (149) and was upregulated in the rabbit ileal loop model (153). However, the *cbb*$_3$ oxidase of *C. jejuni* was concluded to be more important for microaerobic growth, as the authors of this study were unable to generate the mutant strain and the *cbb*$_3$ oxidase had a higher relative affinity for oxygen (149). This was supported as a *C. jejuni CcoN::Cm* (*cbb*$_3$) mutant was unable to colonize the commensal gut of the chicken, while a mutant lacking *cioAB* had no colonization defect (154). *L. monocytogenes* maintains two terminal oxidases, a *bd* and *aa*$_3$-type which allow growth at different oxygen levels. The *bd* oxidase supports growth in atmospheric oxygen and intracellularly, whereas the *aa*$_3$ oxidase supports growth during the initial stages of infection (148). *V. cholerae* contains one *cbb*$_3$ and three *bd* oxidases which have yet to be investigated individually for their functionality during infection and are the subject of work described in this thesis (147).

1.8 – Measuring Oxygen During Infection

As oxygen is a prominent force driving bacterial infection, methods to measure oxygen *in vivo* can further our understanding of oxygen-driven pathogen dynamics during infection. A variety of technologies exist capable of probing oxygen concentrations in model systems, and we discuss some of the more recent tools available in this respect.

1.8.1 – Hypoxia Indicators

One method by which oxygen levels have been measured in animal models is with oxygen-sensitive nitroimidazole compounds, particularly pimonidazole which is suspected to bind to hypoxic tissues at oxygen concentrations <10mmHg O_2 (155).

Pimonidazole binds irreversibly to cellular nucleophiles under hypoxic conditions in the presence of nitroreductase enzymes (156) and can be targeted by secondary fluorescent antibodies in formalin fixed and paraffin embedded tissues to visualize hypoxia in intestinal segments (7, 157). A second hypoxia indicator that has been used is HIF-1. HIF-1 is induced in response to an array of pathogens including bacterial, viral, fungal, and protozoa and is expressed highly in foci of infection where bacterial pathogens readily consume available oxygen (158). Immunohistochemical staining of HIF-1 regulated claudin-1 and GLUT1 has been used to detect tissue hypoxia in fixed tissues of infected animal models (33, 72). These methods are useful for the indirect measurement of oxygen at host cell interfaces but lack the ability to measure oxygen directly and beyond host cell surfaces.

1.8.2 – Phosphorescent Probes

Phosphorescence oximetry is another method by which oxygen levels in the gut can be assessed. Oxyphor G4 and Oxyphor R4 are two oximetry probes that have been especially synthesized for use in *in vivo* tissue samples (159). Oxyphor G4 was used to determine radial oxygen gradients in mouse tissue alongside a novel luminal probe mix OxyphorMicro (3). These probes work by the phosphorescent quenching method. In this method, an excitation fiber excites the probe, and a phosphorescence detector reads the decay rate over short timescales corresponding to the partial pressure of oxygen in the environment, as oxygen quenches the probe (159). Use of these types of probes is challenging in *in vivo* systems as it requires surgical laparotomy in animal models to position excitation and detector wirings near the intestinal wall (3). These phosphorescent probes have seen growing use in emerging microfluidic applications

examining host-pathogen interactions (160, 161). A novel microfluidic device has been developed using a noninvasive phosphorescent film to measure oxygen levels (162), supporting a host-bacteria interface that could be used in future studies of pathogen interactions (163).

1.8.3 – Protein Biosensors

Oxygen-sensitive proteins are also used to measure oxygen levels within cells. A Förster resonance energy transfer (FRET)-based biosensor was developed where yellow fluorescent protein (YFP) and hypoxia-tolerant Flavin-binding fluorescent protein (FbFP) were linked in a biosensor called FluBO (164). Oxygen is required for the maturation of the YFP chromophore which will only receive energy to emit fluorescence from FbFP when oxygen is present (164). However, oxygen-dependent maturation of YFP is irreversible, meaning the dynamic shifts in oxygen availability likely to occur in an *in vivo* host environment are difficult to measure over time. Another sensor, ANA-Y, was recently developed in which a heme-based protein, linked to YFP variant Venus, responds sensitively to oxygen and can measure oxygen levels as low as 6µM (165). This probe does, however, rely on the presence of available heme and functions within a particular range of oxygen availability that may not capture all degrees of oxygen availability during infection. Much of this work has been conducted in batch cultures, but probes such as this could be valuable to measure oxygen exposure during infection, especially when paired with other imaging technologies. Previous work has taken advantage of this approach, using a HIFα luciferase fusion reporter in mice, detecting regions of hypoxia where luciferase bioluminescence was detected by IVIS (166).

1.9 – Conclusions and Future Perspectives

Oxygen is critical in shaping enteric infections, which are a continuing concern for global human health. Investigating the role of oxygen during infection by bacterial pathogens is necessary to our understanding of disease onset and disease progression. How oxygen influences bacterial infection is only recently explored as a crucial element of pathogen fitness and pathogenicity, and we are learning that oxidative metabolism and response networks are essential for fitness within the host environment. Oxygen-directed metabolism, induced in the presence of oxygen, can be essential for pathogen establishment within the intestinal environment. Particularly for pathogens capable of oxidative respiration that maintain a terminal oxidase complex, oxygen-driven population expansion exacerbates disease and promotes dissemination.

Of future interest is the dynamic relationship between resident microbes, pathogens, and host cells that influence oxygen abundance within the gut. The temporal changes in oxygen availability arising from complex host-microbe (pathogenic and commensal) interactions are important to understand for a more complete knowledge of enteric infections and how to combat them. Although recent technologies for measuring oxygen during infection have been discussed, limitations to these approaches make accurate longitudinal measurements difficult. Oxygen is instrumental in enteric infections, and its impact on progression of infectious diseases of the intestinal tract is a rich area of study for future investigators.

Chapter 2 – Aerobic Metabolism in *Vibrio cholerae* is Required for Population Expansion During Infection

2.1 – Preface

Contents of this chapter were published in the journal mBio in 2020 (Citation: Van Alst AV and DiRita VJ. 2021. Aerobic Metabolism in *Vibrio cholerae* is Required for Population Expansion during Infection. *mBio* 11: 5 e01989-20.) Per ASM reuse of published materials guidelines: “Authors in ASM journals retain the right to republish discrete portions of his/her article in any other publication (including print, CD-ROM, and other electronic formats) of which he or she is author or editor, provided that proper credit is given to the original ASM publication. ASM authors also retain the right to reuse the full article in his/her dissertation or thesis.”

2.2 – Abstract

Vibrio cholerae replicates to high cell density in the human small intestine leading to the diarrheal disease cholera. During infection, *V. cholerae* senses and responds to environmental signals that govern cellular responses. Spatial localization of *V. cholerae* within the intestine affects nutrient availability and metabolic pathways required for replicative success. Metabolic processes used by *V. cholerae* to reach such high cell densities are not fully known. We sought to better define the metabolic traits that contribute to high levels of *V. cholerae* during infection. By disrupting the pyruvate dehydrogenase (PDH) complex and pyruvate formate-lyase (PFL), we could differentiate aerobic and anaerobic metabolic pathway involvement in *V. cholerae* proliferation. We demonstrate that oxidative metabolism is a key contributor to the replicative success of *V. cholerae in vivo* using an infant mouse model in which PDH mutants were attenuated 100-fold relative to the wild type for colonization. Additionally, metabolism of host substrates, including mucin, was determined to support *V. cholerae*

growth *in vitro* as a sole carbon source, primarily under aerobic growth conditions. Mucin likely contributes to population expansion during human infection as it is a ubiquitous source of carbohydrates. These data highlight oxidative metabolism as important in the intestinal environment and warrant further investigation of how oxygen and other host substrates shape the intestinal landscape that ultimately influences bacterial disease. We conclude from our results that oxidative metabolism of host substrates is a key driver of *V. cholerae* proliferation during infection, leading to the substantial bacterial burden exhibited in cholera patients.

2.3 – Importance

Vibrio cholerae remains a challenge in the developing world and incidence of the disease it causes, cholera, is anticipated to increase with rising global temperatures and with emergent, highly infectious strains. At present, the underlying metabolic processes that support *V. cholerae* growth during infection are less well understood than specific virulence traits such as production of a toxin or pilus. In this study we determined that oxidative metabolism of host substrates such as mucin contribute significantly to *V. cholerae* population expansion *in vivo*. Identifying metabolic pathways critical for growth can provide avenues for controlling *V. cholerae* infection and the knowledge may be translatable to other pathogens of the gastrointestinal tract.

2.4 – Introduction

Vibrio cholerae causes the diarrheagenic disease cholera in humans and is particularly problematic in regions of the world with poor water sanitation. Ingesting contaminated water sources containing sufficiently high numbers of *V. cholerae* bacterial cells leads to infection characterized by excessive fluid loss and a substantial bacterial burden of *V.*

cholerae during the acute phase of disease. In the human gastrointestinal tract, *V. cholerae* can proliferate to numbers as high as 10^6 to 10^8 cells per gram of stool (167). In this study, we sought to understand the metabolic requirements for *V. cholerae* that support such substantial population expansion within the gut.

The mucous lining of the gastrointestinal tract, which typically serves as a barrier to infection, is saturated with a variety of carbohydrates. Mucin is a glycoprotein and the primary macromolecule of mucus. Mucin consists of a protein backbone decorated with *O*-linked glycan chains containing sugars such as *N*-acetylgalactosamine, *N*-acetylglucosamine, galactose, fucose, and sialic acid (168). Commensal mucin-degrading bacteria, such as *Bacteroides* spp. and *Akkermansia mucinophila*, contain numerous mucinolytic enzymes capable of releasing these sugars from the mucin glycan chain to support growth (168, 169). Mucin degradation is also a feature of bacterial pathogens such as *Shigella flexneri*, *Helicobacter pylori*, and enterohemorrhagic *Escherichia coli* (170–173). *V. cholerae* contains a number of mucolytic glycosyl hydrolases that are predicted to release glycans from mucin polysaccharides (174–176). Indeed, previous studies have linked mucus carbohydrate metabolism with infection, as *V. cholerae* mutants defective for *N*-acetylglucosamine and sialic acid metabolism were attenuated for colonization in the infant mouse (175–177). The mechanism of acquisition of these mucin carbohydrates may be through both phosphoenolpyruvate phosphostransferase-dependent and independent systems to support growth *in vivo* (178). Although mucin can serve as a substrate for growth, chemical reduction of intestinal mucus during infection leads to increased numbers of *V.*

cholerae, indicating that mucus also contributes to intestinal protection and clearance of the bacteria (179).

V. cholerae harbors the complete enzymatic pathways for the Embden-Meyerhof-Parnas pathway (EMP/glycolysis) pathway, the Entner-Doudoroff pathway (ED) pathway, and the pentose phosphate (PP) pathway (180, 181). The EMP and ED pathways predominantly generate the energy necessary for *V. cholerae* growth and proliferation. Additionally, previous work has shown that these pathways promote virulence factor production, although the direct cause for this effect is unknown (181, 182). In contrast, the PP pathway does not appear to play a significant role in the growth or colonization of *V. cholerae* during infection (183). These pathways culminate with the formation of pyruvate, which can then be used by the bacterium to fuel either aerobic or anaerobic metabolism to generate energy for the cell.

To expand our understanding of carbohydrate metabolism and its impact on *V. cholerae in vivo* fitness, we targeted the pyruvate dehydrogenase (PDH) complex and pyruvate formate-lyase (PFL), which both function to convert pyruvate to acetyl coenzyme A (acetyl-CoA) (184, 185). Examination of PDH and PFL mutants enables us to assess the contribution of aerobic and anaerobic metabolism to the expansion of *V. cholerae* during infection. The conversion of pyruvate to acetyl-CoA precedes the tricarboxylic acid (TCA) cycle, as the first step in the cycle requires acetyl-CoA to generate citrate. In previous work, *V. cholerae* mutants defective in the TCA cycle expressed increased levels of *toxT*, which encodes the major virulence gene activator in *V. cholerae.* This

finding suggested a link between acetyl-CoA and virulence expression (186). However, these TCA cycle mutants were not tested *in vivo* and have been investigated only in classical biotype strains, not in strains of the El Tor biotype. Classical *V. cholerae* predominated among epidemic isolates prior to 1961, when it was supplanted by the El Tor biotype (187). The biotypes are differentiated by numerous physiological attributes that contributed to displacement of the classical biotype by the El Tor biotype (188–191). Some of these are encoded on genomic islands unique to the El Tor biotype that contribute to phage resistance or acquisition of substrates (192, 193).

In this study, we assessed pathways of carbohydrate metabolism as they contribute to growth, virulence factor production, and colonization of *V. cholerae* El Tor strain C6706. By targeting the PDH complex and PFL, we are able to draw conclusions about the aerobic and anaerobic metabolic processes that facilitate population expansion of *V. cholerae* during infection. Our results provide evidence supporting the importance of a functional PDH complex during infection, with significantly less reliance on PFL function. This indicates that oxidative metabolism primarily drives the growth and proliferation required to amass the high bacterial cell density observed during the disease cholera. The defects in colonization observed with strains lacking a functional PDH are attributable primarily to metabolic deficiencies, as virulence factor production was unaffected by mutation in these metabolic pathways. Given what is known in regard to oxygen availability within the intestinal environment, being highest in the intestinal crypts and decreasing to near hypoxia in the lumen, we can deduce the biogeographical localization of replicative *V. cholerae* (3). Our work suggests that replication within

intestinal crypt spaces, observed by others (179), is enabled due to the higher oxygenation of this site than of the lumen. Furthermore, by using the physiologically relevant growth substrate mucin, we could closely reflect, and assess, the growth substrates typically encountered by *V. cholerae* during infection. The results of this study further our understanding of central metabolism and its contribution to *V. cholerae* infectivity and *in vivo* growth.

2.5 – Materials and Methods

2.5.1 – Transposon Mutagenesis Library Screen

We used a non-redundant transposon mutant library collection constructed in the El Tor C6706 background (194). Using a 96-well plate replicator, the library was replica plated onto large LB + kanamycin (0.05mg/mL) agar plates and incubated overnight at 37ºC. Subsequently, this LB-grown library was replica plated onto minimal MCLMAN media (195) plates supplemented with 0.5% type III porcine gastric mucin (Sigma). Transposon insertion mutants that were qualitatively defective for growth compared to neighboring transposon insertion mutants were marked as deficient for mucin utilization for further investigation. The complete list of identified mutants is in Table A.1.

2.5.2 – Porcine Small Intestinal Mucus Collection and Mucin Purification

Fresh porcine small intestinal segments were harvested from healthy adult pigs from the Michigan State University Meat Lab. Mucus was scraped from the intestinal segments and purified in a manner similar to that previously described (196). Briefly, crude mucus was solubilized and resuspended in extraction guanidine hydrochloride (extraction GuHCl) (6M guanidine hydrochloride, 5mM EDTA, 0.01M NaH_2PO_4, [pH 6.5]) and

homogenized using a Dounce homogenizer. The crude mucus was then rocked overnight at 4ºC, followed by centrifugation at 14,000rpm and 10ºC for 45min. The supernatant was removed, and samples were washed again with extraction GuHCl. Samples were washed and centrifuged a total of five times or until the supernatant appeared clear for two consecutive washes. Mucin was then solubilized using 20ml of reduction guanidine hydrochloride (Reduction GuHCl) (6M guanidine hydrochloride, 0.1M Tris, 0.5mM EDTA, [pH 8.0]) with the addition of 25mM dithiothreitol (DTT) as powder just before use and rocked for 5 hours at 37ºC. A 75mM iodoacetamide was added after incubation as powder, and samples were rotated in the dark overnight. Samples were then centrifuged at 4,000rpm for 45min at 4ºC. The supernatant was added to dialysis tubing and dialyzed in double-distilled water (ddH_2O) for a total of six changes. The samples were flash-frozen using liquid nitrogen and lyophilized for purified mucin powder.

2.5.3 – Bacterial Strains and Growth Conditions

Vibrio cholerae and *Escherichia coli* strains used in this study are listed in Table A.2. Unless otherwise specified, *V. cholerae* and *E. coli* strains were grown aerobically at 37ºC on LB agar plates or with shaking at 210rpm in LB broth. Where indicated, antibiotics were routinely added to the media at concentrations: 0.1mg /ml streptomycin, 0.1mg/ml ampicillin, and 0.05mg/ml kanamycin. LB media was prepared according to a previously reported recipe (197); however, solid media was made with a 1.5% (wt/vol) concentration of agar.

2.5.4 – Primers

Primers used in this study are listed in Table A.3.

2.5.5 – Plasmid Construction

Plasmid construct inserts were generated by PCR using Phusion high-fidelity polymerase (Thermo Scientific). Vector backbones were generated by plasmid purification using Qiagen Mini Prep Kit and subsequent restriction digest.

A modified pKAS32 suicide vector was constructed to generate *ΔaceE*, *ΔaceF*, and *ΔpflA* strains (198). Primer sets were used to amplify 1,000-bp homologous regions upstream and downstream of the target gene. The pKAS32 vector was restriction digested using SacI and XbaI at 37ºC for 1 h, followed by an additional 30 min at 37ºC with alkaline phosphatase from calf intestine (CIP; New England Biolabs). Vector backbone and upstream and downstream segments were joined using Gibson assembly (New England Biolabs) and subsequently electroporated into electrocompetent *E. coli* S17 λpir and recovered on agar plates with LB ampicillin (0.1 mg/ml).

A description of the contruction of complementation plasmids can be found in the supplemental methods.

2.5.6 – *Vibrio cholerae* Mutant Construction

Wild type *V. cholerae* and *E. coli* strains were mated on LB agar plates at 37ºC overnight. The mating was then plated on LB ampicillin (0.1mg/ml) and polymyxin B (25 U/ml). Colonies were then subjected to streptomycin counterselection as described

previously using LB streptomycin (2.5mg/ml) (198). Colonies were screened for the deletion using primer sets upstream and downstream of the pKAS32 homology regions.

A description of the generation of complementation strains can be found in the supplemental methods.

2.5.7 – Growth Curves

M9 0.5% purified porcine small intestinal mucin (PSIM) was made by combining in a 1:1 mixture 2X M9 minimal media and 2X (1%) PSIM prepared as a final 20-ml volume which was then autoclaved for 20 minutes at 121°C.

Strains were initially grown on LB streptomycin (0.1mg/ml) overnight at 37ºC, and a single colony isolate was used to start a fresh broth culture on LB streptomycin (0.1mg/ml) grown overnight 210rpm at 37ºC. Overnight cultures were washed twice in phosphate-buffered saline and resuspended to an optical density at 600nm (OD_{600}) of 1.0.

Aerobic growth curves

For LB growth curves, a 1:1,000 dilution of a culture at an OD_{600} of 1.0 was used to inoculate prepared medium (either 2ml or 50ml, depending on the experiment) which was grown at 210rpm and 37ºC. For M9 plus 0.5% PSIM, 2ml of media was added to a 15-ml round-bottom tube and inoculated 1:250 with a culture at an OD_{600} of 1.0 and

grown at 210rpm and 37ºC. At each timepoint, 100µl was removed for dilution series plating.

Anaerobic growth curves

Anaerobiosis was achieved using a Coy anaerobic chamber. For LB growth curves, a 1:1,000 dilution of a culture at an OD_{600} of 1.0 was used to inoculate prepared medium and grown statically at 37ºC. WT, *ΔaceE*, and *ΔaceF* growth curves were carried out in 50ml of LB medium in a 125-ml flask, whereas later WT and *ΔpflA* strain LB growth curves were performed in 2ml of LB media in a 15-ml round-bottom tube. For M9 0.5% PSIM, 2ml of medium was added to a 15-ml round-bottom tube and inoculated 1:250 with a culture at an OD_{600} of 1.0 which was grown statically at 37ºC. At each time point, the flask and tubes were swirled or vortexed and 100µl was removed for dilution series plating. For growth curves including 50mM fumarate, sodium fumarate (Sigma) reagent was used.

Complementation growth curves

Methods for complementation growth curves can be found in the supplemental methods.

2.5.8 – AKI Virulence-Inducing Conditions

Standard AKI Conditions

Wild type, *ΔaceE*, *ΔaceF*, and *ΔtoxT* strains were grown statically in 50ml pre-warmed AKI medium in 50ml conical tubes for 4 h at 37ºC, followed by a transfer to 125-ml flasks and shaking at 210rpm and 37ºC (199). One milliliter of medium was removed at

each time point and centrifuged 14,000rpm for 1 min. Supernatant was separated from the pellet and stored at -80ºC for cholera toxin quantification. The bacterial pellet was resuspended in 1ml TRIzol (Ambion Life Technologies) and stored at -80ºC for RNA isolation.

Anaerobic AKI conditions

Wild type, *ΔaceE*, *ΔaceF*, and *ΔtoxT* strains were grown in 50ml pre-warmed oxygen-depleted AKI medium in 50-ml conical tubes statically under anaerobic conditions using a Coy anaerobic Chamber (78). One milliliter of medium was removed at each timepoint and centrifuged 14,000rpm for 1 min. The supernatant was separated from the pellet and stored at -80ºC for cholera toxin quantification.

2.5.9 – Cholera Toxin Quantification by ELISA

Cholera toxin in *V. cholerae* supernatants from standard and anaerobic AKI conditions was quantified by GM1 enzyme-linked immunosorbent assay (ELISA) as previously described (200, 201). GM1-coated microtiter plates were incubated with a 1:20 dilution of culture supernatant and detected using primary anti-cholera toxin and secondary horseradish peroxidase (HRP)-conjugated goat anti-rabbit IgG (Invitrogen). 1-Step Ultra TMB-ELISA (Thermo Scientific) reagent was added and stabilized using 2M sulfuric acid. Colorimetric measurements were read at 450nm, and the toxin concentration was determined by comparison to a standard curve using purified cholera toxin.

2.5.10 – RNA Isolation and Real Time Quantitative PCR (RT-qPCR)

RNA was harvested from AKI toxin-inducing culture pellets preserved in 1ml TRIzol using an RNEasy kit (Qiagen) using on-column DNase digestion (Qiagen) followed by

Turbo DNase digestion (Invitrogen). RNA concentration and quality were measured with a UV/VIS Spectrophotometer and visualized on a 2% agarose gel.

cDNA was generated from RNA using Superscript III reverse transcriptase (Thermo Scientific). RT-qPCRa were carried out using SYBR green master mix (Applied Biosystems) with 5ng cDNA. Primers used to detect *recA*, *toxT*, *ctxA*, and *tcpA* transcripts are listed in Table A.3. Threshold cycle ($\Delta\Delta C_T$) values were calculated using *recA* as the gene of reference (202).

2.5.11 – Infant Mouse Colonization Assays

All animal experiments in this study were approved by the Institutional Animal Care and Use Committee at Michigan State University.

Infant mice were infected as described previously (203). Three- to five- day old CD-1 mice (Charles River, Wilmington, MA) were orogastrically inoculated with approximately 10^6 bacterial cells 2 h after separation from the dam and maintained at 30ºC. Mice were euthanized approximately 20 hours after inoculation. Mouse intestinal segments were weighed and homogenized in 3ml of PBS. Intestinal homogenates were serially diluted and plated on LB streptomycin (0.1mg/ml) for monoassociated infections and LB streptomycin (0.1mg/ml) and 5-bromo-4-chloro-3-indolyl-β-D-galactopyranoside (X-Gal)(0.08mg/ml) for competition infections. Competition infections consisted of a 1:1 mixture of target strains with a *ΔlacZ* strain for differentiation by blue-white screening.

For PDH monoassociated and competition infections, the entire intestinal tract was homogenized for bacterial enumeration. In intestinal segment measurements, approximately 1cm of intestine from each section (proximal, medial, and distal) was homogenized for bacterial enumeration between segments. For PFL monoassociated and competition infections, the intestinal tract was divided into small intestine and large intestine plus cecum. The divided intestinal portions were then homogenized for bacterial enumeration.

2.5.12 – Statistical Methods

For determining the relationship between cholera toxin output versus optical density among WT, *ΔaceE*, and *ΔaceF* strains, a simple linear regression and subsequent slope and intercept analysis were performed using GraphPad Prism software, which follows a method equivalent to analysis of covariance (ANCOVA).

For *in vivo* experiments, CFU-per-gram intestine and competitive index scores were $\log_{10}$ transformed and tested for normality using a Shapiro-Wilks test. Normally distributed data were then analyzed using either parametric Student's *t* test or an analysis of variance (ANOVA) with *post hoc* Tukey's test to test for significance.

For *in vivo* intestinal segment data where bacterial loads were below the limit of detection, a nonparametric Kruskal-Wallis one-way analysis of variance was used with *post hoc* Dunn's test to test for significance.

2.6 – Results

2.6.1 – Transposon Mutagenesis Screen Identified the Pyruvate Dehydrogenase Complex as Important for Growth on Mucin.

We hypothesized that intestinal mucin would serve as a growth substrate for *V. cholerae* during colonization. In a pilot experiment, *V. cholerae* was observed to exhibit enhanced growth in minimal media supplemented with mucin (Figure A.1). We then performed a transposon mutant library screen of *V. cholerae* El Tor strain C6706 on minimal media supplemented with 0.5% mucin (Type III; Sigma). Genes encoding two of the three components of the pyruvate dehydrogenase (PDH) complex were identified in our screen, *aceE* (VC2414) and *aceF* (VC2413) (Table A.1). The third component of the PDH complex, *lpdA* (VC2414), was also defective for growth in our screen; however, growth of this transposon mutant was also severely attenuated for growth on LB, as this enzyme also functions in the alpha-ketoglutarate dehydrogenase (AKGDH) and glycine cleavage multienzyme (GCV) systems (204). Because of its pleiotropic growth defect, we did not further investigate an *lpdA* mutant.

2.6.2 – The Pyruvate Dehydrogenase Complex Supports Aerobic Growth on Mucin.

As a glycoprotein, mucin is coated in glycans, contributing to the protective function of the mucous barrier (205). To study mucin from a physiologically relevant site of infection, and to avoid potential contaminants in commercially purified mucin that may impact *V. cholerae* growth (206), we purified mucin from the small intestine of healthy adult pigs using a guanidine hydrochloride (GuHCl) extraction procedure. The purified mucin was then analyzed by high-performance anion-exchange chromatography coupled with pulsed amperometric detection (HPAEC-PAD; GlycoAnalytics) (207, 208).

Mucin obtained by this method showed high relative presence of mucin carbohydrates galactosamine, glucosamine, galactose, fucose, and sialic acids Neu5Ac and Neu5Gc compared to non-mucin monosaccharides glucose and mannose (Table A.4).

When grown in M9 minimal salts medium supplemented with 0.5% purified small intestinal mucin (PSIM), isogenic *ΔaceE* and *ΔaceF* PDH mutants were defective for growth in aerobically grown cultures compared to the wild type (Figure 2.1A). This phenotype was complemented for both the *ΔaceE* and *ΔaceF* mutants using the isopropyl β-D-1-thiogalactopyranoside (IPTG) inducible pMMB66EH vector in M9 0.5% glucose media (Figure A.2). To verify the PDH complex does not contribute to anaerobic proliferation on mucin, we measured growth under anaerobic conditions. Under these conditions, PDH mutants grew comparably to the wild type (Figure 2.1B). To determine if addition of an alternative electron acceptor would elicit a growth difference between the wild type and PDH mutants, 50mM fumarate, which enhances *V. cholerae* growth via anaerobic respiration (209), was added to the growth medium. No growth disparity was observed between the wild type and PDH mutants with the addition of 50mM fumarate (Figure 2.1C). The observed phenotypes indicate that the PDH complex is not required for anaerobic growth. Energy generation under anaerobic conditions is likely due to an active pyruvate formate-lyase converting pyruvate to formate and acetyl-CoA for mixed acid fermentation (210) and acetolactate synthase, which converts pyruvate to (*S*)-2-acetolactate in the first step of 2,3-butanediol fermentation (191). The growth disparity observed in the minimal mucin medium under aerobic conditions was less pronounced in LB medium, which contains less than 100μM

collective sugars and primarily supports growth through amino acid catabolism (Figure A.3) (211). As a growth defect was observed in LB medium, we wanted to test whether this growth delay was attributable solely to perturbed carbohydrate metabolism, or if growth on amino acids was also negatively impacted by a disrupted PDH complex. In M9 supplemented with 0.2% Casamino Acids under aerobic growth conditions, the *ΔaceE* and *ΔaceF* mutants did not grow at all (Figure A.4). These findings suggest that aerobic amino acid catabolism may also have contributed to the phenotype illustrated in Figure 2.1A, as mucin molecules contain, among other amino acids, proline, threonine, and serine in repeat glycan attachment moieties and have previously been shown to support *V. cholerae* growth *in vitro* (48). It is therefore unclear what component of LB is supporting growth of the *ΔaceE* and *ΔaceF* mutants.

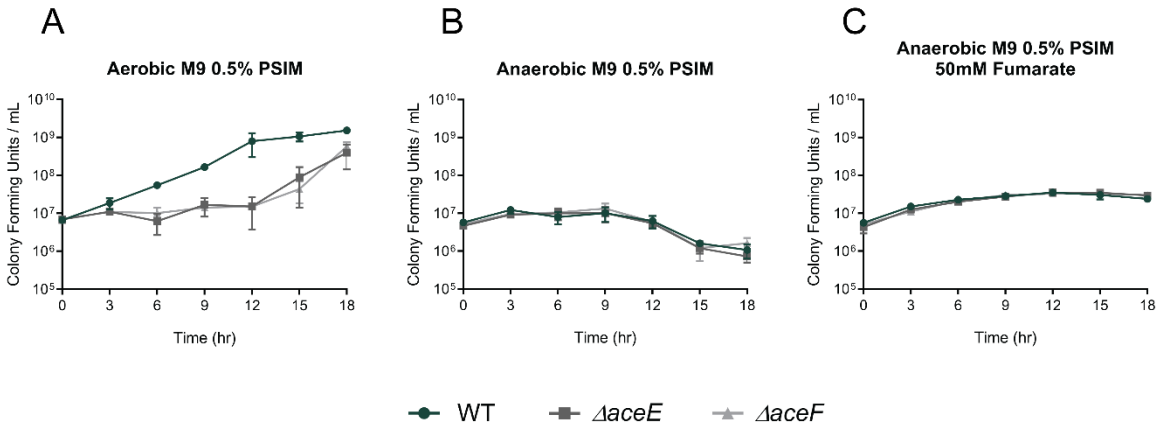

Figure 2.1. Growth curves of WT *ΔaceE*, and *ΔaceF* in M9 minimal media supplemented with 0.5% purified porcine small intestinal mucin. Growth curves of WT, *ΔaceE*, and *ΔaceF* in M9 minimal medium supplemented with 0.5% purified porcine small intestinal mucin (PSIM) grown aerobically (A), anaerobically (B), or anaerobically supplemented with 50mM fumarate (C). Data represent the averages and SEMs for three independent biological replicates.

2.6.3 – Pyruvate Formate-Lyase Supports Anaerobic Growth on Mucin.

As pyruvate formate-lyase (PFL) also converts pyruvate to acetyl-CoA, we sought to investigate the role of PFL in the catabolism of mucin. To accomplish this, an isogenic mutant strain with a deletion of *pflA* (VC1869) was tested for *in vitro* growth on PSIM. In M9 minimal salts media supplemented with 0.5% PSIM, the *ΔpflA* mutant grew comparably to the wild type under aerobic growth conditions (Figure 2.2A) and poorly compared to the wild type (which did not thrive itself) when cultured anaerobically, in both the absence and presence of 50mM fumarate (Figure 2.2B and C). This growth defect was complemented for *pflA* using an IPTG-inducible pMMB66EH vector in M9 0.5% glucose 50mM fumarate medium (Figure A.5). The disparity in growth between wild type and *ΔpflA* strains under anaerobic growth conditions indicates that PFL can indeed generate energy from mucin during anaerobic growth. As PFL is expected to function primarily in the metabolism of carbohydrates, it was not surprising to see growth comparable to that of the wild type in LB medium, both aerobic and anaerobic, but it was intriguing to find *ΔpflA* mutant remained viable longer than wild type in LB medium without the addition of 50mM fumarate (Figure A.6).

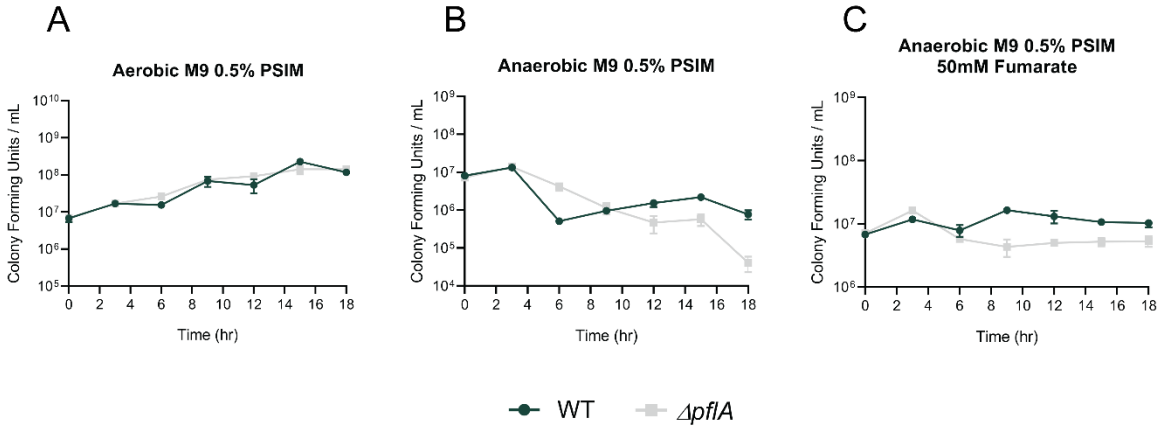

Figure 2.2. Growth curves of WT and *ΔpflA* in M9 minimal media supplemented with 0.5% purified porcine small intestinal mucin. Growth curves of WT and *ΔpflA* in M9 minimal media supplemented with 0.5% purified porcine small intestinal mucin grown aerobically (A), anaerobically (B), or anaerobically supplemented with 50mM fumarate (C). Data represent the averages and SEMs for three independent biological replicates.

2.6.4 – Cholera Toxin Production in PDH Mutants is Equivalent to Wild Type in Both Standard and Anaerobic Toxin-Inducing Conditions.

Cholera toxin is the primary virulence determinant of *V. cholerae*. To determine whether the PDH complex influences production of cholera toxin, wild type and PDH mutant strains were grown under conditions referred to as “AKI” to induce virulence factor production (199). Previous findings with strains of the classical biotype demonstrate that disruption of the TCA cycle increases *toxT* expression and suggests a link between acetyl-CoA and virulence expression (186). As the PDH complex is the primary enzyme responsible for the production of acetyl-CoA under aerobic growth conditions, we anticipated mutants lacking it would produce cholera toxin levels below that of wild type. However, we observed no significant difference in cholera toxin produced in the WT and PDH mutant strains under either standard or anaerobic AKI conditions. For standard AKI conditions, cholera toxin levels were measured as a function of optical density, with the *ΔtoxT* (VC0838) included as a negative control, as ToxT stimulates cholera toxin production (Figure 2.3A) (212). Overall, the wild type produced more total cholera toxin as it reached a higher final optical density than PDH mutants, yet when determining individual cellular capacity for cholera toxin production, it was found that at similar optical densities, cholera toxin output in the PDH mutants was comparable to that in the wild type. Cholera toxin production levels at 4h, 5h, 6h, 7h, 8h, and 24h are provided in

Figure A.7. Cholera toxin levels were also measured after 8h and 20h of growth under anaerobic AKI conditions and were again similar between the wild type and PDH mutant strains (Figure 2.3B and Figure A.7). These findings indicate that the PDH complex does not affect cholera toxin production in El Tor C6706 *V. cholerae*.

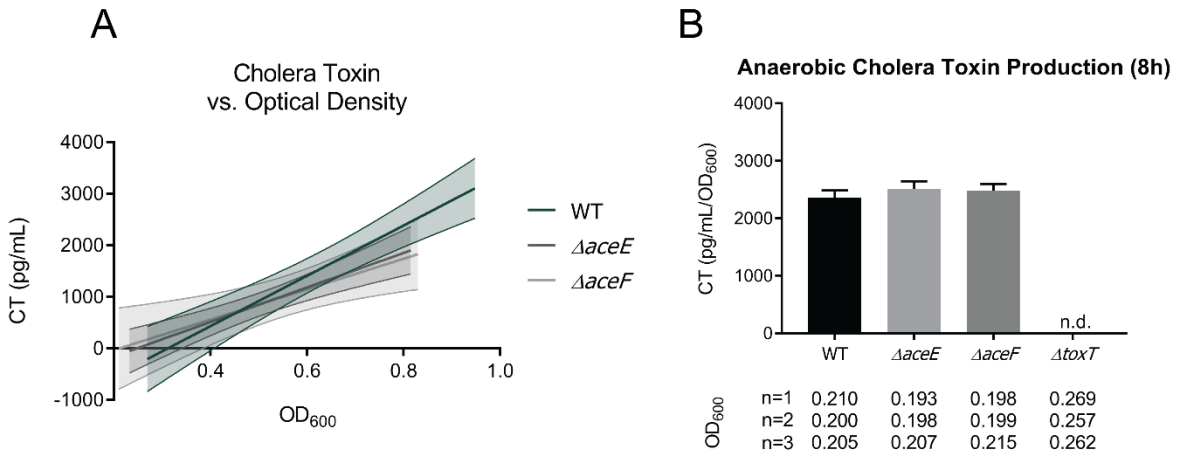

Figure 2.3. Cholera toxin (CT) production for WT, *ΔaceE*, *ΔaceF*, and *ΔtoxT* strains. (A) CT output as a function of optical density (OD_{600}) under standard AKI toxin-inducing conditions. Data points were collected from three biological replicates, and a line of best fit with 95% confidence intervals was plotted. WT ODs higher than 0.9 were excluded to better superimpose with *ΔaceE* and *ΔaceF* OD values. A simple linear regression found no significant differences between WT, *ΔaceE*, and *ΔaceF* strain CT production. *ΔtoxT* control was not plotted because no toxin was detected. Statistical analysis was performed using GraphPad Prism (B) CT values relative to optical density (pg/ml/OD_{600}) under anaerobic AKI toxin-inducing conditions at the 8h time point are reported. The optical densities for the biological replicates are displayed below the corresponding strain on the *x* axis in each graph. Data represent the averages and SEMs for three biological replicates.

2.6.5 – Functional PDH Activity is not Required for Expression of *toxT*, *ctxA*, and *tcpA*.

The relative expression of the master virulence regulator *toxT* and primary virulence factors *ctxA* and *tcpA* was determined by real-time quantitative PCR (RT-qPCR). The 4h and 5h time points of *in vitro* standard AKI conditions were selected to compare relative expression profiles, as *toxT* expression has been observed to be high at these

time points (213). PDH mutant strains at 4h exhibited somewhat elevated levels of *toxT* and *tcpA* and similar *ctxA* expression compared to those of the wild type, with no transcripts detected in the *ΔtoxT* control, as expected (Figure 2.4A). At 5h, PDH mutant strains exhibited wild type *toxT* and *ctxA* expression and a 2-fold reduction in *tcpA* expression (Figure 2.4B). Although there is variability in the expression of these virulence genes at the given time points, we conclude that the PDH complex is not required for virulence gene expression.

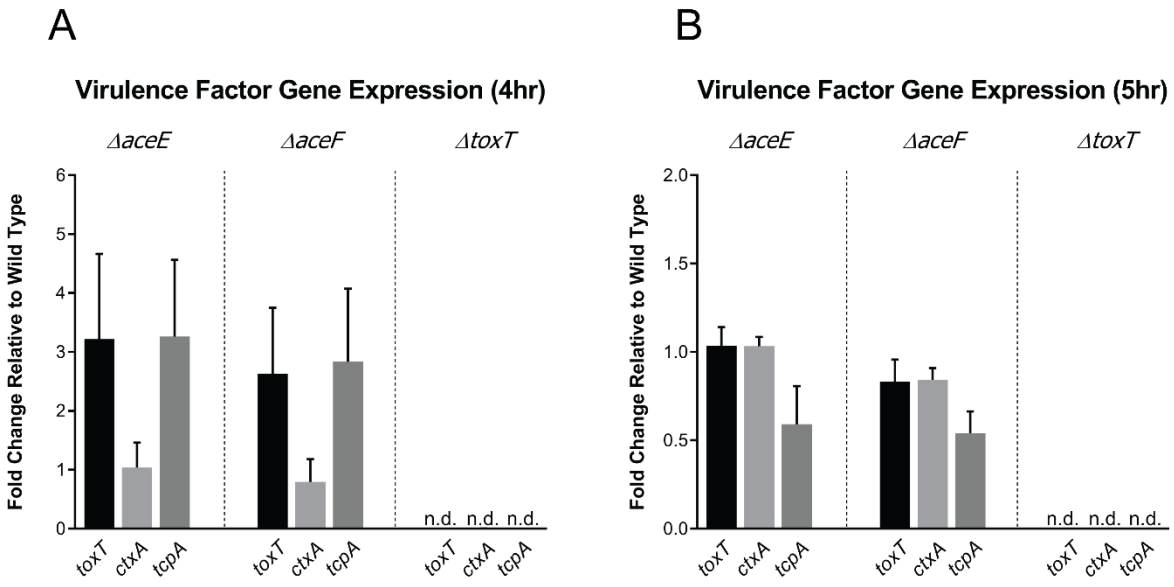

Figure 2.4. Relative fold change of *toxT, ctxA,* and *tcpA* transcript levels compared to wild type expression. RNA was isolated from WT, *ΔaceE, ΔaceF*, and *ΔtoxT* cultures grown under standard AKI toxin-inducing conditions at 4h and 5h. Expression data were calculated by $\Delta\Delta C_T$ using *recA* as an internal control. Data represent the averages and SEMs for three independent biological replicates.

2.6.6 – A Functional Pyruvate Dehydrogenase Complex is Necessary for Colonization of the Infant Mouse.

Based on our findings that *V. cholerae* PDH mutants are defective for aerobic carbohydrate metabolism, we sought to examine whether this pathway was required to support growth *in vivo*. The infant mouse model is used extensively to investigate intestinal colonization by *V. cholerae* (214). Infant mice produce a mucous layer in the intestine that can serve as a substrate for *V. cholerae* growth (179), although they also have reduced resident microbiota and a less developed immune system compared to adult mice (215). The reduction in resident flora increases the necessity for *V. cholerae* to liberate mucin glycans for substrate utilization, as the commensal population does not provide this resource as in other systems (216).

In this study, we orogastrically infected CD-1 mouse neonates with ~10^6 CFU bacterial cells to compare colonizations by wild type and PDH mutant *V. cholerae*. In monoassociated infections, PDH mutants were attenuated for colonization by approximately 100-fold compared to the wild type (Figure 2.5A). We also assessed direct *in vivo* competition with wild type by coinfecting each mutant with a PDH^+ *ΔlacZ* (VC2338) strain of *V. cholerae*. PDH mutant strains exhibited attenuation in competition with the wild type similar to that observed in monoassociated infections, with mutant recovery approximately 100-fold lower than that of the wild type after coinfection (Figure 2.5B). These data indicate a requirement for a functionally active PDH complex to support colonization of the infant mouse, suggesting that oxidative metabolism of carbohydrate substrates is critical for colonization and population expansion.

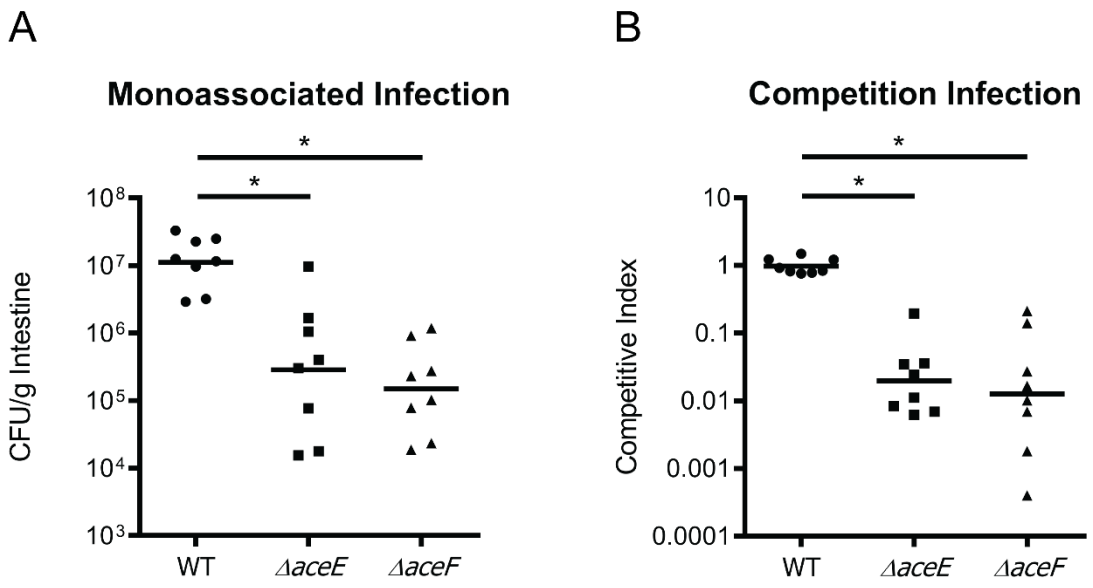

Figure 2.5. Infant mouse colonization assays of WT, *ΔaceE*, and *ΔaceF* after 20h. (A) Monoassociated infections of 3- to 5-day-old infant mice. (B) Competition infections of 3- to 5-day-old infant mice. Competitive index scores were calculated as ratios of output versus input [(target$_{Output}$/*ΔlacZ*$_{Output}$) / (target$_{Input}$/*ΔlacZ*$_{Input}$)]. WT, *ΔaceE*, and *ΔaceF* strains were co-inoculated with an *aceE*$^+$/aceF$^+$ *ΔlacZ* strain (PDH$^+$) to determine the relative fitness of each test strain. Data for each experiment was obtained from eight independent mouse colonization infections in which the entire intestinal tract (small intestine, large intestine, and cecum) was extracted and homogenized for bacterial enumeration. Bars represents geometric mean. Statistical analysis was performed using GraphPad Prism where significance was tested on log-transformed data by ANOVA with *post hoc* Tukey's Test. *, $P<0.05$.

As oxygen levels (5, 8) and mucin composition (217) fluctuate along the length of the small intestine, we investigated the relative importance of PDH function across the longitudinal axis in the infant mouse intestine. One-centimeter-long pieces of intestine were harvested from the proximal, medial, and distal regions of the small intestine and assayed for recoverable CFU. Throughout the small intestine, *V. cholerae* PDH mutants were recovered at levels well below that of the wild type and in some cases were not detected, as counts were below our limit of detection (Figure 2.6A-C). Here we again conclude that the PDH complex promotes *V. cholerae* colonization and that oxidative

metabolism of carbohydrates is a key feature of *V. cholerae* growth and proliferation along the entire length of the small intestine. Additionally, bacterial loads of the PDH mutants across the individual intestinal segments do not appear to reflect the CFU-per-gram counts obtained from analyzing the entire gastrointestinal tract in the previous monoassociated infection (Figure 2.5A). This suggests that the majority of PDH mutants detected in the previous monoinfection experiment resided within either the cecum or large intestine, sites anticipated to support more anaerobic metabolism (5). This finding further supports the necessity for an active PDH, particularly at the primary site of infection in the small intestine.

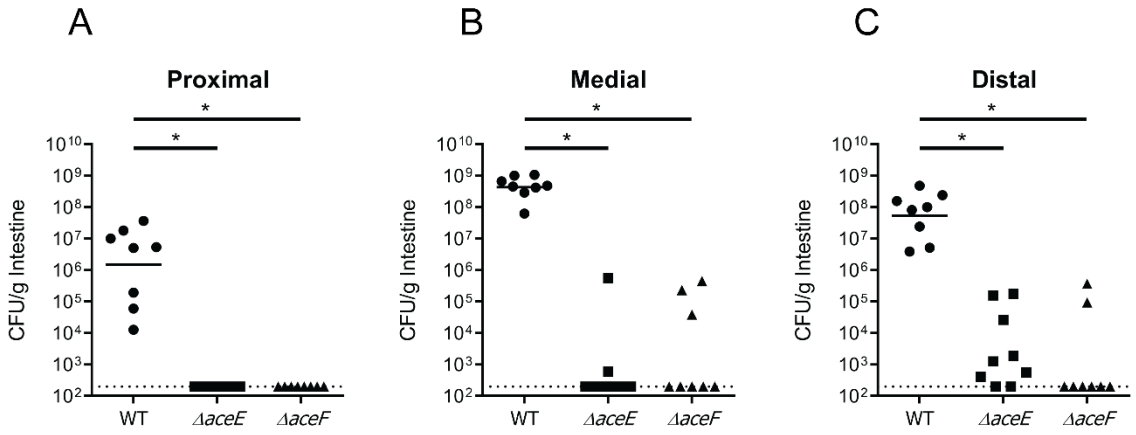

Figure 2.6. Infant mouse colonization of WT, *ΔaceE*, and *ΔaceF* mono-associated infections in proximal, medial, and distal portions of the small intestine after 20h. Infant mouse colonization of WT, *ΔaceE*, and *ΔaceF* monoassociated infections in proximal (A), medial (B), and distal (C) portions of the small intestine after 20h. Data for each segment was obtained from 8 independent mouse colonization infections. The bars represent the geometric means and can only be plotted for the WT strain. Statistical analysis was performed using GraphPad Prism where significance was tested on nontransformed data by Kruskal-Wallis analysis with *post hoc* Dunn's test. *, $P<0.05$.

2.6.7 – Pyruvate Formate-Lyase Provides Minor Growth Support during Infection.

As aerobic metabolism was determined to be beneficial to population expansion of *V. cholerae*, we wanted to explore the contributing effects of anaerobic metabolism to colonization. Oxygen gradation within the small intestine maintains the highest oxygen availability in the intestinal crypts and nears hypoxia at the villus tip (3, 218). To determine if anaerobic proliferation also contributes to population expansion of *V. cholerae* during infection, potentially in the more anoxic lumen of the small intestine, CD-1 mice were infected with ~10^6 CFU of the *ΔpflA* mutant. To accurately assess the importance of PFL during infection, recovery of *V. cholerae* was performed for the small intestine separately from the large intestine. As the large bowel is inherently more anoxic, where PFL would be expected to function more readily, we focused more on assessing the role of PFL in the small intestine as a more clinically relevant site for human *V. cholerae* infection.

In monoassociated infections, the PFL mutant was attenuated for colonization by approximately 2-fold compared to the wild type (Figure 2.7A). These data suggest that PFL, and therefore anaerobic metabolism, provides a less critical level of energy production than PDH to support growth during infection. Our results are consistent with previous studies that investigated anaerobic nitrate respiration demonstrating a similar (2-fold) reduction in colonization of the infant mouse (110). However, in a competition experiment, the *ΔpflA* mutant colonized to levels equivalent to those of the wild type (Figure 2.7B), essentially demonstrating no colonization defect at all. The same

colonization pattern of the PFL mutant strain was observed in the large intestine (Figure A.8).

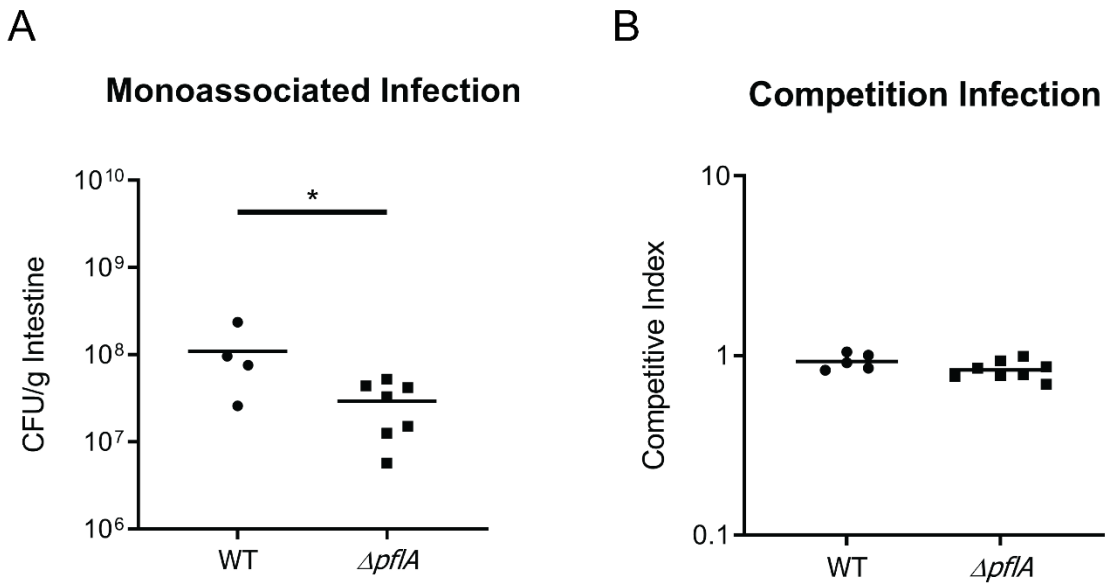

Figure 2.7. Infant mouse colonization assays of WT and *ΔpflA* strains in the small intestine after 20h. (A) Monoassociated infections of 3- to 5-day-old infant mice. (B) Competition infections of 3- to 5-day-old infant mice. Competitive index scores were calculated as a ratios of output versus input [($target_{Output}$/*ΔlacZ*$_{Output}$) / ($target_{Input}$/*ΔlacZ*$_{Input}$)]. WT and *ΔpflA* strains were co-inoculated with a *pflA*+ *ΔlacZ* strain to determine the relative fitness of each test strain. Data for each experiment was obtained from 4 or 5 independent mouse colonization infections for WT and 7 or 8 mouse infections for the *ΔpflA* strain. The bar represents geometric mean. Statistical analysis was performed using Graphpad Prism where significance was tested on log-transformed data by Student's *t* test. *, $P<0.05$.

One hypothesis to explain this lack of fitness defect when coinfected with the wild type is that during coinfection, the *pflA*+ *ΔlacZ* strain may produce acetate, which can be metabolized by the *ΔpflA* mutant to mitigate the 2-fold defect seen in monoassociated infections (219). Acetate would provide acetyl-CoA by way of acetyl-CoA synthase-1 (ACS-1), circumventing the PDH/PFL carbohydrate utilization pathways (220). To test this hypothesis, we first demonstrated that all strains are capable of growth on acetate (Figure A.9). Then, to test whether metabolic rescue of the *ΔpflA* strain by *pflA*+ *ΔlacZ*

occurs, monocultures and competition cultures were grown anaerobically in M9 minimal media with 0.5% glucose. At both the 12h and 20h time points, the PFL mutant was found to be between 2- and 10-fold reduced compared to *pflA+ ΔlacZ* strain for both monoculture and competition comparisons. These findings indicate that the similar output ratios detected in competition *in vivo* assays are unlikely related to acetate supplementation by the *pflA+ ΔlacZ* strain (Figure A.10).

2.7 – Discussion

Oxygen-dependent metabolism is key to pathogenicity for many gastrointestinal microbes. Pathogens that actively manipulate the host environment to oxygenate the gut rapidly proliferate during infection. Although a direct link has yet to be determined, the cholera toxin of *V. cholerae* may increase oxygen availability in the gut through its influence on optimal TCA cycle activity during infection (43). In other gastrointestinal pathogens, oxidative metabolism is supported by inducing inflammation at the site of infection. Inflammation in response to *Citrobacter rodentium* or *Salmonella enterica* serovar Typhimurium infections promotes colonization, proliferation of the microbe, and disease as a result of increased aerobic metabolism (7, 42). While *V. cholerae* infection does not lead to significant changes in gross pathology of intestinal architecture and cholera is not typically characterized as a proinflammatory infection, inflammatory markers are increased in animal models and human infection (221, 222). Whether oxygen levels in the gut are elevated due to this innate immune response has yet to be determined. There is evidence to support inflammation promoting *V. cholerae* colonization in some circumstances. In *V. cholerae* strain V52, the Type VI secretion system (T6SS) increases intestinal inflammation in the infant mouse and promotes

increased colonization levels (223). Also, the newly emerged El Tor Haitian variant strain has higher virulence in animal models, reaching a higher bacterial cell burden than previously characterized strains and causing elevated inflammation and epithelial cell damage (224). Evolved *V. cholerae* strains equipped to withstand an inflamed environment could benefit from increased oxygen availability to generate more energy to support growth and proliferation.

Oxygen contribution to *V. cholerae* pathogenicity has been examined principally in regard to the ToxR/TcpP/ToxT virulence cascade. For example, the regulators AphB and OhrR respond to reduced environmental oxygen by activating *tcpP* expression (79). Further, decreased oxygen levels under stationary culture conditions stimulates ToxR-TcpP interaction (225) and activation of *toxT* transcription (213). Translating these *in vitro* results to the context of oxygen distribution *in vivo* would imply that the anoxic lumen primes *V. cholerae* for virulence gene expression prior to accessing the more oxygenated host epithelium. The radial oxygen gradient within the intestine would therefore influence optimal timing of *V. cholerae* virulence expression. In this work, we sought to explore how oxygen-dependent and independent metabolic pathways influence population expansion during infection, but not necessarily as they relate to virulence gene expression.

Oxygen availability in the crypt spaces of the intestine, along with the presence of carbohydrate-rich mucin molecules, could vastly improve growth and proliferation of *V. cholerae* at this site. The mucous lining of the gastrointestinal tract protects the host

epithelium from both resident and transient microorganisms to maintain gut homeostasis (226). *V. cholerae* has the capacity to bypass this host defense through motility (227) as well as to exploit it for growth substrates. However, this does not suggest that the mucous layer is inconsequential to curtailing the effects of *V. cholerae* pathogenicity. In mice with a chemically degraded mucus layer, *V. cholerae* bacterial counts exceeded that of untreated mice (179), indicating that mucus contributes to abatement of disease. Similarly, *Muc2*$^{-/-}$ mice that lack the primary secretory mucin of the intestinal tract, MUC2, exhibit inflammation in the large intestine due to commensal population interactions with the epithelium as well as exacerbated infection in *Citrobacter rodentium* and *Salmonella* Typhimurium challenge models (228–230). Thus, the mucus serves a protective function against *V. cholerae* yet is exploited to benefit the microbe.

The sequential progression of *V. cholerae* pathogenicity is tightly linked to bacterial-mucin interactions. Adherence to host mucin by GbpA, an *N*-acetylglucosamine binding protein, is a key step in colonizing the small intestine (231). Upon reaching the host epithelium *V. cholerae* establishes an adherent microcolony (232). Within this microenvironment, mucin breakdown products and the presence of oxygen help drive the population expansion of *V. cholerae* (this work). Stimulation of the host epithelium by cholera toxin induces production and secretion of goblet cell mucin (233) in addition to other host-derived nutrients such as iron and long-chain fatty acids (43), and potentially oxygen. As the population of cells rapidly expands, mucin breakdown products stimulate motility of *V. cholerae* (234), a trait required for optimal colonization

of the proximal and medial portions of the small intestine (46, 179, 235). This interaction likely contributes to population dynamics observed for *V. cholerae* whereby it migrates counter to intestinal flow in the later stages of infection to populate the proximal and medial portions of the intestine (236). This motility response acts in coordination with the secreted mucolytic hemagglutinin/protease (HapA) of *V. cholerae*, used during cellular detachment (237, 238). HapA is stimulated both by high cell density through the activity of the regulator HapR, and directly when in the presence of mucin (239). As *V. cholerae* exits the host, a fraction of the population is embedded in mucin (240), which may influence hyperinfectivity of human-passaged *V. cholerae* (241). From initial inoculation into the human gut to the eventual passaging of the bacteria, interactions between *V. cholerae* and mucus substantially influence *V. cholerae* pathogenicity.

Our work postulates that mucin metabolism enhances proliferation of *V. cholerae* during the course of infection. *V. cholerae* is a facultative anaerobe, and we sought to uncover whether aerobic or anaerobic metabolism enables it to grow to high levels during infection. We assessed the *in vivo* fitness of strains lacking either the *aceE*- or *aceF*-encoded components of the pyruvate dehydrogenase (PDH) complex or *pflA*-encoded pyruvate formate-lyase (PFL). These enzymes catalyze production of acetyl-CoA from pyruvate either aerobically (PDH) or anaerobically (PFL). In *Escherichia coli*, PFL is induced only during anaerobiosis, whereas the PDH complex can function in both anaerobic and anaerobic environments (242, 243). However, unlike what is observed in *E. coli*, in our work, *V. cholerae* lacking PFL was not rescued for anaerobic growth to any noticeable extent by having a functional PDH. This enabled us to differentiate the

contribution of aerobic and anaerobic metabolism by investigating PDH and PFL mutants. The significant loss of fitness by the *ΔaceE* and *ΔaceF* strains compared to the wild type strain suggests that *V. cholerae* population expansion in the small intestine is driven largely by aerobic, oxidative metabolism. This is consistent with *V. cholerae* preferentially localizing to the epithelial crypts (179), with greater oxygenation that enables oxidative metabolic pathways to generate energy (3). The radial distribution of oxygen in the intestine therefore biogeographically relegates replicative *V. cholerae* cells primarily to the epithelium, as opposed to the more anoxic lumen. Our results do not completely rule out some anaerobic growth and expansion of *V. cholerae* during infection, as the *ΔpflA* mutant colonized to levels about half those of the wild type, similar to what is observed with other anaerobic metabolism-deficient strains (110, 191, 209). Additionally, there is recent evidence to suggest that multiple anaerobic metabolic pathways function in tandem to support growth in anoxic conditions. A double mutant in ethanol fermentation and nitrate respiration showed a significant reduction in colonization, compared to single mutants that were near-wild type levels of colonization (111).

While expansion of *V. cholerae in vivo* evidently proceeds primarily through aerobic production of acetyl-CoA using PDH as opposed to anaerobic acetyl-CoA production using PFL, how it uses its reducing equivalents to generate energy from the electron transport chain is less certain from our work. Oxygen as a terminal electron acceptor is certainly possible given the availability of oxygen within the crypt epithelium and the presence of four terminal oxidase complexes in the *V. cholerae* genome (147), which

will be the subject of future investigation. Previous *in vivo* transposon mutagenesis studies indicate that terminal oxidase function supports colonization, in particular a high affinity *cbb*$_3$ oxidase (244, 245). *V. cholerae* also maintains nitrate, fumarate, TMAO, and DMSO reductases that can function as terminal electron acceptors in anaerobic respiration (147). Fumarate and TMAO support *V. cholerae* growth in anaerobic conditions (209), as does nitrate when in an alkaline environment (110), albeit not to the extent observed for oxidative growth. This is primarily due to the relatively low redox potentials of fumarate and TMAO relative to O_2 and *V. cholerae* requiring alkaline pH environments for nitrate respiration, as it lacks a nitrite reductase needed to eliminate this toxic compound (110). DMSO, on the other hand, was not shown to support *V. cholerae* growth at all (209). However, growth *in vivo* with addition of the alternative electron acceptor TMAO induces high levels of cholera toxin (209). Infant mice infected with an inoculum of El Tor strain N16961 mixed with TMAO exhibited more severe signs of infection, suggesting a TMAO-dependent toxin production effect. Although anaerobic terminal reductases may not be the principal mode of *V. cholerae* growth and expansion *in vivo*, they are still likely to contribute to *V. cholerae* pathogenesis. Resolution of the role of different terminal reductases regarding growth and pathogenicity *in vivo* also awaits future examination by investigating *V. cholerae* terminal reductase mutants.

2.8 – Acknowledgements

We thank Dr. Jeremiah Johnson for insights and encouragement in initiating this study. AJV was supported in part by SUTL and FAST Fellowships from Michigan State University, and by the Bertina Wentworth Fellowship in the Department of Microbiology

& Molecular Genetics at Michigan State University. This work was supported in part by the Rudolph Hugh Endowment (VJD) at Michigan State University.

Chapter 3 – Oxidative respiration through the *bd*-I and *cbb*$_3$ oxidases is required for *Vibrio cholerae* pathogenicity and proliferation *in vivo*.

3.1 – Preface

Contents of this chapter are unpublished and soon to be submitted for publication. This chapter includes one experiment conducted by a fellow graduate student in the lab of Dr. Victor DiRita, Lucas Demey. This contribution helped generate Figure B.8.

3.2 – Abstract

Respiration is an energy generating process that supports growth and proliferation of many enteric pathogens. *Vibrio cholerae*, the bacterial pathogen that causes the disease cholera, is capable of both aerobic and anaerobic respiration. However, despite knowledge that oxygen diffuses from host tissue into the intestinal lumen, the role of aerobic respiration in supporting *V. cholerae* growth during infection has yet to be defined. Here, we show that *V. cholerae* colonization of the infant mouse requires aerobic respiration, but not anaerobic respiration, to support growth and proliferation. Using Multiplex Genome Editing by Natural Transformation (MuGENT) we created a septuple knockout strain lacking the capacity to produce any of the four terminal oxidase complexes (*cbb*$_3$*, bd*-I*, bd*-II*,* and *bd*-III) where the resulting strain effectively functions as a strict anaerobic variant of *V. cholerae.* In infant mouse infections, this resulted in a near 10^6-fold reduction in colonization. Characterization of individual oxidases identified the *cbb*$_3$ and *bd*-I oxidases, but not the *bd*-II or *bd*-III oxidases, as essential for colonizing the small intestine of the infant mouse. Unexpectedly, the *bd*-I oxidase was determined to be the primary oxidase in *V. cholerae*, only the second example of a *bd*-type oxidase serving as the primary oxidase supporting energy acquisition both inside and outside of a host for a bacterial pathogen. In addition to determining the oxidase requirements of *V. cholerae,* the results of this study further

implicate oxygen as a critical electron acceptor that shapes the progression of enteric infections.

3.3 – Introduction

Respiration promotes growth and proliferation of bacterial cells (138). Energy acquisition through respiration relies on the metabolism of exogenously acquired substrates and the presence of terminal electron acceptor molecules to generate chemical energy, which is stored in the form of ATP to power cellular processes required for growth. Although not considered canonical virulence factors, metabolism and energy generative processes are required by pathogens to thrive during infection. Here we investigate respiration as a potent driver of replication during infection by the bacterial gastrointestinal pathogen *Vibrio cholerae* (246).

Vibrio cholerae is a facultative anaerobe that grows in both aerobic and anaerobic environments (247). Respiration in *V. cholerae* is achieved aerobically through the terminal reduction of molecular oxygen or anaerobically through the terminal reduction of various alternative electron acceptors (110, 209). Recent evidence suggests there is combined contribution of both aerobic and anaerobic metabolism to *V. cholerae* growth *in vivo* (103, 111). This may be attributed to the radial and longitudinal gradients of oxygen availability in the intestinal tract enabling metabolism through both pathways in response to *in vivo* localization (8).

We sought to investigate the relative contributions of aerobic and anaerobic respiration *in vivo* using an infant mouse model of colonization. *V. cholerae* encodes four terminal

oxidases and four terminal reductases that support respiration (147, 248). The terminal oxidases include one *cbb*$_3$ heme-copper oxidase (249, 250) and three *bd*-type oxidase complexes capable of catalyzing the 4 H^+/O_2 reduction of oxygen to water (137). *cbb*$_3$ oxidases (251, 252) and *bd* oxidases (253–255) have a low K_m for oxygen and are typically induced under microaerobiosis, a feature particularly beneficial for pathogens colonizing near hypoxic environments of the human host (54, 135, 256). *V. cholerae* also carries out anaerobic respiration through four terminal reductases that use nitrate, fumarate, trimethylamine-N-oxide (TMAO) or biotin sulfoxide (BSO) (112, 209, 248, 257). Previous work found that abrogation of nitrate reductase activity reduced colonization in a streptomycin-treated adult mouse by approximately 2-fold (110) and concomitant disruption in fermentative pathways further reduced colonization, revealing a dependency between nitrate reduction and fermentation (111). Additionally, TMAO influences virulence gene expression in *V. cholerae* when added exogenously, however, whether reduction of TMAO is required for this response is not clear (209, 258). In this study, we looked to more thoroughly examine the complete suite of terminal electron accepting complexes encoded by *V. cholerae* and assess the pertinence of each terminal electron acceptor molecule to *in vivo* infection.

By targeting terminal oxidase and terminal reductase complexes of *V. cholerae*, we can better understand the respiratory processes occurring during disease and identify which terminal electron accepting complexes are most critical to *in vivo* fitness. This work highlights that oxygen, although present at low levels diffusing from the host epithelium, is sufficient and essential to supporting *V. cholerae* growth in the infant mouse. These

findings change how we understand the host environment during *V. cholerae* pathogenesis and how oxygen may function in the pathogenicity of other bacterial pathogen elicited diseases.

3.4 – Materials and Methods

3.4.1 – Bacterial Strains and Growth Conditions

Bacterial strains used in this study are listed in Supplemental Table 3. *Vibrio cholerae* El Tor C6706 was used as the wild type strain in this study and served as the strain background for all *V. cholerae* mutant derivatives. Strains were grown primarily on LB agar and used to inoculate 4mL LB media in preparation for subsequent assays. Addition of antibiotics when required were in given concentrations: streptomycin (100µg/ml), spectinomycin (200µg/ml), and ampicillin (100µg/ml). Strains were grown at 37°C for all growth assays. Aerobic growth assays were performed at atmospheric oxygen concentrations whereas anaerobiosis for anaerobic growth was maintained using a Coy anaerobic chamber.

3.4.2 – MuGENT Mutant Strain Construction

MuGENT generated mutant strains were constructed using Enhanced Multiplex Genome Editing by Natural Transformation (259). Linear segments of *V. cholerae* genomic DNA were amplified using a primer with intentional base changes designed to introduce a frameshift mutation, removal of ATG start codon, insertion of 3-frame stop codons, and offsetting of the ribosomal binding site while also inserting a universal primer binding site. These fragments, along with a fragment containing an antibiotic resistance cassette in pseudogene VC1807 were transformed into a *V. cholerae*

ΔrecJΔxseA pMMB-tfoX strain. Once all mutants were integrated into the genome of carrier strains, a more traditional MuGENT approach (260) was used to amplify ~2Kb arms of homology on either side of the mutated site in each carrier strain to introduce into wild type *V. cholerae* by natural transformation, which maintains functional *recJ* and *xseA*. Candidate colonies were screened via colony PCR for target loci in a multiplex PCR reaction and confirmed by screening purified genomic DNA of each isolate. Strains were serially passaged in LB media to cure the pMMB-tfoX plasmid, where cured strains became sensitive to ampicillin 100µg/ml. Primers used to generate and confirm MuGENT mutant strains are listed in Supplemental Table 4.

3.4.3 – Isogenic Deletion Mutant Strain Construction

Isogenic deletion strain constructs were generated using the positive allelic exchange vector pKAS32 (198). Plasmid constructs were generated by first amplifying and purifying 1Kb DNA fragments upstream and downstream of target loci that contain homology base pairing to pKAS32. The pKAS32 vector was isolated from *E. coli* pKAS32 cultures using a QIAprep Spin Miniprep Kit (Qiagen) and restriction digested with SacI and XbaI. DNA fragments and digested pKAS32 backbone were combined using Gibson Assembly (New England Biolabs) and transformed into *E. coli* ET12567 *ΔdapA* diaminopimelic acid auxotroph mating strain. Newly formed pKAS32 constructs were sequenced and correct vectors conjugated into *V. cholerae*. *V. cholerae*-pKAS32 strains were outgrown in LB at 37°C 210rpm and subjected to >2500µg/ml streptomycin to select for strains that have excised the plasmid from its genome. Candidate mutant strains were screened by colony PCR and confirmed by screening purified genomic

DNA. Primers to generate and confirm pKAS32 deletion strains are listed in Supplemental Table 4.

3.4.4 – *V. cholerae* Terminal Oxidase Strain Growth Curves

Bacterial strains were grown either aerobically or anaerobically on LB streptomycin (100µg/ml) agar media and after 16-18h used to inoculate 4mL LB media. After 16h, bacterial strains were concentrated to a 1.0 OD_{600}. 700µl LB media was inoculated 1:1000 (0.7µl) with the 1.0 OD_{600} resuspensions, vortexed, and aliquoted in triplicate 200µl volumes in a 96-well plate. Optical density was recorded every hour for the duration of the growth curve. Deoxygenated LB was used for anaerobic growth and benchtop LB used for aerobic growth.

3.4.5 – *V. cholerae* Terminal Reductase Strain Growth Curves

Bacterial strains were grown on LB streptomycin (100µg/ml) agar media and after 16-18h used to inoculate 4mL LB media. After 16h, bacterial strains were concentrated to a 1.0 OD_{600}. 700µl LB media was inoculated 1:1000 (0.7µl) with the 1.0 OD_{600} resuspensions, vortexed, and aliquoted in triplicate 200µl volumes in a 96-well plate. Optical density was recorded every hour for the duration of the growth curve. Deoxygenated LB was used for anaerobic growth curves and benchtop LB used for aerobic growth curves. Concentrations of alternative electron acceptors supplemented to LB media were as follows: 50mM sodium fumarate (Sigma), 50mM trimethylamine-N-oxide (TMAO) (Sigma), 50mM sodium nitrate (Sigma), and 50mM dimethyl sulfoxide (DMSO) (Sigma). For strains grown in 50mM LB Nitrate media, after 3h 5µM sodium hydroxide (Fisher Chemical) final concentration was added to alkalinize the growth media to support continued nitrate respiration.

3.4.6 – Wild Type Aerobic, Microaerobic, and Anaerobic RNA Isolation and Real-Time Quantitative PCR (RT-qPCR)

For each growth condition (aerobic / microaerobic / anaerobic) 4mL of LB media was placed in each environment at 37°C to temper the media prior to inoculation in an effort to equalize the oxygen content and to pre-warm the media. Media was inoculated 1:1000 (4µl) with a 1.0 OD_{600} wild type *V. cholerae* inoculum and grew shaking 210rpm for the aerobic culture and static for both microaerobic and anaerobic cultures. After 4h, culture tubes were centrifuged 4000rpm, 4°C, for 10min and cell pellets were resuspended in 1mL TRIzol (Invitrogen). RNA was isolated from TRIzol suspensions using an RNeasy kit (Qiagen) coupled with an on-column DNase digestion (Qiagen) and Turbo DNase digestion (Invitrogen). RNA concentrations were measured with a UV/VIS Spectrophotometer and visualized on a 2% agarose gel.

cDNA was generated from RNA using Superscript III reverse transcriptase (Thermo Scientific). RT-qPCRs were performed using SYBR green master mix (Applied Biosystems) with 5ng of cDNA. Primers used to detect *recA*, cbb_3 (VC1442), *bd*-I (VC1844), *bd*-II (VCA0872), and *bd*-III (VC1571) are listed in Table 4. Threshold cycle ($\Delta\Delta C_t$) values were calculated using *recA* as the gene of reference.

3.4.7 – Infant Mouse Colonization Assays

All animal experiments in this study were approved by the Institutional Animal Care and Use Committee at Michigan State University.

Infant mice were infected as described previously (203). Briefly, three- to five-day-old mouse neonates (Charles River, Wilmington, MA) were orogastrically infected with approximately 10^6 bacterial cells following 2 hours of separation from dam mice and maintained at 30°C for 20h. After 20h, mice were euthanized, and intestinal segments weighed and homogenized in 4mL phosphate buffered saline (PBS). Intestinal homogenates were serially diluted and plated for CFU counts.

For monoassociated infections, dilutions were plated on LB streptomycin (100 µg/mL) for growth and enumeration. For MuGENT strain competition assays, dilutions were also plated on LB spectinomycin (200 µg/ml) for differentiation from co-infected wild type *V. cholerae.*

3.4.8 – CoMPAS Infant Mouse Infection and Sequencing

Wild type, ^{Mu}*cbb*$_3$, ^{Mu}*bd*-I, ^{Mu}*bd*-II, and ^{Mu}*bd*-III MuGENT strains were combined in equal ratios and a total of 6 infant mice were infected with a final 0.01 OD_{600} inoculum, approximately ~10^6 CFU. Remaining inoculum volume was spun down at 4°C, 4000rpm, for 10min and where DNA of the inoculum pool (IP) was isolated using a QIAamp PowerFecal Pro DNA Kit (Qiagen). After 20h infection, small intestinal segments were homogenized and pooled from the 6 infant mice. Pooled homogenates were filtered on ice using a 70µm filter to remove residual intestinal tissue. From here, DNA of the mouse pool (MP) was isolated using a QIAamp PowerFecal Pro DNA Kit (Qiagen).

Recovered DNA samples were normalized to 100ng/µl and subsequently, multiplex amplicon sequencing was performed on both inoculum and mouse pools. Amplification targets included the primary subunit of each MuGENT oxidase complex (VC1442, VC1844, VCA0872, and VC1571) as well as *toxT* (VC0838) which is present in all input strains. Primers used are listed in Supplemental Table 4, amplification was carried out for 30 cycles. PCR products were purified using the QIAquick PCR Purification Kit (Qiagen) and quantified by Qubit dsDNA HS and normalized to 20ng/µl for MiSeq amplicon sequencing by the MSU RTSF Genomics Core (Michigan State University). Sequencing was conducted on a MiSeq Nano v2 flow cell using a 2x250bp paired end format. Sequence barcodes were trimmed and target loci read counts were quanitified using Geneious software.

3.4.9 – *In vitro* Competition Assays

Bacterial strains were grown in 4mL LB media for 16-18h and resuspended to 1.0 OD_{600}. Wild type and an individual target strain were combined in a 1:1 ratio and used to inoculate deoxygenated LB for anaerobic competitions or benchtop LB for aerobic competitions. Anaerobic competitions were grown at 37°C static and aerobic competitions were grown 37°C 210rpm shaking. After 20h of growth, cultures were serially diluted and plated for colony forming units. WT vs. Aero7 and WT vs. Ana4 competitions were plated on LB streptomycin (100µg/ml), and LB spectinomycin (200µg/ml) to determine strain ratios. Individual deletion strain competitions were plated on LB Str100 X-Gal 40µg/ml for blue-white screening to determine strain ratios.

3.5 – Results

3.5.1 – Constructing Terminal Electron Acceptor Mutant Strains

Vibrio cholerae terminal electron acceptor mutants were generated using the multiplex genome editing technique MuGENT (259) and by a positive allelic exchange vector pKAS32 (198) in an El Tor C6706 *V. cholerae* background. Target loci and their relative chromosomal locations are depicted in Figure 3.1A. In MuGENT-generated mutant strains, target loci are disrupted by a frameshift mutation, removal of ATG start codon, insertion of 3-frame stop codons, and offseting of the ribosomal binding site. This is combined with the insertion of a universal detection sequence at each target locus and a spectinomycin cassette insert into pseudogene VC1807 for naturally competent cell selection that has no *in vitro* fitness cost (260) (Figure B.1). MuGENT generated strains are designated with a superscript 'Mu' (^{Mu}). Mutant strains constructed via pKAS32 have the complete coding sequence for all subunits of target terminal electron acceptor complexes excised, generating isogenic deletion strains. Select strains were verified by whole genome sequencing which indicated no nucleotide polymorphisms in most strains and where present were found in hypothetical protein regions of the genome predicted to have no impact on bacterial cell fitness (Supplemental Table 1).

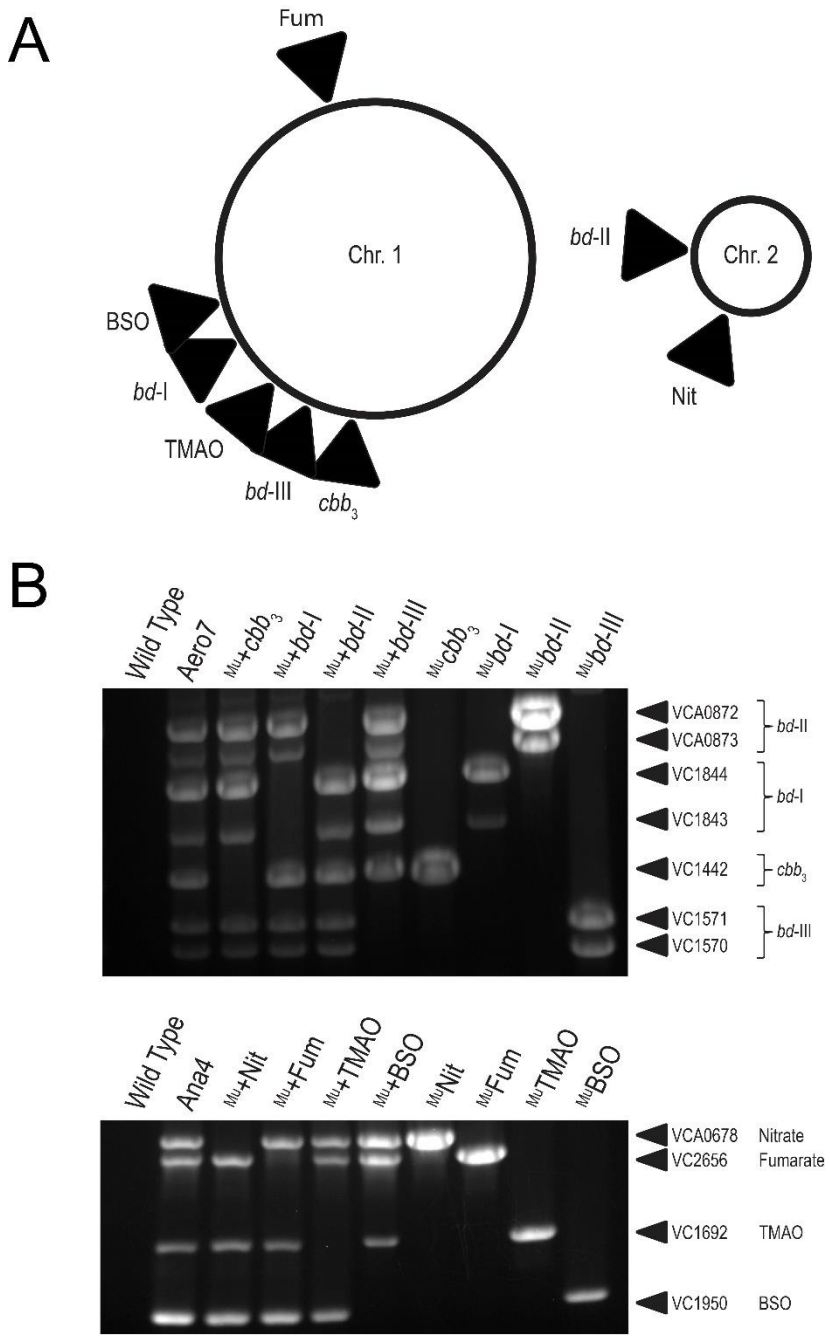

Figure 3.1. Verification of MuGENT generated mutant strains. (A) Chromosomal map of *V. cholerae* terminal electron reducing complex loci. (B) Multiplex allele-specific PCR (MASC-PCR) of *V. cholerae* terminal electron reducing complexes MuGENT mutants. Lanes are labelled with the strain name where a strain preceded by a '^{Mu}+' (Lanes 3-6) indicates it is the indicated oxidase complex as the sole remaining functional oxidase in that strain and strains preceded by a '^{Mu}' (Lanes 7-10) indicates that the specified locus is the targeted knock out. Targeted gene loci are labelled to the right of each gel image. The presence of a band indicates a targeted

knockout in the gene locus whereas the absence of a band indicates the wild type gene is present.

V. cholerae encodes one *cbb*$_3$ oxidase and three *bd*-type oxidase complexes (147) (Figure 3.1A). Cytochrome oxidase *cbb*$_3$ is a four subunit (VC1439-VC1442) cytochrome c containing terminal oxidase of which the coding sequence for the primary subunit, CcoN (VC1442), was disrupted to generate MuGENT knockout strains. CcoN is the first open reading frame in the operon and contains the active site for reducing oxygen to water (261); its disruption was sufficient for abolishing *cbb*$_3$ cytochrome c activity (Figure B.2A). For each of the three *bd*-type oxidases, *bd*-I (VC1844-43), *bd*-II (VCA0872-73), and *bd*-III (VC1570-71), both subunits of each complex were disrupted. Mutations in each target locus were confirmed by multiplex allele-specific PCR (MASC-PCR) (178) where the presence of a DNA band indicates successful genomic editing at the indicated locus via MuGENT (Figure 3.1B). To further validate the function of each oxidase, isogenic deletion strains were also generated for select terminal oxidases via pKAS32 positive allelic exchange.

V. cholerae also encodes four alternative terminal reductase complexes (147) capable of reducing alternative electron acceptors that can support respiration in the absence of oxygen. The four terminal reductases include a fumarate reductase (VC2656-59), trimethylamine-N-oxide (TMAO) reductase (VC1692-94), nitrate reductase (VCA0676-0680), and a biotin sulfoxide reductase (BSO) (VC1950-51). For each of these multi-subunit complexes, the active reducing subunit was disrupted via MuGENT and confirmed by MASC-PCR (Figure 3.1B).

3.5.2 – *In vitro* Characterization of Terminal Electron Acceptor Complex Mutants

Terminal Oxidase Growth Characterization

V. cholerae oxidase mutant strains were grown in LB media in aerobic and anaerobic conditions. Inocula were prepared anaerobically to ensure consistent growth of oxidase-deficient strains. After anaerobic preparation of inocula, both *cbb*$_3$ and *bd*-I oxidase complexes were found to be required for wild type levels of growth in aerobic conditions whereas *bd*-II and *bd*-III oxidases were not (Figure 3.2A). Cultures lacking the *cbb*$_3$ oxidase grew at a consistently lower optical density and never reached the peak OD_{600} of wild type. The *bd*-I oxidase was determined to be the most critical oxidase complex for supporting aerobic respiration in *V. cholerae*, as cells lacking it showed drastically reduced growth. This finding was unexpected as electron transport and oxygen reduction by the *cbb*$_3$ oxidase is more efficient at generating a proton gradient (and therefore ATP) for the cell (262). Electrons passed to the *cbb*$_3$ oxidase are shuttled through the bc_1 complex, which accounts for a $\Delta 6H^+$ proton gradient (263) along with translocation of two additional protons coupled to the terminal reduction of oxygen by the *cbb*$_3$ complex (264). The *bd*-I reducing pathway generates a relatively weaker proton gradient resulting in less ATP for the cell (137, 265). Thus our observation that it serves as the primary oxidase in *V. cholerae* under atmospheric oxygen conditions was unanticipated. All oxidase-disrupted mutants grew comparably to wild type in anaerobic conditions (Figure 3.2B) suggesting the observed defect in aerobic growth is not due to a general growth defect imposed by the mutations. *In vitro* competition assays were also performed, demonstrating a competitive defect for both *cbb*$_3$ and *bd*-I deficient strains in aerobic conditions (Figure 3.2C-D). These growth phenotypes were

recapitulated in M9 0.2% D-glucose media, although *bd*-I deficient strains were further hampered for growth aerobically and showed a minor shift in reaching exponential phase anaerobically (Figure B.3).

We hypothesized that *bd*-I deficient strains grown anaerobically may experience a growth lag prior to expression of alternative oxidases, such as the *cbb*$_3$ oxidase (Figure B.2B), accounting for the observed growth kinetics. To test this, we prepared inocula aerobically and observed the growth phenotype. In this condition, strains lacking *bd*-I oxidase grew to wild type optical density (Figure 3.2E) indicating that delayed expression of alternative oxidases when inocula are prepared anaerobically may account for the observed growth lag. Similar growth patterns were observed in anaerobic growth conditions for inocula of aerobically prepared oxidase mutants (Figure 3.2F). We examined expression patterns of wild type *V. cholerae* under anaerobic, microaerobic, and aerobic conditions, by qRT-PCR $\Delta\Delta C_t$ analysis using *recA* as the gene of reference. Expression values are reported relative to *bd*-III expression in anaerobic conditions, which served as the baseline for comparison among the oxidases (Figure 3.2G). The *cbb*$_3$ and *bd*-I oxidases were more highly expressed relative to *bd*-II and *bd*-III. In anaerobic conditions, *bd*-I oxidase was expressed nearly 10-times higher than *cbb*$_3$ oxidase whereas in the presence of oxygen (microbaerobic or aerobic) *cbb*$_3$ oxidase was expressed slightly higher than *bd*-I. We conclude that the *bd*-I oxidase is critical for aerobic respiration in *V. cholerae* during transition from an anaerobic to aerobic environment and hypothesize that expression of the *cbb*$_3$ oxidase is delayed during this transition period.

Further characterization of the oxidase complexes was carried out using double, triple, and quadruple oxidase mutant strains. Isogenic double and triple deletion strains, as well as quadruple oxidase MuGENT mutant Aero7, were grown in aerobic and anaerobic conditions in LB from inocula grown anaerobically (Figure 3.2H-I). Strain +*bd*-I, harboring solely a functional *bd*-I oxidase, grew to near wild type levels while strains +*cbb*$_3$ and +*bd*-III, having solely the *cbb*$_3$ or *bd*-III oxidase complex, grew after a considerable lag phase. This lag phase, however, was reduced when inocula were adapted to an aerobic environment prior to the growth assay (Figure 3.2J-K). Strain Aero7, defective for production of all terminal oxidases encoded by *V. cholerae*, and strain +*bd*-II, containing only the *bd*-II oxidase, were completely deficient for aerobic growth. This was further exemplified for Aero7 by a near 10^7-fold attenuation in *in vitro* competition assays (Figure 3.2L). These observed growth phenotypes were recapitulated in M9 0.2% D-glucose media (Figure B.3). Additionally, triple oxidase MuGENT mutant growth mirrored that observed in isogenic deletion strains, although strain ^{Mu}+*bd*-III (encoding only *bd*-III) exited lag phase more rapidly (Figure B.4). From these results, we conclude that *cbb*$_3$, *bd*-I, and *bd*-III oxidases support aerobic growth of *V. cholerae* to varying degrees while *bd*-II does not. Despite its low mRNA expression level in wild type cells relative to other oxidases, *bd*-III oxidase supported +*bd*-III aerobic growth, particularly when culture inocula were grown aerobically.

Taken together, these findings make clear that *bd*-I oxidase is the primary oxidase in *V. cholerae*, priming a transition from anaerobic to aerobic environments and functioning as the primary oxidase in atmospheric oxygen environments. To our knowledge, *V.*

cholerae and *Listeria monocytogenes* (148) are the only pathogens demonstrated to preferentially use a *bd*-type oxidase in lieu of a heme-copper oxidase such as the bo_3 oxidase of *Escherichia coli* (141) and *Salmonella* Typhimurium (7), the cbb_3 oxidase of *Psuedomonas aeruginosa* (266), *Campylobacter jejuni, and Helicobacter pylori* (267), or the aa_3 oxidase of *Staphylococcus aureus* (268) to support growth in atmospheric oxygen.

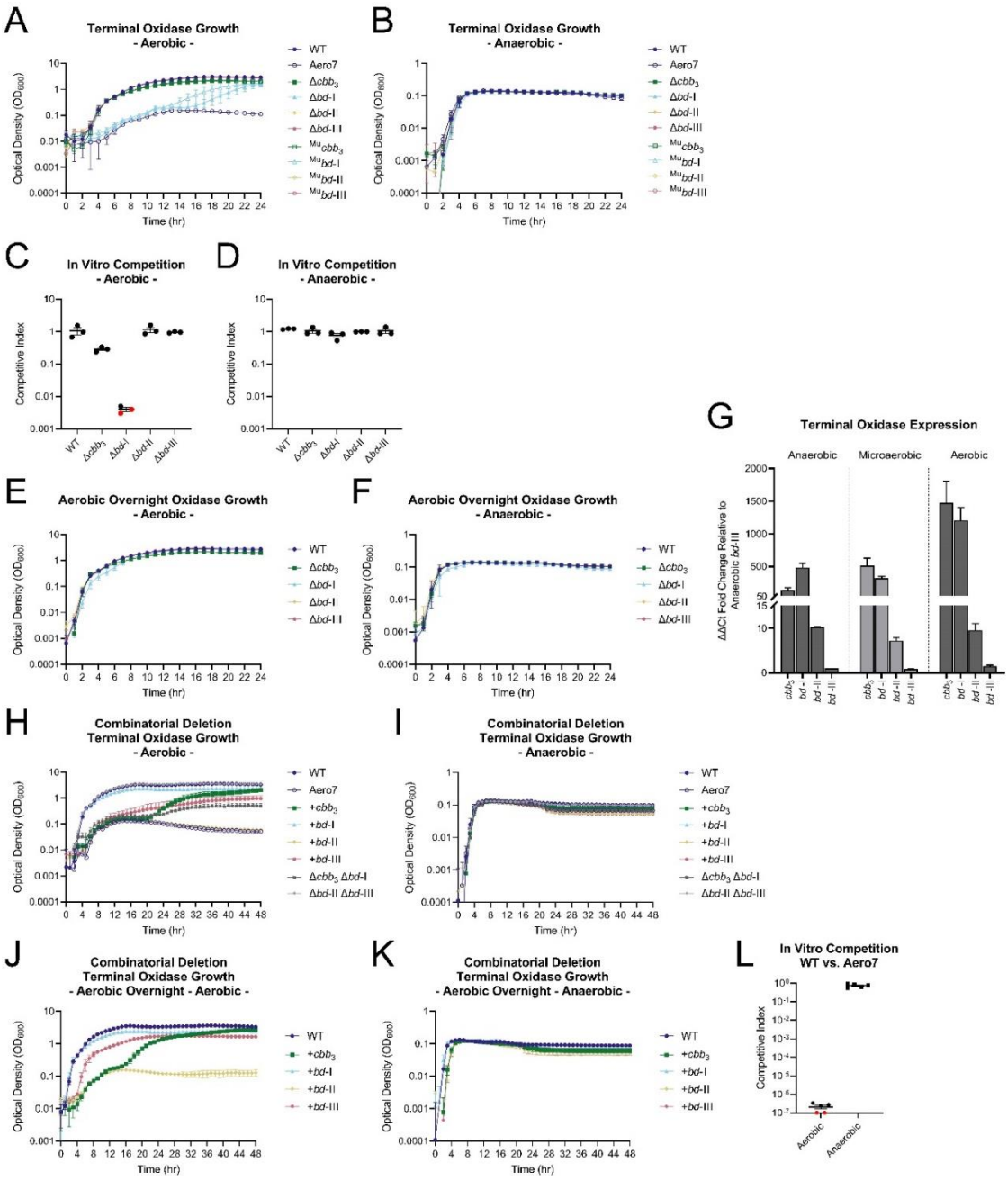

Figure 3.2. Terminal oxidases support aerobic growth in *V. cholerae*. Growth characteristics of the terminal oxidases in *V. cholerae.* (A-B) Single terminal oxidase mutants, both MuGENT and isogenic deletion, growth in LB. Inoculums were prepared anaerobically and subsequently grown in aerobic and anaerobic conditions, respectively. (C-D) Single terminal oxidase isogenic deletion strain *in vitro* LB competition assays in both aerobic and anaerobic conditions, respectively. Competitive index scores were calculated as a ratio of output versus input [(Target$_{Output}$/*ΔlacZ*$_{Output}$) / (Target$_{Input}$/*ΔlacZ*$_{Input}$)], where a *ΔlacZ* strain served as a psuedo-wild type to determine relative fitness via blue-white screening. Red dots indicate the limit of detection where no CFUs were recovered for these trials. (E-F)

Single terminal oxidase isogenic deletion mutant growth in LB where inoculums were prepared aerobically and subsequently grown in aerobic and anaerobic conditions, respectively. (G) *In vitro* expression of terminal oxidases in anaerobic, microaerobic, and aerobic growth conditions.(H-I) Combinatorial terminal oxidase deletion mutant growth in LB. Inoculums were prepared anaerobically and subsequently grown in aerobic and anaerobic conditions, respectively. Triple deletion mutant strains have a '+' with an oxidase name (e.g. +*cbb*$_3$), indicating the sole remaining oxidase, with the other three oxidases disrupted by mutation. (J-K) Combinatorial terminal oxidase deletion mutant growth in LB. Inoculums were prepared aerobically and subsequently grown in aerobic and anaerobic conditions, respectively. (L) *In vitro* aerobic and anaerobic competition assay between Aero7 and Wild Type *V. cholerae* with competitive index scores calculated as [(Aero7$_{Output}$/WT$_{Output}$) / (Aero7$_{Input}$/WT$_{Input}$)]. Growth curves are an average of three biological replicates where error bars represent the standard error of the mean. Bars for *in vitro* competitions and expression data represent the arithmetic mean where error bars represent the standard error of the mean.

Growth of Mutants Lacking Terminal Reductases

MuGENT terminal reductase *V. cholerae* mutants were prepared aerobically and used to inoculate fresh LB with and without alternative electron acceptors in both aerobic and anaerobic conditions. Individual reductase MuGENT-derived mutant strains were made lacking the active subunit of fumarate reductase (VC2656), TMAO reductase (VC1692), nitrate reductase (VCA0678), and BSO reductase (VC1950). And a combinatorial mutant was also constructed, denoted Ana4, in which all reductases were disrupted.

All terminal reductase mutants, including Ana4, grew similarly to wild type in LB in both aerobic and anaerobic growth conditions. However, when grown anaerobically in the presence of the alternative electron acceptors fumarate, TMAO, nitrate, or DMSO, mutant strains were defective for growth compared to wild type (Figure 3.3A-D). This indicated that the MuGENT-generated reductase mutants were defective for reductase function. As Ana4 was reduced for growth in the presence of all alternative electron

acceptors, we concluded it adequately represented a strain incapable of utlizing these molecules to support growth and included it in our *in vivo* analysis described below. The presence of these alternative electron acceptors under aerobic conditions led to varying growth responses by wild type *V. cholerae*. With fumarate or DMSO, growth was boosted, however, with either nitrate or TMAO growth was reduced (Figure B.5A-D).

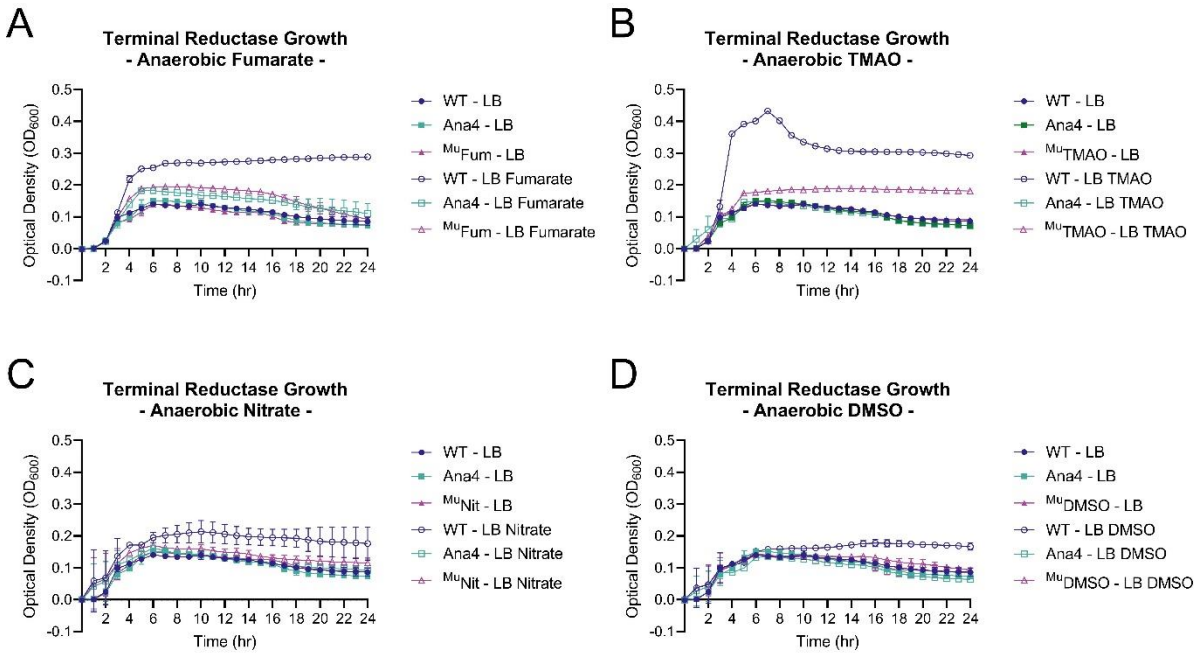

Figure 3.3. Terminal reductase mutants are reduced for anaerobic growth in the presence of cognate electron acceptor molecules. Growth characteristics of terminal reductases of *V. cholerae*. MuGENT generated terminal reductase mutants grown in LB in the presence and absence of alternative electron acceptors (A) 50mM fumarate, (B) 50mM trimethylamine-N-oxide (TMAO), (C) 50mM nitrate, and (D) 50mM dimethyl sulfoxide (DMSO). Inoculums were prepared aerobically subsequently grown in anaerobic conditions. Growth curves are an average of three biological replicates where error bars represent the standard error of the mean.

3.5.3 – Aero7 and Ana4 Infant Mouse Infections

To examine the importance of aerobic and anaerobic respiration during infection, *V. cholerae* Aero7 and Ana4 MuGENT strains were tested for their ability to colonize the

infant mouse intestinal tract. Single strain and competition infections in neonatal mice were performed for both strains.

Aero7 was severely attenuated for colonization of the small intestine, in both single strain and competition infections (Figure 3.4A-B). In single strain infections, wild type *V. cholerae* was recovered near 10^8 CFU/g intestine whereas Aero7 was recovered near 10^3 CFU/g intestine, a 5-log decrease in colonization. This reduction was also observed in the competition infections where the competitive index (CI) score of Aero7, calculated as $[[Aero7_{Output}/WT_{Output}] / [Aero7_{Input}/WT_{Input}]]$ was approximately 10^{-5}. Aero7 competed better In the large intestine, although was still at a fitness disadvantage, with a CI of 10^{-3}. Its greater fitness in the large intestine may be due to the more anaerobic environment of this site, which has a more complex microbiota (269) (Figure B.6A-B). That Aero7 is considerably less fit in the infant mouse small intestine is relevant as this is the site of infection in humans. We conclude from these findings that maintaining functional terminal oxidases, and therefore aerobic respiration, is critical for *V. cholerae* to establish infection and proliferate.

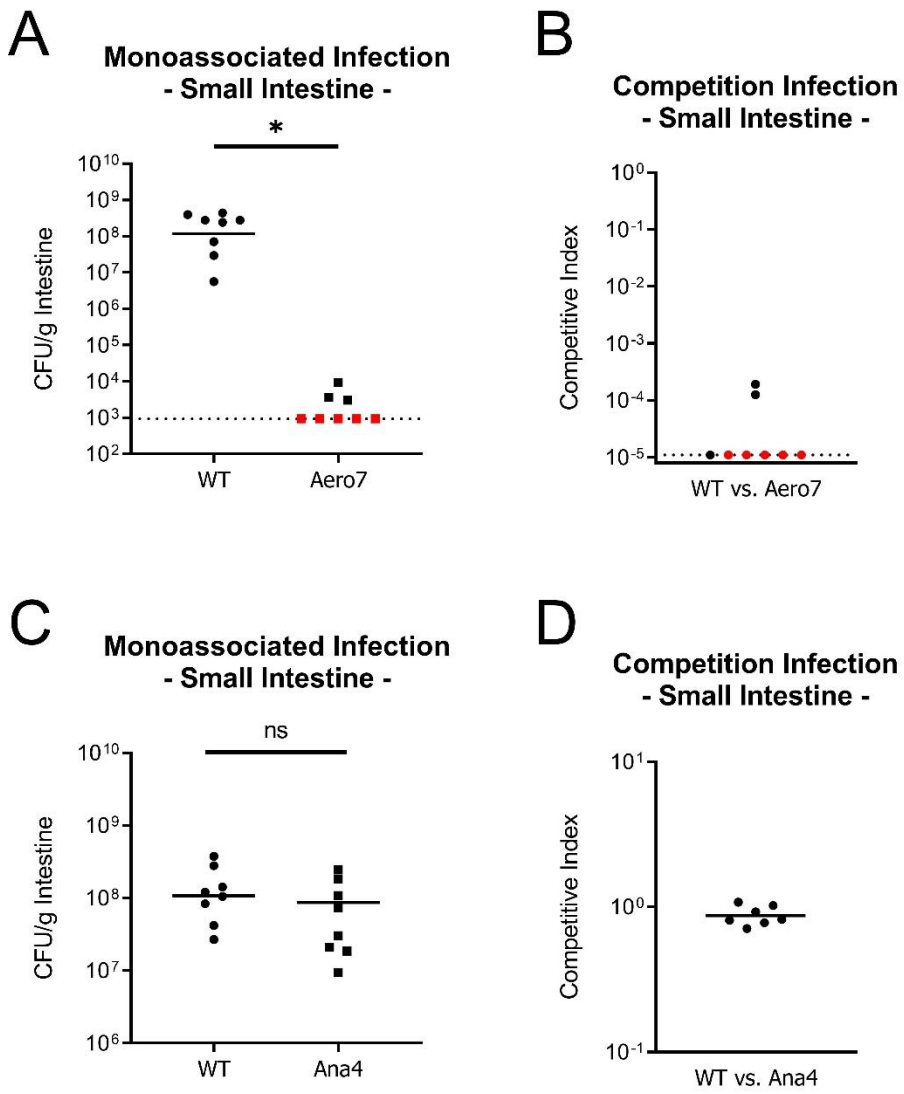

Figure 3.4. Aerobic respiration, and not anaerobic respiration, is required for growth and colonization of the infant mouse small intestine. Aero7 and Ana4 small intestine colonization in monoassociated and competition infections. (A) Monoassociated infection of strain Aero7. (B) Competition infection of strain Aero7. (C) Monoassociated infection of strain Ana4. (D) Competition infection of strain Ana4. Bars represent the geometric mean. Horizontal dashed lines indicate the limit of detection (LOD) and red dots indicate recovered CFUs were below the LOD. Competitive index scores were calculated as [($Mutant_{Output}/WT_{Output}$) / ($Mutant_{Input}/WT_{Input}$)]. Statistical analysis was performed using GraphPad PRISM. *, $P < 0.05$. A Mann-Whitney U-test was used in the determination of significance between WT and Aero7. A Student's T-test was performed on log transformed data in the determination of signifance between WT and Ana4.

In contrast to a strain lacking all terminal oxidases, the Ana4 mutant lacking all terminal reductases, which is deficient for anaerobic growth with specific alternative electron acceptors (Figure 3.3A-D), colonized both the small and large intestines to wild type levels in both single strain and competition infections (Figure 3.4C-D and Figure B.6C-D). The lack of an observable phenotype in our experiments differs from an earlier study demonstrating a two-fold reduction in colonization by a mutant strain of *V. cholerae* lacking nitrate reductase (*napA*; VCA0678) in the adult streptomycin-treated mouse model (110). This two-fold reduction may be observed in adult mice, but not infant, as the adult gut has greater anaerobic luminal volume compared to the limited luminal space in the infant. Nitrate availability has also been shown to increase following streptomycin treatment, which may contribute to the observed colonization discrepancy between wild type and *napA V. cholerae* (270), as lacking a functional nitrate reductase may incur a greater fitness cost in the streptomycin-treated adult mouse.

Overall, our data suggests that anaerobic respiration using alternative electron acceptors is not a prominent feature of *V. cholerae* growth during infection of the infant mouse. The slight growth defect reported with a nitrate reductase mutant in the streptomycin-treated adult mouse (110) suggests that there may be a limited role for anaerobic respiration although more work is required to ascertain the effects of a mature, non-disturbed microbiota on these questions.

3.5.4 – Individual Oxidase Function During Infection

Comparative Multiplex PCR Amplification Sequencing (CoMPAS)

To examine the requirements of the terminal oxidases of *V. cholerae in vivo*, we took a novel approach that combines elements of insertion-site sequencing (Tn-Seq) with targeted amplification of MuGENT generated oxidase mutations (Comparative Multiplex PCR Amplicon Sequencing (CoMPAS)). Individual terminal oxidase MuGENT strains were pooled along with a wild type strain in equal proportions, and the pool was used to infect infant mice. Small intestinal segments were pooled from 6 mice and genomic DNA extracted along with the input inoculum for CoMPAS analysis.

Mutant allele abundances were determined for each oxidase complex and relative sequence abundances were normalized to *toxT* gene amplification (Figure 3.5A). Sequence coverage for each pool are presented in Supplemental Table 2. Comparative index scores are reported for each of the primary oxidase subunits VC1442 (cbb_3), VC1844 (*bd*-I), VCA0872 (*bd*-II), and VC1571 (*bd*-III). Comparative index scores were calculated as [(Output $Pool_{\text{Target Reads}}$ / Output $Pool_{toxT\ \text{Reads}}$) / (Input $Pool_{\text{Target Reads}}$ / Input $Pool_{toxT\ \text{Reads}}$)]. In this experiment, ^{Mu}*bd*-I oxidase knockout strain was underrepresented in the output sequencing pool approximately 10-fold relative to the input. Conversely, all other MuGENT oxidase mutant strains were within a 2-fold change relative to the input. Overall, the *bd*-I oxidase was determined to be the most important oxidase complex supporting growth *in vivo*.

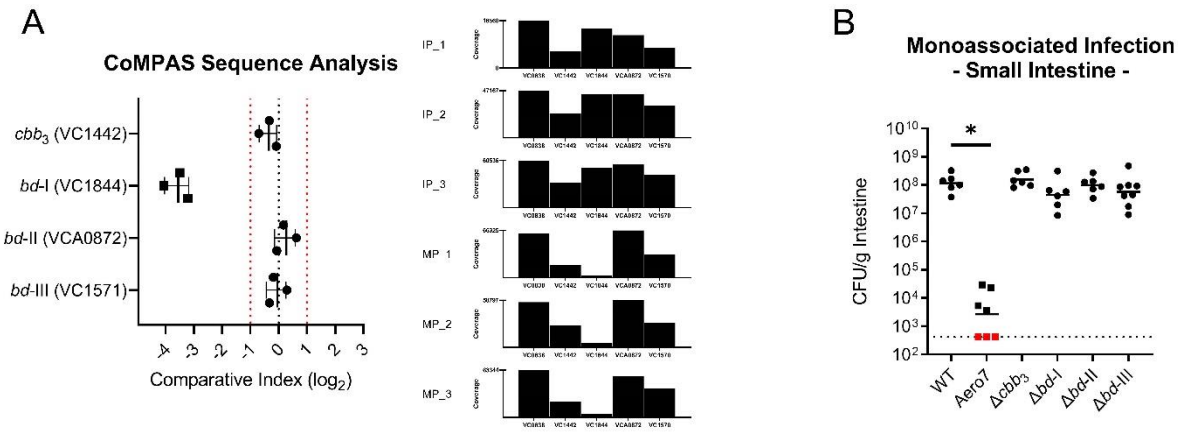

Figure 3.5. Terminal oxidases are functionally redundant in supporting colonization of the infant mouse small intestine. Single oxidase *in vivo* colonization dynamics in the small intestine. (A) Comparative Multiplex PCR Amplification Sequencing (CoMPAS) sequence analysis. Comparative index scores were calculated as [(Output Pool$_{\text{Target Reads}}$ / Output Pool$_{toxT\ \text{Reads}}$) / (Input Pool$_{\text{Target Reads}}$ / Input Pool$_{toxT\ \text{Reads}}$)]. Vertical red dashed lines indicate a 2-fold change in output to input sequence ratios. Sequence coverage for each input pool (IP) and associated mouse output pool (MP) are shown in the bar plots. (B) Individual oxidase deletion monoassociated infections. Bars represent the geometric mean. Horizontal dashed lines indicate the limit of detection (LOD) and red dots indicate recovered CFUs were below the LOD. Statistical analysis was performed using GraphPad PRISM. *, $P < 0.05$. A Mann-Whitney U-test was used in the determination of significance between WT and Aero7 whereas an Analysis of Variance with post-hoc Dunnett's multiple comparisons test was conducted on log transformed CFU/g intestine for all other strain comparisons.

Single Oxidase Complex Deletion Infections

Isogenic terminal oxidase deletion strains were also examined for colonization levels in single strain infections of the infant mouse. Loss of any one of the terminal oxidases did not result in a colonization defect in the small or large intestine of the infant mouse (Figure 3.5B and Figure B.7A). Wild type and mutant strains colonized to approximately 10^8 CFU/g intestine. These findings indicate that in single strain infections, functional redundancy exists among the oxidases that support aerobic respiration during infection. As multiple oxidases were shown to support aerobic growth of *V. cholerae* in our growth assays, we hypothesized that the *cbb*$_3$, *bd*-I, and potentially the *bd*-III oxidase could all

be supporting growth *in vivo*. This hypothesis also reflects data present in a large Tn-Seq dataset where transposon insertions into the *cbb*$_3$, *bd*-I, and *bd*-III oxidases showed a reduced capacity for colonization (244).

Counter to the observed defect in a ^{Mu}*bd*-I knockout strain in our CoMPAS analysis, no colonization defect was present in monoassociated infections. We reasoned that a *bd*-I oxidase deficient strain was capable of colonizing the infant mouse, however, as cultures prepared anaerobically were delayed for aerobic growth as in Figure 3.2A, this growth delay resulted in the *bd*-I deficient strain being outcompeted during the pooled mouse infection.

For all oxidase mutants, one concern is that disruption to oxidase function may impact other requirements for colonization such as virulence factor production or protection against reactive oxygen species (ROS). To address whether mutations in the oxidases alter production of virulence factors required for colonization, TcpA protein levels in the mutants were examined as described in Supplemental Materials and Methods and were equivalent to wild type production (Figure B.8). As oxidative stress can also prevent bacterial growth *in vivo* and the *bd* oxidases of *Escherichia coli* exhibit low levels of catalase activity (150), we tested the minimum inhibitory concentraion of hydrogen peroxide on *V. cholerae* oxidase mutants, observing no growth defects for any mutant strain (Figure B.9). These findings support our conclusions that observed colonization defects can be attributed to a reduction in respiratory energy generation and not related

to virulence factor production or increased ROS sensitivity that could have also limited colonization efficiency.

3.5.5 – Determining Functionally Redundant Oxidases During Infection

To identify which oxidases primarily support growth *in vivo*, triple oxidase isogenic deletion strains were used to colonize the infant mouse. By infecting with triple mutants, we could determine the importance of the single remaining oxidase. Strain +*bd*-I expressing solely the *bd*-I oxidase colonized comparable to wild type and strain +*cbb*$_3$ with a functional *cbb*$_3$ oxidase colonized at a ~1.5-fold reduction compared to wild type (Figure 3.6A). This finding further supports *bd*-I oxidase as the primary oxidase of *V. cholerae*. Strains containing solely the *bd*-II or *bd*-III oxidase were unable to colonize (Figure 3.6A). This pattern of colonization was also reflected in the large intestine, however with higher levels of recovered CFU/g intestine, again likely due to the more anaerobic environment (Figure B.7B). As the *cbb*$_3$ oxidase was determined to be less expressed and inactive in anaerobic conditions (Figure 3.2G and Figure B.2B), and mouse inocula were prepared anaerobically prior to infection, we investigated whether preparation in aerobic conditions could prime expression and activation of the *cbb*$_3$ oxidase to better support growth *in vivo*. Despite preparing +*cbb*$_3$ oxidase cultures aerobically, we still observed a significant ~1-log reduction in colonization (Figure 3.6B). However, the colonization efficiency of aerobically grown +*cbb*$_3$ cultures was improved compared to anaerobically prepared +*cbb*$_3$ cultures but was not enough to support wild type levels of colonization. No significant difference was detected in the large intestine, which was also previously observed in the anaerobically prepared culture infections (Figure B.7C).

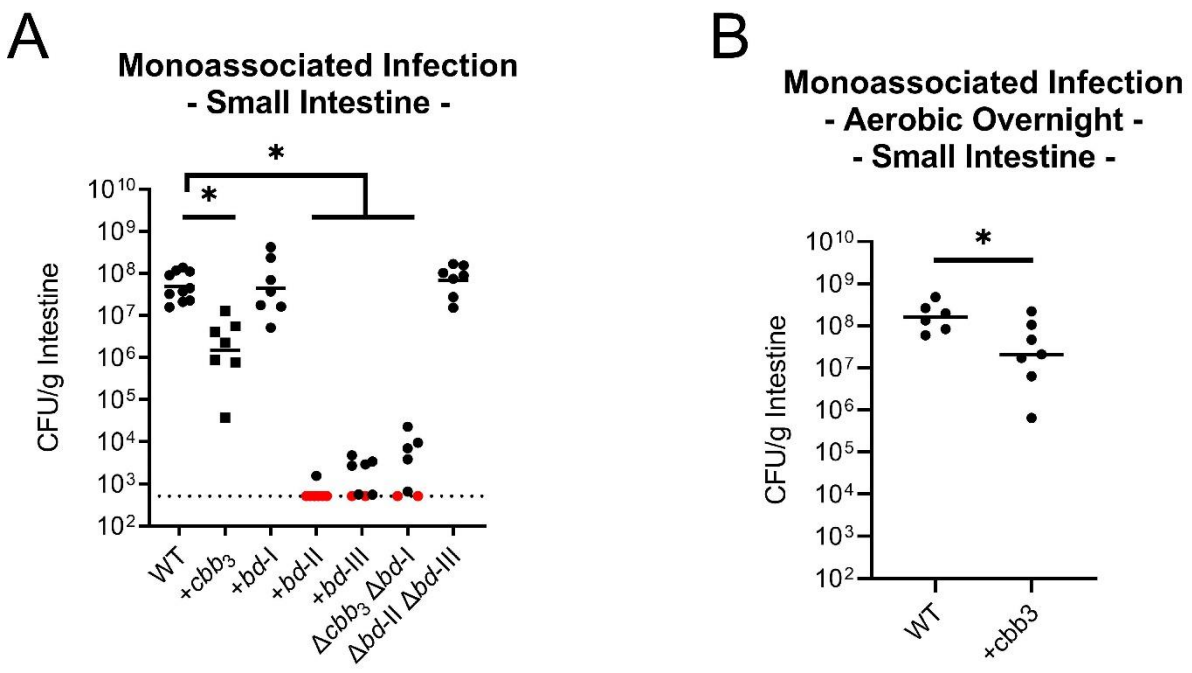

Figure 3.6. *bd*-I oxidase alone supports wild type levels of colonization in the infant mouse small intestine with *cbb*$_3$ supporting colonization to a lesser extent. (A) Combinatorial oxidase deletion i*n vivo* colonization dynamics in the small intestine. (B) Colonization of aerobically prepared wild type and +*cbb*$_3$ oxidase inoculums. Triple deletion mutant strains have a '+' with an oxidase name (e.g. +*cbb*$_3$), indicating the sole remaining oxidase, with the other three oxidases disrupted by mutation. Bars represent the geometric mean. Horizontal dashed lines indicate the limit of detection (LOD) and red dots indicate recovered CFUs were below the LOD. Statistical analysis was performed using GraphPad PRISM. *, $P < 0.05$. A Mann-Whitney U-test was used in the determination of significance between WT and +*bd*-II, +*bd*-III, and Δ*cbb*$_3$Δ*bd*-I whereas an Analysis of Variance with post-hoc Dunnett's multiple comparisons test was conducted on log transformed CFU/g intestine for all other strain comparisons.

As the +*bd*-III oxidase strain could grow *in vitro* in aerobic LB conditions following aerobic overnight preparation while lacking both *cbb*$_3$ and *bd*-I oxidases, we looked to determine whether wild type expression levels of *bd*-III oxidase could support aerobic growth in this strain. By $\Delta\Delta C_t$ qRT-PCR analysis, +*bd*-III aerobic growth was supported by increased expression of *bd*-III transcript, minimally 40x higher than wild type. We hypothesized that this increased expression may be due to selective pressure for

mutations that increase *bd*-III expression. A variant strain, +*bd*-III^{V} was isolated that supported high levels of aerobic growth and exhibited increased expression of the *bd*-III oxidase (Figure B.10B-D). We determined the genome sequence of this variant, identifying a mutation in *chrR* (VC2301), encoding an anti-sigma factor for SigmaE, which controls *bd*-III expression (Supplemental Table 1) (271). In infant mouse infections, +*bd*-III^{V} colonized near one order of magnitude lower than wild type in the small intestine of the infant mouse and was comparable to wild type in the large intestine (Figure B.10E-F). Comparatively in infant mouse infections, the +*bd*-III^{V} strain performed significantly better than +*bd*-III in the initial colonization infections (Figure 3.6A). In wild type *V.* cholerae, we found that the *bd*-III oxidase is not typically expressed and does not contribute to *in vivo* colonization, however, in scenarios where the *bd*-III oxidase is the sole remaining oxidase and is expressed, it can support aerobic growth and *in vivo* colonization.

3.6 – Discussion

Oxidative respiration is required for population expansion of *V. cholerae* in the infant mouse where the *cbb*$_3$ and *bd*-I oxidases function as the terminal reducing complexes during infection. This is also the first instance where a *bd* oxidase was determined to support growth of a bacterial pathogen in aerobic conditions and is also necessary for the transition from an anaerobic to aerobic environment. The finding that the *cbb*$_3$ and *bd*-I oxidases of *V. cholerae* are necessary for aerobic respiration in the low oxygen environment of the small intestine aligns well with the typically low K_m observed for each of these classes of oxidases (54, 135, 256, 272–274). This work highlights that the low

oxygen level in the small intestine is sufficient and essential for *V. cholerae* growth and implicates oxygen as a key electron acceptor for bacterial pathogenesis in the gut.

Chapter 4 – Concluding Remarks

4.1 – Conclusions and Significance

Prior to this work, the influence of oxygen on the pathogenicity of *V. cholerae in vivo* was an unexplored area of research. It has been well established that preparation of laboratory grown *V. cholerae* can be carried out aerobically (275) and that toxin inducing conditions required aeration (199), but the role of oxygen as it supports growth *in vivo* during infection was first examined in the work presented in Chapters 2 and 3.

4.1.1 – Metabolic Pathways Important for *In Vivo* Growth

Through the investigation of *V. cholerae* metabolism via the pyruvate dehydrogenase (PDH) complex, we concluded that aerobic metabolism is a key driver of *V. cholerae* population expansion during infection (103). Under aerobic conditions, the PDH complex converts pyruvate to acetyl-CoA to feed into the TCA cycle, providing reducing molecules for the electron transport chain (ETC), supporting aerobic respiration. We first established that *V. cholerae* was capable of aerobic growth on mucin when the PDH complex was intact. We then sought to further investigate the role of the PDH complex and, therefore, aerobic metabolism *in vivo*. As the intestine contains many substrates in addition to mucin, we were unable to determine whether mucin-specific metabolism is essential for proliferation *in* vivo. *V. cholerae* colonization is elevated in mice treated with the mucolytic agent N-acetyl-L-cysteine (NAC), indicating that mucus primarily serves as a barrier to colonization and may only secondarily act as a substrate for growth (179). From our results, we were able to conclude that aerobic metabolism as a whole is essential to colonization, a new finding in the field of *V. cholerae* research. We further examined the relationship between aerobic and anaerobic metabolism by investigating a pyruvate formate-lyase (PFL) mutant which also converts pyruvate to

acetyl-CoA, but only under anaerobic conditions. As no significant defect in colonization was observed, we concluded that anaerobic respiration plays only a minor role in colonization of the infant mouse. Anaerobic metabolism of *V. cholerae* during infection has been investigated by another group, however our data suggest that aerobic metabolism is substantially more important for efficient colonization (111).

4.1.2 – Respiration of *V. cholerae* During Infection

After determining that aerobic metabolism is key to the fitness of *V. cholerae* during infection, we wanted to further define how oxidative respiration controls proliferation during infection. The PDH complex, in addition to its role in supporting aerobic respiration, leads to the generation of other metabolic intermediates that can promote cell viability. To directly examine oxidative respiration, we targeted the terminal oxidase complexes of *V. cholerae*. By generating individual and combinatorial oxidase mutant strains, both through modified multiplex genome editing through natural transformation (MuGENT) and pKAS positive allelic exchange vector approaches, we were able to show conclusively the necessity of oxidative respiration during *V. cholerae* infection. Of the four terminal oxidase complexes of *V. cholerae*, the *cbb*$_3$ and *bd*-I oxidases support growth in the infant mouse intestine. Between these two, the *bd*-I oxidase is dominant in supporting aerobic growth, both in atmospheric and *in vivo* conditions. Typically, *bd*-type oxidases are induced under microaerobic conditions characteristic of the host environment, which is consistent with the importance of this oxidase *in vivo*. Identifying *bd*-I as the primary oxidase active in atmospheric oxygen conditions was unexpected and offers insight into the oxygen response pathways of *V. cholerae* both inside and outside of the host environment.

Overall, results presented in this thesis support a model of *V. cholerae* pathogenesis in which oxygen is a key metabolic factor that promotes growth and proliferation during infection. The implications of this work further our understanding of *V. cholerae* biology and present a new view of *V. cholerae* disease progression reliant on oxidative respiration and growth.

4.2 – Future Directions

The influence of oxygen on the pathogenicity of *V. cholerae* had been under-explored prior to this work. An avenue for future work is to explore how oxygen is generated in the intestine during *V. cholerae* infection. As discussed in Chapter 1, oxygen regulation in the intestines is controlled through a combination of host-microbe interactions. How *V. cholerae* affects levels of gut oxygenation during infection and how it interacts with each of these factors that maintain physiological hypoxia in the gut has yet to be explored. Addressing alterations in host metabolism, changes in microbiota-produced short chain fatty acids, and perturbations to the resident aerotolerant microbial populations are key areas of research open for investigation as each plays a role in oxygen regulation in the gut.

The first consideration in pursuing future research in this area requires a re-evaluation of the infant mouse model. The infant mouse model reflects human infection to the degree that the toxin-coregulated pilus is required for colonization of the infant mouse intestine, just as it is required for microcolony formation in the human gut (232, 276). However, cholera toxin, which directly elicits water efflux from human host tissues, does not cause similar diarrheal symptoms in the infant mouse. Additionally, the infant mouse

intestine is naïve both in terms of its innate immunity and composition of a commensal microbiota. To account for deficiencies of the infant mouse, at least in part, further research may benefit from both infant and adult rabbit infection models (277, 278). Both models elicit diarrheal-like symptoms characteristic of human disease, resulting in high fluid accumulation in the lumen of the intestines due to cholera toxin production. To establish oxygen-dependent *V. cholerae* growth in the rabbit models, we would infect the infant rabbit with our WT, Aero7, Δ*cbb*$_3$, Δ*bd*-I, Δ*cbb*$_3$Δ*bd*-I, and Δ*bd*-IIΔ*bd*-III strains. This experiment would further examine the role of the terminal respiratory oxidases *in vivo* and provide confidence for further work in these models. Additionally, examination of host factors that contribute to oxygen levels in the gut, through immunohistochemical staining of HIF regulated claudin-1 or GLUT-1 or, alternatively, pimonidazole dye detection (for examples) may help to investigate *V. cholerae*-induced oxygen changes in the gut following infection, although these would be limited to single time point measurements (33, 72, 155).

The role of cholera toxin (CT) in supporting aerobic metabolism of *V. cholerae* is of interest as the toxin directly affects epithelial cell signaling (279) and drastically changes the luminal environment through diarrheal disease symptoms. In a comparison study of wild type and Δ*ctxA* mutant in the infant rabbit, CT production led to induction of aerobic metabolic pathways (43). Production of CT was linked to increased expression of TCA metabolic genes in the ileum of rabbits (43), including expression of *sucA*, an indicator of aerobic metabolism (42, 280). In the same study, L-lactate metabolism was also induced in infecting *V. cholerae* cells (43). Shifts in host cell metabolism from oxygen-

dependent β-oxidation to anaerobic glycolysis leads to the secretion of lactate into the gut (11). By observing an increase in L-lactate metabolism, we hypothesize that *V. cholerae* CT is leading to a shift in host enterocyte cell metabolism. This shift results in excess oxygen no longer being used for β-oxidation to diffuse into the gut lumen, increasing luminal concentrations of oxygen. Lastly, CT has also been implicated in disrupting intestinal barrier integrity (281) which may contribute to oxygen availability in the gut to support *V. cholerae* growth and proliferation during infection.

To probe the effects of CT on host cell-mediated gut oxygenation, purified CT could be administered to intestinal cell lines, such as polarized T84 epithelial cells (282), to determine if host cell metabolism changes as a result. This could be addressed through monitoring changes in the cell transcriptome with RNA-Seq. Additionally, we can apply fluidic devices that mimic the intestinal environment (283) to measure changes in oxygen availability (162) following administration of purified CT. This would directly test whether oxygen concentrations shift as a result of CT-mediated effects on host cells; although it may be challenging to delineate oxygen changes due to shifts in metabolism or weakening of barrier function in this experimental setup.

Inflammation caused by infection is also of interest for future work. Although cholera is not traditionally considered an inflammatory disease, emerging lineages of *V. cholerae* isolates induce gross pathological alterations to infected tissues (224). Even in the absence of gross pathology changes, inflammatory markers are present in the infant mouse model, which may influence oxygen availability in the gut (221). Neutrophil

recruitment is essential for combating *V. cholerae* during early stages of infection in the adult mouse model (284) and this can lead to higher gut oxygenation. To investigate the role of inflammation for *V. cholerae* aerobic growth, adult mice can be pre-treated with TNBS (285) or DSS (286) to induce inflammation. The colonization capacity of WT *V. cholerae* in the inflamed gut can then be determined. Development of a 3-5 day old infant mouse inflammation model would also be beneficial for studying colonization of *V. cholerae*. To date, a 10-day old TNBS infant mouse model has been studied (287), but would need to be appropriately tested for *V. cholerae* colonization efficacy. As Haitian isolate strains were phenotypically linked to a hypervirulent strain (288), it may be worthwhile to identify and clone evolved genes whose products may contribute to increased inflammation into 7th pandemic El Tor and Classical *V. cholerae* to examine whether inflammation is maintained and if this benefits colonization. Genomic comparisons between the Haitian El Tor variant and the El Tor and Classical biotypes may provide insight into genetic factors that engender host inflammatory responses and support colonization in the inflamed intestine.

Finally, as the intestinal microbiota also plays a significant role in oxygen regulation in the gut, examining interactions between *V. cholerae* and host microbiota would also be of interest. In the human intestinal tract, *V. cholerae* must compete with resident microbiota for niche establishment in order to cause disease. *V. cholerae* can directly kill resident microbes through its Type VI secretion system (45, 46) to reduce competitor populations, including other facultative anaerobes of the gut capable of utilizing oxygen for respiration. Additionally, changes in the microbiota as a result of diarrheal flushing of

resident populations is also anticipated to affect oxygen concentrations in the gut. Adult mice treated with streptomycin to alter the microbiota have been used to study *V. cholerae* infection, but this alteration may confound the interpretation of data from experiments aimed to understand how the microbiota contributes to oxygenation (270). *V. cholerae* infection of zebrafish alters host microbiota composition (289), and this model may be worth exploring as well. By removing short chain fatty acid-producing microorganisms, host cells can no longer obtain adequate amounts of butyrate to grow via oxygen-dependent β-oxidation, shifting host cells to anaerobic glycolysis, leading to an increase in oxygen diffusion to the gut lumen. The infant and adult rabbit models may be key to investigating this relationship. These models, particularly the adult model, would involve a more established microbiota where significant alterations to commensal taxa may be observed following *V. cholerae* infection.

APPENDICES

APPENDIX A

Supplemental Material for Chapter 1

A.1 – Supplemental Methods

A.1.1 – *Vibrio cholerae* Initial Growth on Sigma Type III Porcine Gastric Mucin

Strains were grown on LB + 0.1mg/mL streptomycin plates overnight at 37ºC and a single colony isolate used to start a fresh LB + 0.1mg/mL streptomycin broth culture grown overnight 210rpm at 37ºC. Overnight cultures were washed in PBS and resuspended to an optical density 1.0 OD_{600}. 700µl of either LB, MCLMAN + 0.5% Mucin (Sigma Type III porcine gastric mucin), or MCLMAN minimal media was inoculated 1:1000 with the 1.0 OD_{600} culture. Triplicate 200µl aliquots were dispensed in a 96-well plate and optical densities recorded every 30min for 24h.

A.1.2 – Complementation Plasmid Construction

Complementation plasmid construct open reading frame inserts were generated by PCR using Phusion high-fidelity polymerase (Thermo Scientific). pMMB66EH vector backbones were generated by plasmid purification using Qiagen Mini Prep Kit and subsequent restriction digested using BamHI and HindIII at 37ºC for 1 hour followed by an additional 30 minutes at 37ºC with alkaline phosphatase from calf intestine (CIP) (New England Biolabs). Constructs were assembled using Gibson assembly (New England Biolabs) and were electroporated into electrocompetent S17 λpir *E. coli* and recovered on LB + 0.1mg/mL ampicillin agar plates.

A.1.3 – *Vibrio cholerae* Complementation Strain Construction

Complementation strains were made by mating S17 λpir E. coli pMMB66EH complementation strains with *ΔaceE*, *ΔaceF*, and *ΔpflA* mutant strains and recovered on LB + 0.1mg/mL ampicillin + 25 U/mL polymyxin B agar plates. Strains were verified

using pMMB66EH plasmid-specific primers to detect the full length insert and additional sequencing primers to verify construct sequence.

A.1.4 – Complementation Growth Curves for *ΔaceE* and *ΔaceF*

M9 + 0.5% glucose was prepared and 2mL prewarmed media inoculated 1:250 with 1.0 OD600 culture and grown 210rpm at 37ºC. For wild type control and ΔaceE complementation strains, 1mM isopropyl-β-D-thiogalactoside (IPTG) was added to induce ectopic expression from the complementation vector. For the ΔaceF complementation strain, 0.01mM IPTG was added to induce vector expression. At each timepoint, 100µl was removed for dilution series plating.

A.1.5 – Complementation Growth Curves for *ΔpflA*

M9 + 0.5% glucose 50mM fumarate media was prepared and 700µl was inoculated 1:250 with 1.0 OD600 culture. Triplicate 200µl aliquots were dispensed in a 96-well plate and grown statically at 37ºC in anaerobic conditions. Optical densities were recorded every 1h for 24h. For both WT control and pflA complementation strains, 1mM isopropyl-β-D-thiogalactoside (IPTG) was added to induce ectopic expression from the complementation vector.

A.2 – Supplemental Tables and Figures

Table A.1. Transposon mutagenesis screen results.

NR Well Location	Locus Tag	Gene Name	Gene Description	Gene Role
9-E1	VC2482	ilvH	acetolactate synthase III, small subunit	Amino acid biosynthesis
10-D1	VC0029	ilvE	branched-chain amino acid amiotransferase	Amino acid biosynthesis
9-E12	VCA0684	thiE	thiamin-phosphate pyrophosphorylase	Biosynthesis of cofactors, prosthetic groups, and carriers
17-F8	VC0061	thiC	thiamin biosynthesis protein ThiC	Biosynthesis of cofactors, prosthetic groups, and carriers
33-G10	VC1296	thiD	phosphomethylpyrimidine kinase	Biosynthesis of cofactors, prosthetic groups, and carriers
12-E7	VC2481	serA	D-3-phosphoglycerate dehydrogenase	Amino acid biosynthesis
28-B11	VC2345	serB	phosphoserine phosphatase	Amino acid biosynthesis
28-H7	VC2363	thrB	homoserine kinase	Amino acid biosynthesis
33-G6	VC2362	thrC	threonine synthase	Amino acid biosynthesis
10-F1	VC1169	trpA	tryptophan synthase, alpha subunit	Amino acid biosynthesis
33-H10	VC1170	trpB	tryptophan synthase, beta subunit	Amino acid biosynthesis
34-C5	VC1174	trpE	anthranilate synthase component I	Amino acid biosynthesis
5-H6	VC0705	pheA	chorismate mutase/prephenate dehydratase	Amino acid biosynthesis
25-C3	VC0056	aroE	shikimate 5-dehydrogenase	Amino acid biosynthesis
9-B1	VC0149	epsC	general secretion pathway protein C	Protein fate
28-E3	VC2725	epsL	general secretion pathway protein L	Protein fate
33-E3	VC1709		zinc protease, insulinase family	Protein fate
1-F3	VC1181	cydD	transport ATP-binding protein CydD	Transport and binding proteins
12-G7	VC2270	ribE	riboflavin synthase, alpha subunit	Biosynthesis of cofactors, prosthetic groups, and carriers
23-C6	VC2268	ribE	6,7-dimethyl-8-ribityllumazine synthase	Biosynthesis of cofactors, prosthetic groups, and carriers
28-H2	VC0094	ubiA	4-hydroxybenzoate octaprenyltransferase	Biosynthesis of cofactors, prosthetic groups, and carriers
23-C8	VC2628	aroB	3-dehydroquinate synthase	Amino acid biosynthesis
5-A12	VC2414	aceE	pyruvate dehydrogenase, E1 component	Energy metabolism
32-A1	VC2413	aceF	pyruvate dehydrogenase, E2 component, dihydrolipoamide acetyltransferase	Energy metabolism
27-A7	VC2544	fbp	fructose-1,6-bisphosphatase	Energy metabolism
4-H4	VC0604	acnB	aconitate hydratase 2	Energy metabolism
26-A10	VC1487		conserved hypothetical protein	Hypothetical proteins
3-C8	VC0849		conserved hypothetical protein	Hypothetical proteins

Table A.2. Bacteria strain list.

Strain	Description	Reference
Vibrio cholerae		
V. cholerae C6706 El Tor biotype (Wild type)	Wild type strain	Waters Lab Collection
V. cholerae ΔaceE (VC2414)	Isogenic deletion strain	This study
V. cholerae ΔaceF (VC2413)	Isogenic deletion strain	This study
V. cholerae ΔpflA (VC1869)	Isogenic deletion strain	This study
V. cholerae ΔlacZ (VC2338)	Isogenic deletion strain	This study
V. cholerae ΔtoxT (VC0838)	Isogenic deletion strain	Waters Lab Collection
V. cholerae pMMB66EH (empty vector)	Complementation verification strain	This study
V. cholerae ΔaceE pMMB66EH (empty vector)	Complementation verification strain	This study
V. cholerae ΔaceE pMMB66EH-*aceE*	Complementation verification strain	This study
V. cholerae ΔaceF pMMB66EH (empty vector)	Complementation verification strain	This study
V. cholerae ΔaceF pMMB66EH-*aceF*	Complementation verification strain	This study
V. cholerae ΔpflA pMMB66EH (empty vector)	Complementation verification strain	This study
V. cholerae ΔpflA pMMB66EH-*pflA*	Complementation verification strain	This study
Escherichia coli		
E. coli MCH100λpir pKAS32 (empty vector)	Plasmid vector strain	Lab Collection
E. coli S17 pMMB66EH (empty vector)	Plasmid vector strain	Lab Collection
E. coli S17 λpir 3-7	Cloning vector recipient	Lab Collection

Table A.3. Primer list.

	Primer Name	Primer Sequence (5' -> 3')	Description	Reference
Mutant Construction Primers				
aceE VC2414	*aceE* Upstream Homology F	GTGGAATTCCCGGGAGAGCTCAATATTTTTGCTGTTTAATCAACTCTTG	pKAS32 construction primer	This study
	aceE Upstream Homology R	CATTACTTTTCCTACCTTCAAGGCGATCTATCCTTCTGTTGG	pKAS32 construction primer	This study
	aceE Downstream Homology F	CCAACAGAAGGATAGATCGCCTTGAAGGTAGGAAAAGTAATG	pKAS32 construction primer	This study
	aceE Downstream Homology R	CCGCGGACATGTACAGAGCTGCACGACTGGAGAAGCATG	pKAS32 construction primer	This study
	aceE pKAS32 Seq Primer F1	GAACTGGAGAGACTGATAGTGGAAG	pKAS32 sequencing primer	This study
	aceE pKAS32 Seq Primer F2	CAGAATTTTAAACTCTTACATCGC	pKAS32 sequencing primer	This study
	aceE pKAS32 Seq Primer R1	CAAAAGGTGCAGGTACTTCCAT	pKAS32 sequencing primer	This study
	aceE pKAS32 Seq Primer R2	CTGCACCTTCCGCTTCAA	pKAS32 sequencing primer	This study
	aceE Deletion Detection F	CACCTCTAGCCCATCAAGTCC	Isogenic deletion verification primer	This study
	aceE Deletion Detection R	GTAGTTCTGTACGTCTTCTTTCAGG	Isogenic deletion verification primer	This study
aceF VC2413	*aceF* Upstream Homology F	GTGGAATTCCCGGGAGAGCTTTCTTACTACAAAGAAGCGACTTC	pKAS32 construction primer	This study
	aceF Upstream Homology R	TTTCGCCACCCGAGAATGCGCTTAAGCGTACAGCGGGTTGGT	pKAS32 construction primer	This study
	aceF Downstream Homology F	ACCAACCCGCTGTACGCTTAAGCGCATTCTCGGGTGGCGAAA	pKAS32 construction primer	This study
	aceF Downstream Homology R	CCGCGGACATGTACAGAGCTCTTTCGCTTCAACGGCGGTC	pKAS32 construction primer	This study
	aceF pKAS32 Seq Primer F1	GTACAACGCTGAACGGTGAA	pKAS32 sequencing primer	This study
	aceF pKAS32 Seq Primer F2	ATCGCAGCGACTGACTACAT	pKAS32 sequencing primer	This study
	aceF pKAS32 Seq Primer R1	CAGCGCATCGGTTGAATC	pKAS32 sequencing primer	This study
	aceF pKAS32 Seq Primer R2	GCTCATTTCGACCTCTTGTAGTC	pKAS32 sequencing primer	This study
	aceF Deletion Detection F	TCCGTCAAATCGGTATCTACA	Isogenic deletion verification primer	This study
	aceF Deletion Detection R	CGCATCGTAACGCTCAGCT	Isogenic deletion verification primer	This study
pflA VC1869	*pflA* Upstream Homology F	GTGGAATTCCCGGGAGAGCTTCACTGACTCGCAAAAAAG	pKAS32 construction primer	This study
	pflA Upstream Homology R	AGAGGATGAAGAGCGCTTCTCAGTTATG	pKAS32 construction primer	This study
	pflA Downstream Homology F	AGAAGCGCTCTTCATCCTCTCGACGTTATC	pKAS32 construction primer	This study
	pflA Downstream Homology R	TGCGCATGCTAGCTATAGTTAACTCGCGGTTCAGTTCAC	pKAS32 construction primer	This study
	pflA pKAS32 Seq Primer F	AATCTCAGACACCTTGTTTGAC	pKAS32 sequencing primer	This study
	pflA pKAS32 Seq Primer R	GCCAGATATAAAGGGAGTTAAGC	pKAS32 sequencing primer	This study
	pflA Deletion Detection F	GCTGTTGCTTCACTACTGAG	Isogenic deletion verification primer	This study
	pflA Deletion Detection R	GGATTCTTGCATCGCATGATAC	Isogenic deletion verification primer	This study
lacZ VC2338	*lacZ* Upstream Homology F	GTGGAATTCCCGGGAGAGCTGCCACCAAACACTAAGCTTC	pKAS32 construction primer	This study
	lacZ Upstream Homology R	GCTCTCTGGCCCCTCAAGCCGAGGAGTAAAG	pKAS32 construction primer	This study
	lacZ Downstream Homology F	GGCTTGAGGGGCCAGAGAGCCTTAAGGC	pKAS32 construction primer	This study
	lacZ Downstream Homology R	TGCGCATGCTAGCTATAGTTTAGCACGTGAAGCCGGTG	pKAS32 construction primer	This study
	lacZ pKAS32 Seq Primer F	GATAACCAATCGCAAAACCAACTT	pKAS32 sequencing primer	This study
	lacZ pKAS32 Seq Primer R	TCTCATCCGTCAAGGACATAGAAAC	pKAS32 sequencing primer	This study
	lacZ Deletion Detection F	GAAATTGATCGGTCGATAGGCTG	Isogenic deletion verification primer	This study
	lacZ Deletion Detection R	CCGAGTCCATAACTCTTATCCTTCTTA	Isogenic deletion verification primer	This study
pKAS32	pKAS32 Multiple Cloning Site Seq Primer F	GCCTCTAAGGTTTTAAGTTT	pKAS32 specific sequencing primer	Lab Collection
	pKAS32 Multiple Cloning Site Seq Primer R	CTTTCAAGGTAGCGGTTACC	pKAS32 specific sequencing primer	Lab Collection
toxT VC0838	1531	CAACTTCTGTAGTTAATGCAATTCCC	toxT deletion verification primer	Waters Lab Collection
	1532	CCCTCCAGTAAATTTTCATAAATGTCG	toxT deletion verification primer	Waters Lab Collection
Complementation Primer Sets				
aceE VC2414	pMMB66EH *aceE* ORF F	CAGGAAACAGAATTCCCGGGATGTCTGACATGAAGCATGAC	pMMB66EH *aceE* ORF construct primer	This study
	pMMB66EH *aceE* ORF R	CTCATCCGCCAAAACAGCCATTAAGCGTACAGCGGGTGG	pMMB66EH *aceE* ORF construct primer	This study
	pMMB66EH *aceE* ORF Seq Primer 1	CTGCGTGCATCGAAGAAAGA	pMMB66EH *aceE* ORF sequencing primer	This study
	pMMB66EH *aceE* ORF Seq Primer 2	CTGTTATGGGTAACGGTAAG	pMMB66EH *aceE* ORF sequencing primer	This study
	pMMB66EH *aceE* ORF Seq Primer 3	GTACCTGAAACTGGAAGAAG	pMMB66EH *aceE* ORF sequencing primer	This study
	pMMB66EH *aceE* ORF Seq Primer 4	GCGTGGATGGCGGGTGAC	pMMB66EH *aceE* ORF sequencing primer	This study
aceF VC2413	pMMB66EH *aceF* ORF F	CAGGAAACAGAATTCCCGGGTTGAAGGTAGGAAAAGTAATG	pMMB66EH *aceF* ORF construct primer	This study
	pMMB66EH *aceF* ORF R	CTCATCCGCCAAAACAGCCATTACAGTACCAGACGACG	pMMB66EH *aceF* ORF construct primer	This study
	pMMB66EH *aceF* ORF Seq Primer 1	AGCAGCGGCAGCACCAGC	pMMB66EH *aceF* ORF sequencing primer	This study
	pMMB66EH *aceF* ORF Seq Primer 2	AGATCAAAGTGGCTACAGGCGA	pMMB66EH *aceF* ORF sequencing primer	This study
	pMMB66EH *aceF* ORF Seq Primer 3	GAGCAAAACGCGATGGAAGC	pMMB66EH *aceF* ORF sequencing primer	This study
pflA VC1869	pMMB66EH *pflA* ORF F	CAGGAAACAGAATTCCCGGGATGTCTACCATTGGTCGAATTC	pMMB66EH *pflA* ORF construct primer	This study
	pMMB66EH *pflA* ORF R	CTCATCCGCCAAAACAGCCATCAATATTTTACGTTTGAGTGATAC	pMMB66EH *pflA* ORF construct primer	This study
pMMB66EH	pMMB66EH Multiple Cloning Site Seq Primer F	TGCATAATTCGTGTCGCTCA	pMMB66EH specific sequencing primer	This study
	pMMB66EH Multiple Cloning Site Seq Primer R	CTACGGCGTTTCACTTCTGA	pMMB66EH specific sequencing primer	This study
RT-qPCR Primer Sets				
toxT VC0838	toxT qPCR F	ACTGATGATCTTGATGCTATGGAG	qPCR Primer	This study
	toxT qPCR R	CATCCGATTCGTTCTTAATTCACC	qPCR Primer	This study
ctxA VC1475	*ctxA* qPCR F	TGGAATCCCACCTAAAGCAG	qPCR Primer	This study
	ctxA qPCR R	TTGTTAGGCACGATGATGGA	qPCR Primer	This study
recA VC0543	*recA* qPCR F	GGGTAACCTCAAGCAATCCA	qPCR Primer	This study
	recA qPCR R	CCACTCTTCGCCTTCTTTG	qPCR Primer	This study
tcpA VC0828	*tcpA* qPCR F	ACGCAAATGCTGCTACACAG	qPCR Primer	This study
	tcpA qPCR R	CCCCTACGCTTGTAACCAAA	qPCR Primer	This study

Table A.4. Purified porcine small intestinal mucin monosaccharide and sialic acid analysis determined by High-Performance Anion-Exchange Chromatography coupled with Pulsed Amperometric Detection (HPAEC-PAD). (GlycoAnalytics).

Monosaccharide	Amount (nmole/5µg of sample)
Fucose	0.17
Galactosamine	0.14
Glucosamine	0.14
Galactose	0.17
Glucose	0.01
Mannose	0.02
Sialic Acid	**Amount (pmole/2µg of sample)**
Neu5Ac	8.54
Neu5Gc	6.90

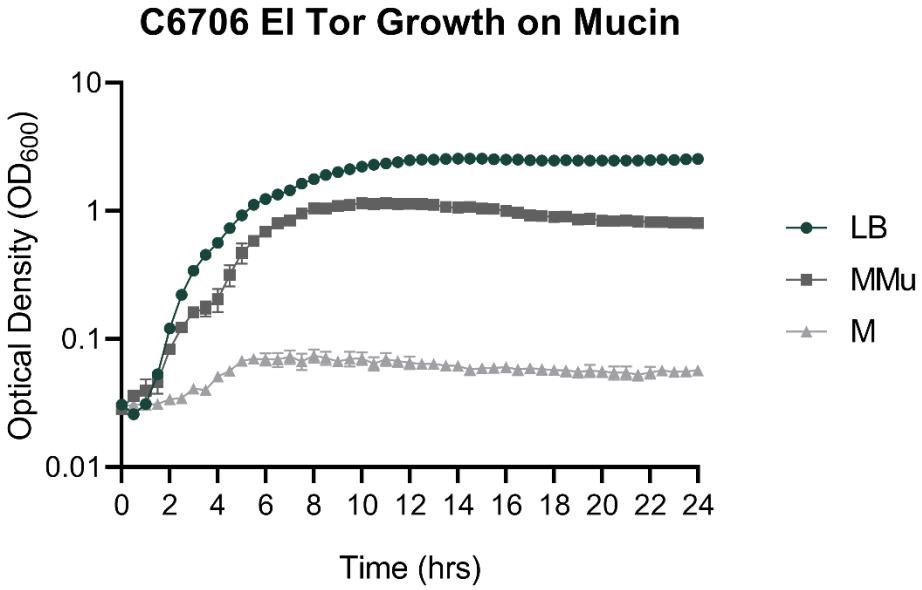

Figure A.1. *V. cholerae* C6706 El Tor wild type growth in LB, minimal 0.5% mucin, and minimal media with no added carbon source. *V. cholerae* C6706 El Tor wild type growth in LB, minimal 0.5% mucin (Sigma Type III porcine gastric mucin) (MMu), and minimal media with no added carbon source (M). Data represent the average and SEM for three independent biological replicates.

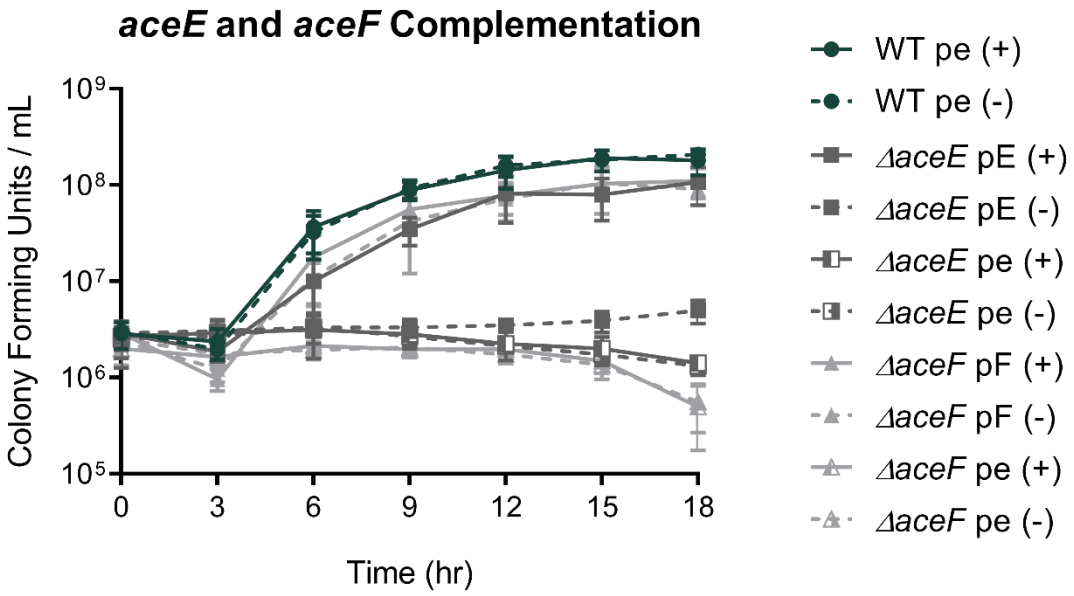

Figure A.2. Complementation growth curves of *ΔaceE* and *ΔaceF* in M9 0.5% glucose media. *ΔaceE* and *ΔaceF* strains were complemented with IPTG-inducible vector pMB66EH. WT and *ΔaceE* strains were induced with 1mM IPTG whereas *ΔaceF* was induced with 0.01mM IPTG. (+) indicates the addition of IPTG inducer whereas (-) indicates the lack thereof. 'pe' denotes an empty vector control whereas 'pE' and 'pF' indicate the complementation plasmid contains the *aceE* and *aceF* open reading frames, respectively. Data represent the average and SEM for three independent biological replicates.

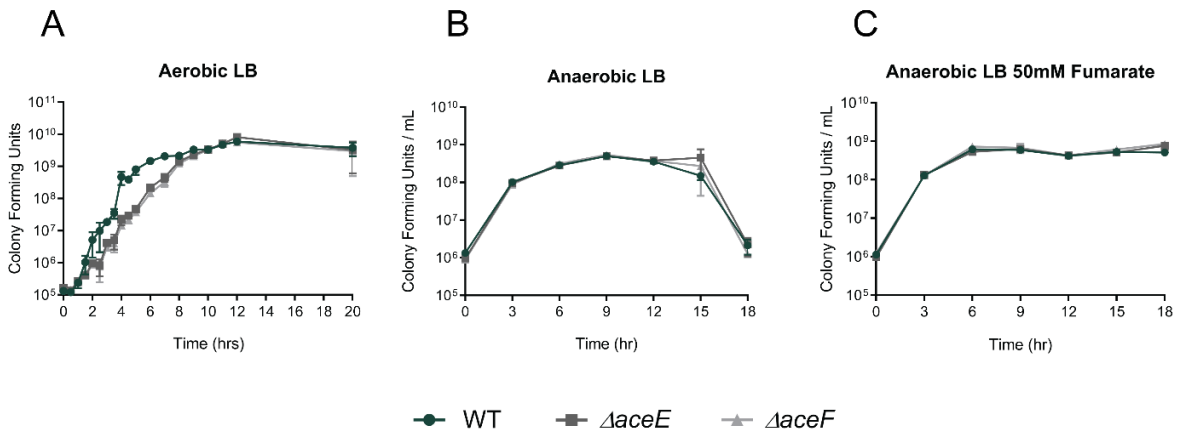

Figure A.3. Growth curves of WT, *ΔaceE*, and *ΔaceF* in LB media grown aerobically, anaerobically, or anaerobically supplemented with 50mM fumarate. Growth curves of WT (green circle) *ΔaceE* (dark grey square) and *ΔaceF* (grey triangle) in LB media grown (A) aerobically, (B) anaerobically, or (C) anaerobically supplemented with 50mM fumarate. Data represent the average and SEM for three independent biological replicates.

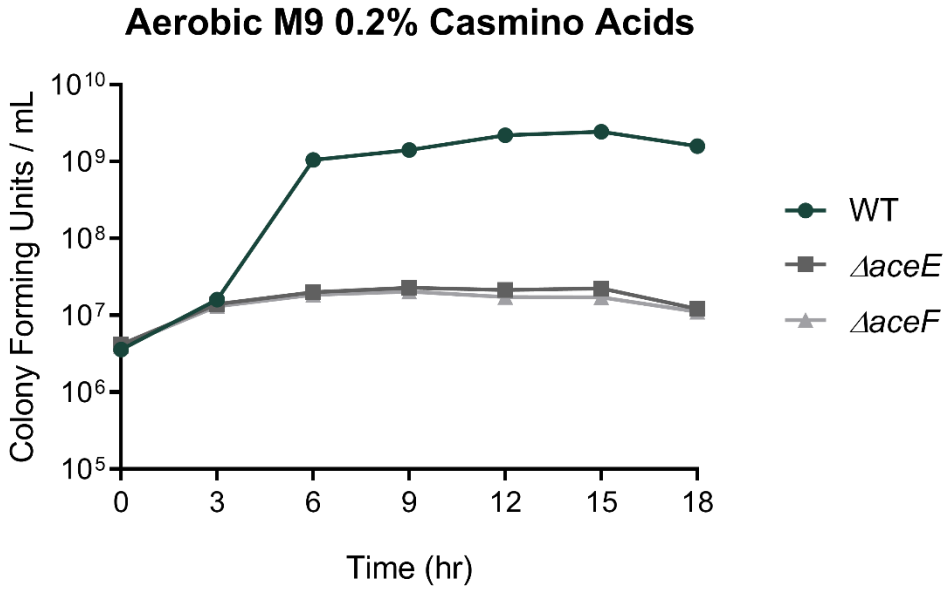

Figure A.4. Growth curves of WT, *ΔaceE*, *ΔaceF* in M9 0.2% Casamino acid media grown aerobically. Growth curves of WT (green circle), *ΔaceE* (dark grey square), *ΔaceF* (grey triangle) in M9 0.2% Casamino acid media grown aerobically. Data represent the average and SEM for three independent biological replicates.

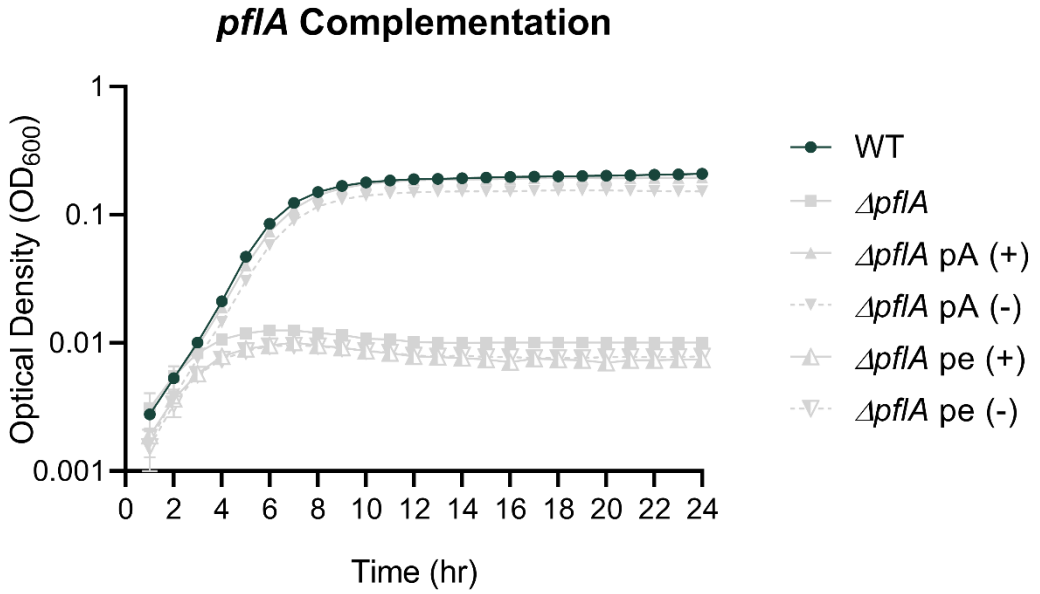

Figure A.5. Complementation growth curve of *ΔpflA* in M9 0.5% glucose 50mM fumarate media grown anaerobically. *ΔpflA* strain was complemented with IPTG-inducible vector pMB66EH. WT and *ΔpflA* strains were induced with 1mM IPTG. (+) indicates the addition of IPTG inducer whereas (-) indicates the lack thereof. 'pe' denotes an empty vector control whereas 'pA' indicates the complementation plasmid contains the *pflA* open reading frame. Data represent the average and SEM for three independent biological replicates.

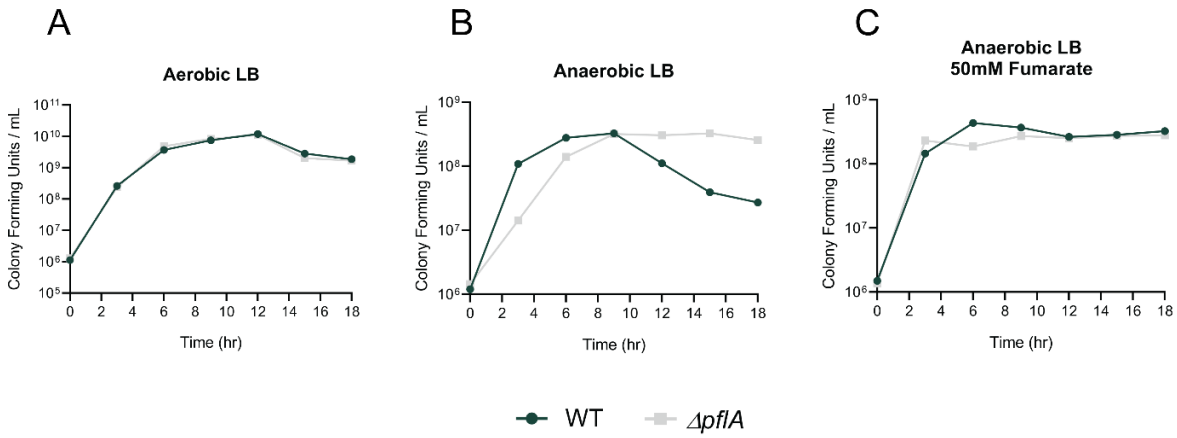

Figure A.6. Growth curves of WT and *ΔpflA* in LB media grown aerobically, anaerobically, or anaerobically supplemented with 50mM fumarate. Growth curves of WT (green circle) and *ΔpflA* (light grey square) in LB media grown (A) aerobically, (B) anaerobically, or (C) anaerobically supplemented with 50mM fumarate. Data represent the average and SEM for three independent biological replicates.

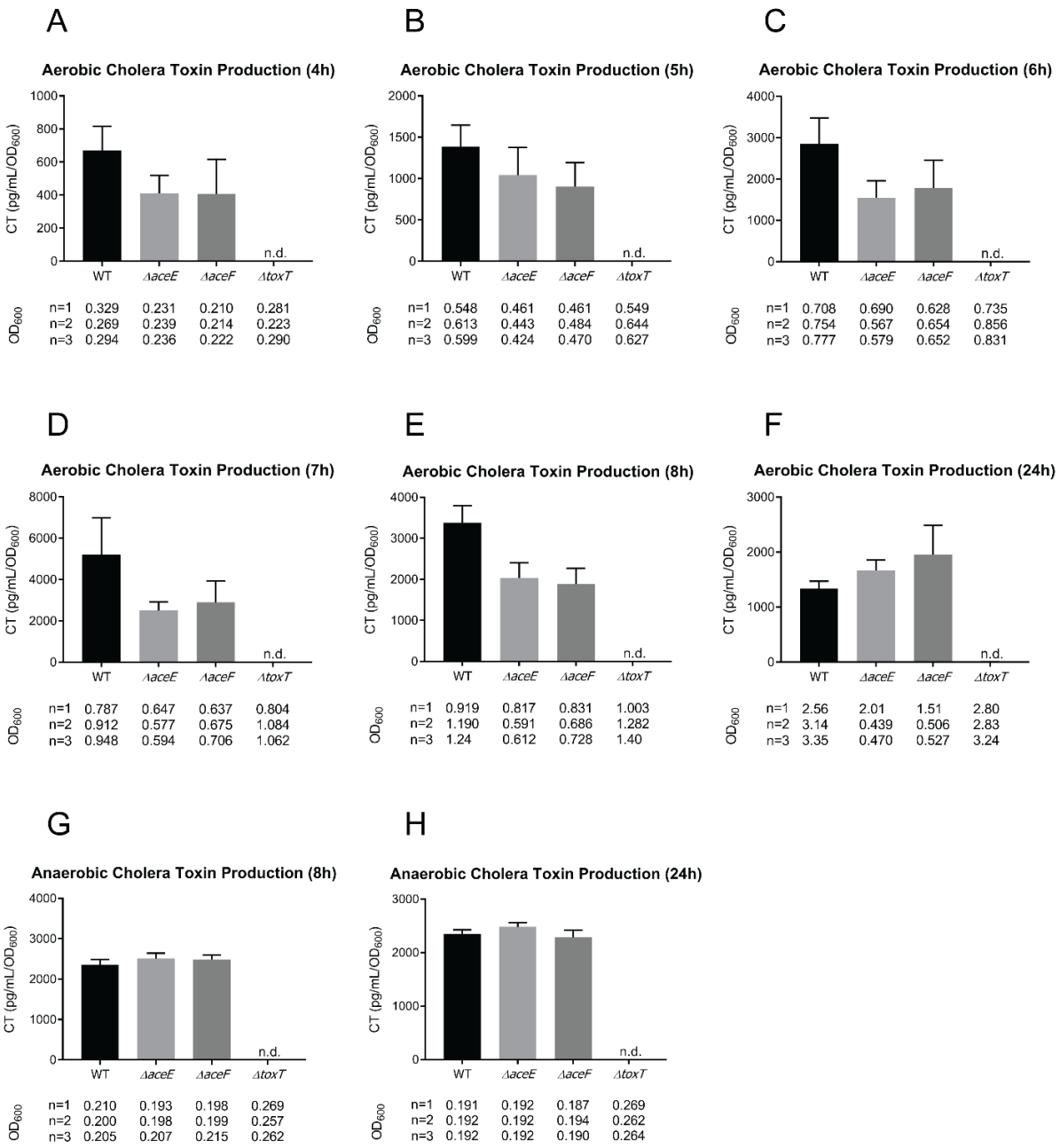

Figure A.7. Cholera toxin (CT) production for WT, *ΔaceE*, *ΔaceF*, and *ΔtoxT* strains. CT values relative to optical density (pg/mL/OD_{600}) are reported under standard AKI toxin-inducing conditions (A-F) and anaerobic AKI conditions (G-H). (A-F) CT levels were measured at 4h, 5h, 6h, 7h, 8h, and 24h. (G-H) CT levels were measured at 8h and 24h. The optical densities for the biological replicates are displayed below the corresponding strain on the x-axis. Data represent the average and SEM for three biological replicates. Panel G is a duplicate graph of Figure 2.3B and is included here for convenient comparison with the 24h timepoint.

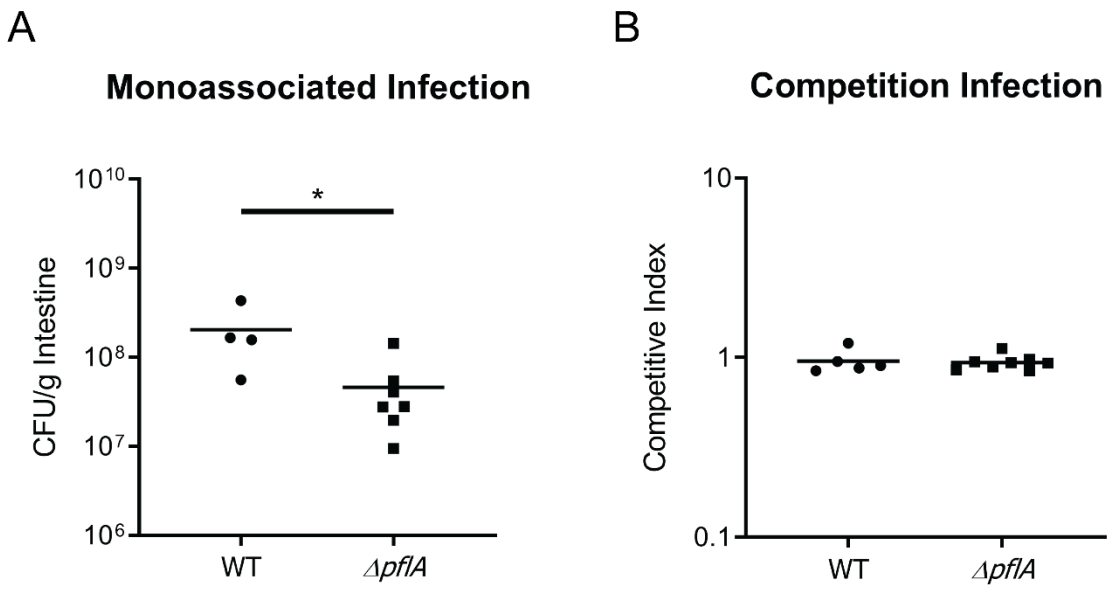

Figure A.8. Infant mouse colonization assays of WT and *ΔpflA* in the large intestine after 20h. (A) Mono-associated infections of 3-5 day old infant mice reported as CFU/g intestine. (B) Competition infections of 3-5 day old infant mice reported as a competitive index score calculated as a ratio of output versus input [($Target_{Output}$/*ΔlacZ*$_{Output}$) / ($Target_{Input}$/*ΔlacZ*$_{Input}$)]. WT and *ΔpflA* strains were co-inoculated with a *pflA*+ *ΔlacZ* strain to determine the relative fitness of each test strain. Data for each experiment was obtained from 4-5 independent mouse colonization infections for WT and 7-8 mouse infections for *ΔpflA*. The bar represents geometric mean. Statistical analysis was performed using GraphPad PRISM where significance was tested on log transformed data by Student's t-test; * indicates $p<0.05$.

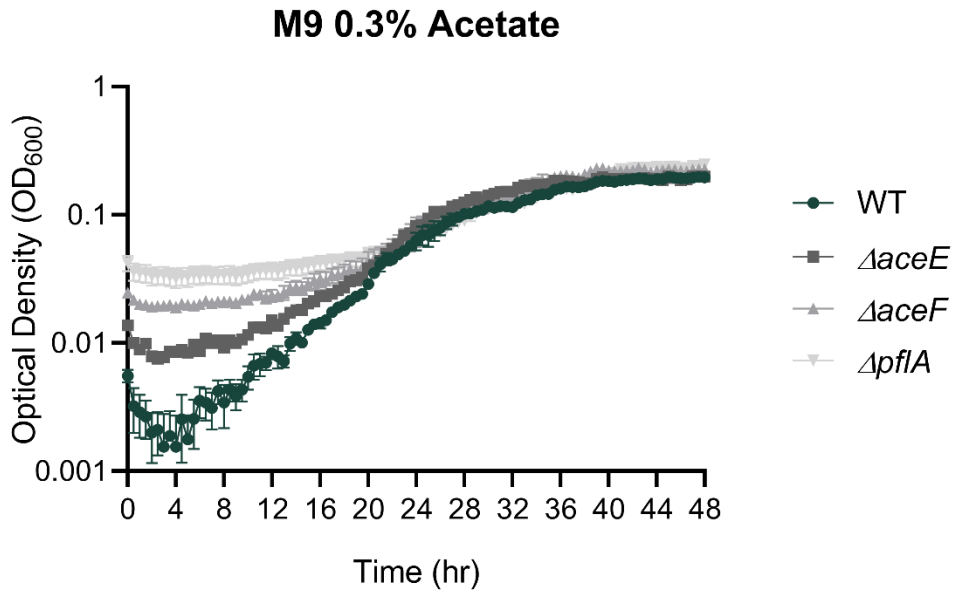

Figure A.9. Growth curves of WT, *ΔaceE*, *ΔaceF* and *ΔpflA* in M9 0.3% acetate. Growth curves of WT (green circle), *ΔaceE* (dark grey square), *ΔaceF* (grey triangle) and *ΔpflA* (light grey inverted triangle) in M9 0.3% acetate. Data represent the average and SEM for three independent biological replicates.

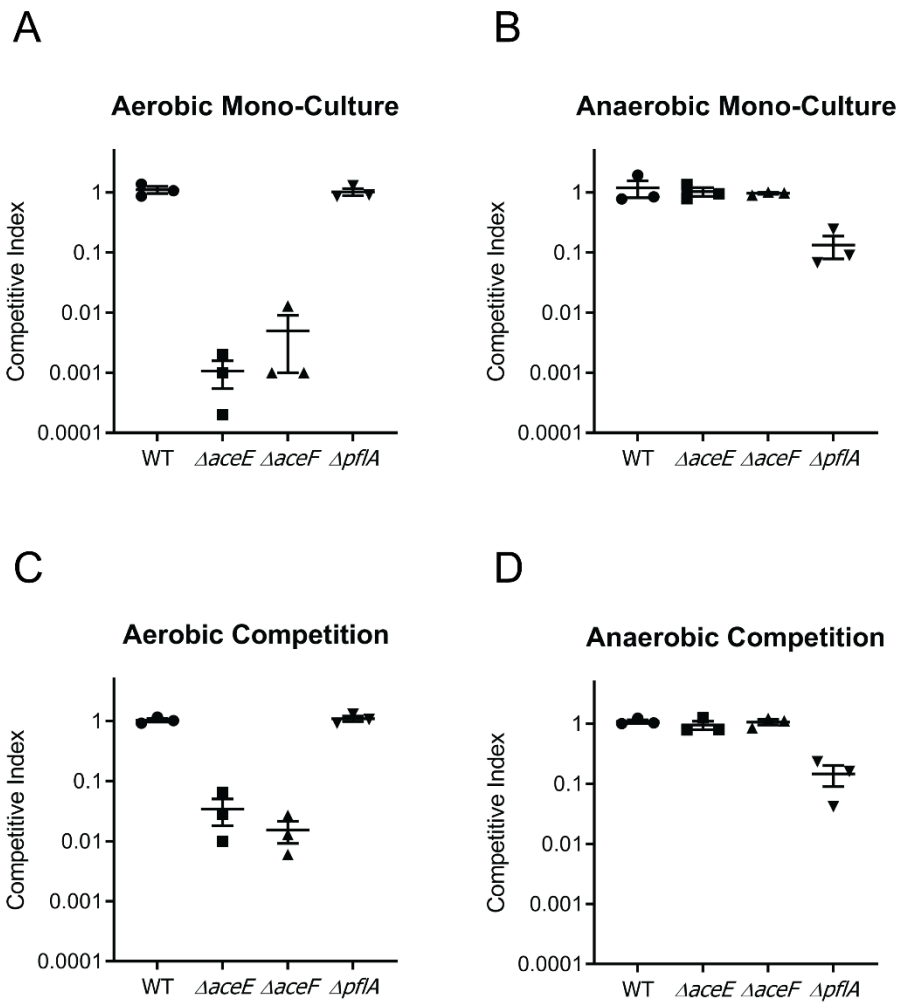

Figure A.10. *In vitro* mono-culture and competition assays of WT, *ΔaceE*, *ΔaceF*, and *ΔpflA* in M9 0.5% glucose after 20h. (A-B) Mono-culture competitive index scores were calculated as a ratio of endpoint culture to initial culture of test strains versus a PDH+/PFL+ *ΔlacZ* strain grown in separate culture tubes; [($Target_{Endpoint}$/$\Delta lacZ_{Endpoint}$) / ($Target_{Initial}$/$\Delta lacZ_{Initial}$)]. (C-D) Competitive index scores were calculated as a ratio of output versus input [($Target_{Output}$/$\Delta lacZ_{Output}$) / ($Target_{Input}$/$\Delta lacZ_{Input}$)]. Strains were co-inoculated with a PDH+/PFL+ *ΔlacZ* strain to determine the relative fitness of each test strain. Data for each experiment was obtained from 3 biological replicates.

APPENDIX B

Supplemental Material for Chapter 2

B.1 – Supplemental Methods

B.1.1 – Hydrogen Peroxide (H_2O_2) Sensitivity Assay

Bacterial strains were grown ON in 4mL LB Str100 broth. After ~16h of growth, cultures were diluted to 1.0 OD600. In a 96-well plate all wells were filled with 100µl LB broth and in the second row 100µl of LB 20mM H_2O_2 (Fisher Chemical) was added and serially diluted to the last row where 100µl was removed leaving a volume of 100µl in all wells. In a 2mL tube, 1.7µl of fresh LB was inoculated 1:500 (2:1000 / 3.4µl) with the 1.0 OD600 cultures. Tubes were vortexed and inoculated media was distributed in duplicate columns for each strain and included blank LB control lanes. 96-well plates were grown at 37°C 210rpm on a plate shaker for 20h. After 20h, the OD600 was read and percent bacterial growth was determined in comparison to the first row which lacks added H_2O_2.

B.1.2 – AKI Virulence Inducing Conditions

Standard AKI Conditions

Bacterial strains were struck on LB streptomycin (100µg/ml) plates and used to inoculate 4mL LB media. After ~16h bacterial strains were diluted to a 1.0 OD600. These cultures were then used to inoculate 40mL prewarmed AKI media 1:5000 (8µl) which were then inverted and set to grow static at 37°C for 4h. After the 4h timepoint, 19mL of culture was transferred to sterile 125mL Erlenmeyer flasks and grown at 37°C, 210rpm, for an additional hour to the experiment 5h timepoint. At both the 4h and 5h timepoint, samples for cholera toxin and TcpA quantification were taken. At the 4h and 5h timepoints, 20mL and 10mL of culture, respectively, were centrifuged at 4000rpm, 4°C, for 10min. For cholera toxin analysis, 1mL of supernatant was removed and stored at -80°C. For TcpA quantification, the bacterial pellet was resuspended in Resuspension

Buffer (50mM Tris-HCl pH 7.4, 50mM EDTA pH 8.0) and transferred to a 1.7mL Eppendorf tube where an equal volume of Lysis Buffer (1% SDS, 10mM Tris-HCl pH 7.4) was added. The bacterial solution was vortexed for 10s, boiled for 10min, and then stored at -80°C.

Anaerobic AKI Conditions

Bacterial strains were struck on LB streptomycin (100µg/ml) plates and used to inoculate 4mL LB deoxygenated media. After ~16h bacterial strains were concentrated and resuspended to a 1.0 OD600 anaerobically. These cultures were then used to inoculate 40mL prewarmed deoxygenated AKI media 1:5000 (8µl) which were then inverted and set to grow static at 37°C for 8h. After 8h, tubes were removed from the anaerobic chamber and 20mL volume centrifuged at 4000rpm, 4°C, for 10min. For cholera toxin analysis, 1mL of supernatant was removed and stored at -80°C. For TcpA quantification, the bacterial pellet was resuspended in Resuspension Buffer (50mM Tris-HCl pH 7.4, 50mM EDTA pH 8.0) and transferred to a 1.7mL Eppendorf tube where an equal volume of Lysis Buffer (1% SDS, 10mM Tris-HCl pH 7.4) was added. The bacterial solution was vortexed for 10s, boiled for 10min, and then stored at -80°C.

B.1.3 – *V. cholerae* Terminal Oxidase Strain M9 Glucose Growth Curves

Bacterial strains were struck on LB streptomycin (100µg/ml) and used to inoculate 4mL LB deoxygenated media. After ~16h bacterial strains were concentrated to a 1.0 OD600 anaerobically. These cultures were used to inoculate 700µl M9 0.2% Glucose 1:250 (2.8µl), vortexed, and aliquoted in triplicate 200µl volumes in a 96-well plate. Optical density was recorded every hour for the duration of the growth curve. Deoxygenated M9

0.2% Glucose was used for anaerobic growth curves and benchtop media used for aerobic growth curves.

B.1.4 – Oxidase TMPD Test Strips

Bacterial strains were tested for functional cytochrome c oxidase *cbb*$_3$ using a rapid test DrySlide containing $N_1N_1N'_1N'$-tetramethyl-*p*-phenylene-diamine dihydrochloride (Wurster's blue; TMPD). Strains were grown on LB Str100 agar media 18-24h and cell collections spotted onto DrySlide using a wooden applicator. Color was allowed to develop, and images taken.

B.1.5 – Whole Genome Sequencing Submission and Analysis

DNA of select *V. cholerae* strains was submitted to the Microbial Genome Sequencing Center (MiGS) for whole genome sequencing following sample submission guidelines. Reads were trimmed for low quality base calls and aligned to NCBI reference genome ASM1308507v1, El Tor C6706 *V. cholerae* using Geneious software to generate genome assemblies. Genomes were aligned using Mauve and genomic polymorphisms recorded.

B.1.6 – TcpA Western Protein Electrophoresis and Immunodetection

Bacterial stains were grown under standard and anaerobic AKI conditions (199). Briefly, for standard AKI conditions, 40ml of AKI media was inoculated (1:5000) with a 1.0 OD_{600} bacterial cell suspension and incubated at 37°C static for 4hr and switched to shaking for one additional hour at which point sample cell pellets were harvested. For anaerobic AKI conditions, 40ml of deoxygenated AKI media was inoculated (1:5000) with a 1.0 OD_{600} bacterial cell suspension and incubated at 37°C static for 8hr in

anaerobic conditions at which point sample cell pellets were harvested. Bacterial cell pellets were first resuspended in resuspension buffer (50mM Tris-HCl pH 7.4, 50mM EDTA pH 8.0), lysed with addition of a lysis buffer (1% SDS, 10mM Tris-HCl pH 7.4), and boiled 10 minutes. After cell lysis, the total protein concentration of each sample was measured via Bradford assay (Sigma Aldrich). Samples were subsequently diluted to a final concentration of 0.5 µg total protein/µl. Samples were loaded on an SDS page gel which contained 12.5% acrylamide and run at 120 volts for 1.5 hours. Proteins were transferred to a nitrocellulose membrane using a semi dry electroblotter (Fisher Scientific) overnight at 35 mA. Membranes were blocked with 15 ml of blocking buffer (5% non-fat milk, 2% bovine serum albumin, 0.5% Tween-20, in Tris-buffered saline) for 1 hour at room temperature. α-TcpA antibodies were diluted 1:100,000 in 5% non-fat milk and incubated with the membranes for 1 hour at room temperature. Membranes were washed three times for five minutes with Tris-buffered saline. Goat anti-Rabbit IgG-HRP antibodies (Sigma Aldrich) were diluted 1:2,000 in 5% non-fat milk in Tris-buffered saline and incubated as before. Membranes were washed three times for five minutes with Tris-buffered saline, and then incubated with SuperSignal HRP Chemiluminescence substrate (Thermo Fisher) for five minutes at room temperature. Membranes were then imaged with an Amersham Imager 600.

B.2 – Supplemental Tables and Figures

Table B.1. Whole Genome Sequencing SNP analysis annotation.

Alignment Strain	Chromosome	Name	Minimum	Maximum	Length	Change	Polymorphism Type	Locus	Protein
Ana4	1	A	1532419	1532419	1	G -> A	SNP (transition)	VC1492	Conserved Hypothetical Protein
bd-II 2B-1-1	2	CCAGAA	306,404	306,403	0	(ACCAGA)11 -> (ACCAGA)12	Insertion (tandem repeat)	VCA0283	Hypothetical Protein
bd-III 3-2-1? Large col	1		626,770	626,774	5	-GTCGA	Deletion	VC2301	ChrR; anti-sigma factor for SigE; transcriptional regulator

Table B.2. CoMPAS sequencing reads.

Sequencing Pool	Target Locus Sequence Counts				
	VC0838	VC1442	VC1844	VCA0872	VC1570
IP_1	16560	5896	13952	11529	7178
IP_2	47167	24594	44075	43971	32435
IP_3	60536	32368	51376	55351	42435
MP_1	62075	17503	3113	66325	32888
MP_2	56408	27681	5676	58797	30870
MP_3	63344	20741	4742	55125	38790

IP = Input Pool
MP = Mouse Output Pool

Table B.3. Bacteria strain list.

Strain	Description	Reference
Vibrio cholerae		
V. cholerae C6706 El Tor biotype (Wild type)	Wild type strain	Waters Lab Collection
V. cholerae ΔlacZ (VC2338)	ΔVC2338 Isogenic deletion strain	Lab Collection
V. cholerae ΔtoxT (VC0838)	ΔVC0838 Isogenic deletion strain	Waters Lab Collection
V. cholerae E7946 TND0195	ptac-TfoX ΔVC2417 ΔVC0766 ΔVC1807::Kan+	PMID: 28575400
V. cholerae E7946 TND0191	ΔVC2417 ΔVC0766 ΔVC1807::Spec+	PMID: 28575400
V. cholerae E7946 SAD030	Parent strain E7946	PMID: 28575400
V. cholerae E7946 SAD034	ΔVC1807::Kan^{r} (50ug/mL)	PMID: 28575400
V. cholerae E7946 SAD033	ΔVC1807::Spec^{r} (200ug/mL)	PMID: 28575400
V. cholerae E7946 SAD530	ΔVC1807::Tm^{r} (10ug/mL)	PMID: 28575400
V. cholerae C6706 pMMB-tfoX 1	Waters WT + Ankur SM10 strain pMMB-tfoX plasmid	This study
V. cholerae C6706 Δ501bp recJ Δ501bp xseA pMMB-tfoX 1	Waters Δ501bp recJ Δ501bp xseA + Ankur SM10 strain pMMB-tfoX plasmid	This study
Terminal oxidase mutant strains		
pKAS32-derived isogenic deletion strains		
V. cholerae Δcbb$_3$	ΔVC1439-1442	This study
V. cholerae Δbd-I	ΔVC1844-43	This study
V. cholerae Δbd-II	ΔVCA0872-73	This study
V. cholerae Δbd-III	ΔVC1571-70	This study
V. cholerae Δbd-I *Δbd*-II *Δbd*-III	+*cbb*$_3$ Strain	This study
V. cholerae Δcbb$_3$ *Δbd*-II *Δbd*-III	+*bd*-I Strain	This study
V. cholerae Δcbb$_3$ *Δbd*-I *Δbd*-III	+*bd*-II Strain	This study
V. cholerae Δcbb$_3$ *Δbd*-I *Δbd*-II	+*bd*-III Strain	This study
V. cholerae Δcbb$_3$ *Δbd*-I	+*bd*-II & + *bd*-III Strain	This study
V. cholerae Δbd-II *Δbd*-III	+*cbb*$_3$ & *bd*-I Strain	This study
V. cholerae Δcbb$_3$ *Δbd*-I *Δbd*-II Variant (+*bd*-III^{V})	+*bd*-III^{V} Variant Strain	This study
MuGENT-derived knockout strains		
V. cholerae Aero7	^{Mu}VC1442; ^{Mu}VC1844-43; ^{Mu}VCA0872-73; ^{Mu}VC1571-70	This study
V. cholerae ^{Mu}*cbb*$_3$	^{Mu}VC1442	This study
V. cholerae ^{Mu}*bd I*	^{Mu}VC1844-43	This study
V. cholerae ^{Mu}*bd II*	^{Mu}VCA0872-73	This study
V. cholerae ^{Mu}*bd III*	^{Mu}VC1571-70	This study
V. cholerae ^{Mu}*bd I* ^{Mu}*bd II* ^{Mu}*bd III*	^{Mu}+*cbb*$_3$ Strain	This study
V. cholerae ^{Mu}*cbb*$_3$ ^{Mu}*bd II* ^{Mu}*bd III*	^{Mu}*bd*-I Strain	This study
V. cholerae ^{Mu}*cbb*$_3$ ^{Mu}*bd I* ^{Mu}*bd III*	^{Mu}+*bd*-II Strain	This study
V. cholerae ^{Mu}*cbb*$_3$ ^{Mu}*bd I* ^{Mu}*bd II*	^{Mu}+*bd*-III Strain	This study
Terminal reductase mutant strains		
MuGENT-derived knockout strains		
V. cholerae Ana4	^{Mu}VC2656; ^{Mu}VCA0678; ^{Mu}VC1692; ^{Mu}VC1950	This study
V. cholerae ^{Mu}*Fum*	^{Mu}VC2656 (Fumarate reductase)	This study
V. cholerae ^{Mu}*Nit*	^{Mu}VCA0678 (Nitrate reductase)	This study
V. cholerae ^{Mu}*TMAO*	^{Mu}VC1692 (TMAO reductase)	This study
V. cholerae ^{Mu}*DMSO*	^{Mu}VC1950 (BSO reductase)	This study
V. cholerae ^{Mu}*Nit* ^{Mu}*TMAO* ^{Mu}*DMSO*	^{Mu}+Fum Strain	This study
V. cholerae ^{Mu}*Fum* ^{Mu}*TMAO* ^{Mu}*DMSO*	^{Mu}+Nit Strain	This study
V. cholerae ^{Mu}*Fum* ^{Mu}*Nit* ^{Mu}*DMSO*	^{Mu}+TMAO Strain	This study
V. cholerae ^{Mu}*Fum* ^{Mu}*Nit* ^{Mu}*TMAO*	^{Mu}+DMSO Strain	This study
Escherichia coli		
E. coli MCH100λpir pKAS32 (empty vector)	Plasmid vector strain	Lab Collection
E. coli ET12567 *ΔdapA*	Conjugation vector strain; diaminopimelic acid auxotroph	PMID: 26166710

Table B.4. Primer list.

	Primer Name	Primer Sequence (5' -> 3')	Description	Reference
MuGENT Construction Primers				
MuGENT Construction Primers	AV MuGENT Mutant Seeking F	CAAGCCGCTTAAACTGAATTAGC	Common F oligo to detect all MuGENT inactivating mutations	This study
	AV xseA MuGENT 2Kb Up F	CATATTGCGGGGCACG	*ΔrecJ* introduction from TND0195; WT repair from Waters C6706 F	This study
	AV xseA MuGENT 2Kb Down R	TTCTGGCCGCTCCATTG	*ΔrecJ* introduction from TND0195; WT repair from Waters C6706 R	This study
	AV recJ MuGENT 2Kb Up F	TTAAAGTGAGAGGCGATTCTTTTAC	*ΔxseA* introduction from TND0195; WT repair from Waters C6706 F	This study
	AV recJ MuGENT 2Kb Up R	TTATTCAATTAGTTAGTATGCATGGGG	*ΔxseA* introduction from TND0195; WT repair from Waters C6706 R	This study
	AV DOG0223 xseA 501bp Confirming Primer R	AGGATGCTGTTTATCAAGCTTGTG	R to detect exoVII 501bp mutation in Vc – 449bp Fragment	PMID: 28575400
	AV VC2417 recJ 501bp Confirming Primer R	CAGTTGCAAACGCTCACAAAAC	R to detect recJ 501bp mutation in Vc – 550bp Fragment	This study
Terminal oxidase primers	AV VC1442 cbb3 Gene Inactivation Primer F	GTGGTGTTACGACGAAAGTCGTGTTGGAAGTAAAAGTGTA caagccgcttaaactgaattagcAACAAAACTACAACTATACCGTGGTC	F to create VC1442 knockout	This study
	AV VC1442 cbb3 Gene Inactivation Primer R	TGCCGTCTTGATAAGCCAAACG	R to create VC1442 knockout	This study
	AV VC1844 Gene Inactivating Primer F	GTTGCAACAACAAATTTTTTTTGTAGCAAAGTGTTATAGT caagccgcttaaactgaattagcGACACAAAGGAGTTACCATGATCG	F to create VC1844 knockout	This study
	AV VC1844 Gene Inactivating Primer R	AACGCCAGCGTTACCTAAAC	R to create VC1844 knockout	This study
	AV VC1843 Gene Inactivating Primer F	GTCTGTTCAGGATCAAGTCAACCGCCAAGTTGAAGCATAA caagccgcttaaactgaattagcGGTGGGTACTGATTGGTGTG	F to create VC1843 knockout	This study
	AV VC1843 Gene Inactivating Primer R	TATGGGCTGATGGAACCGAC	R to create VC1843 knockout	This study
	AV VCA0872 Gene Inactivating Primer F	CACTTCAAAAGCTGTGCTGAAATGCCTTCCAATTCTTGAT caagccgcttaaactgaattagcAATTATCGCGTTTGCAGTTCG	F to create VCA0872 knockout	This study
	AV VCA0872 Gene Inactivating Primer R	CTGGATGTCGCATCCCAC	R to create VCA0872 knockout	This study
	AV VCA0873 Gene Inactivating Primer F	TTATACGAGCATAAGTTGGCACAACAAGTACAATATTAGG caagccgcttaaactgaattagcGGCTGATCGGTGCATTGC	F to create VCA0873 knockout	This study
	AV VCA0873 Gene Inactivating Primer R	TCCAGCTCGAGCCTTCTG	R to create VCA0873 knockout	This study
	AV VC1571 Gene Inactivating Primer F	TAAAGATGGTGGTTAGTGTTAACCCCATCACTGGTTTGTT caagccgcttaaactgaattagcTCCAATTCGCTGCCAATATCAG	F to create VC1571 knockout	This study
	AV VC1571 Gene Inactivating Primer R	ACCATTATCGTCGTCACTCATG	R to create VC1571 knockout	This study
	AV VC1570 Gene Inactivating Primer F	ACCGCAAGTTTCACCAAGCTCTACAAAGGCCGCGTTATAA caagccgcttaaactgaattagcTTATGTACGCGGTGTTGGATG	F to create VC1570 knockout	This study
	AV VC1570 Gene Inactivating Primer R	GCACACGAATTTACGGTGATC	R to create VC1570 knockout	This study
	AV VC1442 cbb3 Conf Prmr New R	TGC GAA CAG CAC GAG AGA C	Mutant Verification Primer - 850bp Fragment	This study
	AV VC1844 bd I Conf Prmr New R	ATA GTG GCC ATA CTG TTG GG	Mutant Verification Primer - 1200bp Fragment	This study
	AV VC1843 bd I Conf Prmr New R	TAG CGT CAG CTT GCT TGA AG	Mutant Verification Primer - 1000bp Fragment	This study
	AV VCA0872 bd II Conf Prmr New R	CGA GCA ACG GTG ACT ATG AG	Mutant Verification Primer - 1500bp Fragment	This study
	AV VCA0873 bd II Conf Prmr New R	AAA TGG TAT GCG AGC GTG ATC	Mutant Verification Primer - 1350bp Fragment	This study
	AV VC1571 bd III Conf Prmr New R	CAC CAA GAT CTG CAC AGG AAT C	Mutant Verification Primer - 700bp Fragment	This study
	AV VC1570 bd III Conf Prmr New R	AGG AAA ACT AAA CCA ACG TTC TGC	Mutant Verification Primer - 625bp Fragment	This study
Terminal reductase primers	AV VC1950 BSO Gene Inactivating Primer F	TCTTCCAGCACCATGCCAAAGATATGGTTAGCCACTGAGT caagccgcttaaactgaattagcTAAAAGGCACTGGTATGGCTGCCGGTG	F to create VC1950 knockout	This study
	AV VC1950 BSO Gene Inactivating Primer R	AAAGCAGCAAGTCGGTTAAGAAC	R to create VC1950 knockout	This study
	AV VC1692 TMAO Gene Inactivating Primer F	AAAACACTCTTCAGATTTCGCTGAAGGCCACCACTAAGCA caagccgcttaaactgaattagcAAGGTGTCGCAACCACCAG	F to create VC1692 knockout	This study
	AV VC1692 TMAO Gene Inactivating Primer R	GCTGGCTTGAGGGATAACG	R to create VC1692 knockout	This study
	AV VC2656 Fumarate Gene Inactivating Primer F	TTGAAAACTCTAGGTACTGAAACGAACTCAGTCCATAAAA caagccgcttaaactgaattagcTCGCAGTCATCGGCGC	F to create VC2656 knockout	This study
	AV VC2656 Fumarate Gene Inactivating Primer R	CTGGGTTCAACATCGCG	R to create VC2656 knockout	This study
	AV VCA0678 Nitrate Gene Inactivating Primer F	CACTGGAAATACCTTTTCTGAACTCGAGGGTAATGTATAA caagccgcttaaactgaattagcCGGCGGTTGCAGGGATC	F to create VCA0678 knockout	This study
	AV VCA0678 Nitrate Gene Inactivating Primer R	GCTTAATACTTGGTCTGGGCTG	R to create VCA0678 knockout	This study
	AV VC1950 BSO Confirming Primer R	CGCCCGCCATACTCATATAG	Mutant Verification Primer - 500bp Fragment	This study
	AV VCA0678 Nitrate Conf Prmr New R	GAC ATC ACT TTG GTG TTT GGA TC	Mutant Verification Primer - 1200bp Fragment	This study
	AV VC1692 Conf Prmr 700bp	AGA CTG GTG CGT TTC ACA G	Mutant Verification Primer - 700 bp Fragment	This study
	AV VC2656 Fumarate Confirming Primer R	ACAGATAAATGGCAGACGTTCTTG	Mutant Verification Primer - 1000bp Fragment	This study

Table B.4 (cont'd)

CoMPAS MASC-Primer Set				
Multiplex Allele-Specific PCR Sequencing Primers	AV 6-48 MuGENT AmpSeq F	ACACTGACGACATGGTTCTACACAAGCCGCTTAAACTGAATTAGC	MuGENT Mutant Seeking Amplicon Sequencing Primer F	This study
	AV VC1442 AmpSeq 125R	TACGGTAGCAGAGACTTGGTCTCTAATTGAGCGGCAATCAAAAC	VC1442 Amplicon Sequencing Primer R 125bp	This study
	AV VC1844 AmpSeq 125R	TACGGTAGCAGAGACTTGGTCTTCCCTAGAGTGAGGGGAAC	VC1844 Amplicon Sequencing Primer R 125bp	This study
	AV VCA0872 AmpSeq 125R	TACGGTAGCAGAGACTTGGTCTAAATCGACTCCATGATAGCGAG	VCA0872 Amplicon Sequencing Primer R 125bp	This study
	AV VC1571 AmpSeq 125R	TACGGTAGCAGAGACTTGGTCTGTGTTCGTAAATAACGCCATTTG	VC1571 Amplicon Sequencing Primer R 125bp	This study
	AV VC0838 toxT AmpSeq 125F	ACACTGACGACATGGTTCTACAGTTCACTAAAATCTTACATTCTTGGTG	VC0838 toxT Amplicon Sequencing Primer F 125bp	This study
	AV VC0838 toxT AmpSeq 125R	TACGGTAGCAGAGACTTGGTCTACCATTTACCACTTCAGAAAGG	VC0838 toxT Amplicon Sequencing Primer R 125bp	This study
pKAS32 Mutant Construction Primers				
Terminal oxidase pKAS32 primers	AV VC1844_43 1Kb Up F	gtggaattcccgggagagctGTGAAGGCCCAGCTGCAC	pKAS bd I Deletion Construct Upstream 1Kb Fragment	This study
	AV VC1844_43 1Kb Up R	tgagcgtccAGAACAACAATTACAATGTTAAAAAAACTATAACACTTTGC	pKAS bd I Deletion Construct Upstream 1Kb Fragment	This study
	AV VC1844_43 1Kb Dwn F	ttgttgtctGGAGCGCTCATTATGTGG	pKAS bd I Deletion Construct Downstream 1Kb Fragment	This study
	AV VC1844_43 1Kb Dwn R	tgcgcatgctagctatagttGTCACTGCAGTTTAACTCC	pKAS bd I Deletion Construct Downstream 1Kb Fragment	This study
	AV VC1844_43 Seq F 1Kb Up	TGTTCTTGAGCCATTTCTCATT	pKAS bd I Deletion Construct Sequencing Primer F	This study
	AV VC1844_43 Seq R 1Kb Dwr	CGTGCAATGTTTTCTTACCTAATGA	pKAS bd I Deletion Construct Sequencing Primer R	This study
	AV VC1844_43 >1Kb Up F (2)	TGGAAAAAGCGGGAGATTTAGC	pKAS bd I Genome Deletion Verification Primer F	This study
	AV VC1844_43 >1Kb Dwn R (2	AAAGCGGTCTTCAAAGGTATC	pKAS bd I Genome Deletion Verification Primer R	This study
	AV VCA0872_73 1Kb Up F	gtggaattcccgggagagctTATGCTTACAATCTTGCAC	pKAS bd II Deletion Construct Upstream 1Kb Fragment	This study
	AV VCA0872_73 1Kb Up R	gcgaatacctCCATCGTAAGATGGCTTTAC	pKAS bd II Deletion Construct Upstream 1Kb Fragment	This study
	AV VCA0872_73 1Kb Dwn F	cttacgatggAGGTATTCGCATGTGGTATTTC	pKAS bd II Deletion Construct Downstream 1Kb Fragment	This study
	AV VCA0872_73 1Kb Dwn R	tgcgcatgctagctatagttTCAGCATGAGCAAATAGC	pKAS bd II Deletion Construct Downstream 1Kb Fragment	This study
	AV VCA0872_73 Seq F 1Kb Up	GCAGCATCCCGATCCAG	pKAS bd II Deletion Construct Sequencing Primer F	This study
	AV VCA0872_73 Seq R 1Kb Dv	GTCACTAAGTGCTCGTTTTACTA	pKAS bd II Deletion Construct Sequencing Primer R	This study
	AV VCA0872_73 >1Kb Up F	TGGCAGCCAAACGCTAAG	pKAS bd II Genome Deletion Verification Primer F	This study
	AV VCA0872_73 >1Kb Dwn R	GTGAGTGATGAGAATGATGTGAAG	pKAS bd II Genome Deletion Verification Primer R	This study
	AV VC1570_71 1Kb Up F	gtggaattcccgggagagctGAGTTTGTGCTTGATAAAG	pKAS bd III Deletion Construct Upstream 1Kb Fragment	This study
	AV VC1570_71 1Kb Up R	gtagtaaaggCTCTTTTCCTCAAAAAATGAAAC	pKAS bd III Deletion Construct Upstream 1Kb Fragment	This study
	AV VC1570_71 1Kb Dwn F	aggaaaagagCCTTTACTACACTTGAATCCAAAC	pKAS bd III Deletion Construct Downstream 1Kb Fragment	This study
	AV VC1570_71 1Kb Dwn R	tgcgcatgctagctatagttAATTGCCGGCTTAGGTGTG	pKAS bd III Deletion Construct Downstream 1Kb Fragment	This study
	AV VC1570_71 Seq F 1Kb Up	TTATTATCACATTACTGCTGATTGC	pKAS bd III Deletion Construct Sequencing Primer F	This study
	AV VC1570_71 Seq R 1Kb Dwr	GCGATCCGCAATCAAAAG	pKAS bd III Deletion Construct Sequencing Primer R	This study
	AV VC1570_71 >1Kb Up F	GCCGCTTGTTTAATGTAGGC	pKAS bd III Genome Deletion Verification Primer F	This study
	AV VC1570_71 >1Kb Dwn R	GCAACCCCCAATACCATTCG	pKAS bd III Genome Deletion Verification Primer R	This study
	AV cbb3 1Kb Up F	gtggaattcccgggagagctGAGATCAATGCCGTGCCG	pKAS cbb3 Deletion Construct Upstream 1Kb Fragment	This study
	AV cbb3 1Kb Up R	tattagaatgGCTTCCAATGTTTAATTAACTACACTTTTAC	pKAS cbb3 Deletion Construct Upstream 1Kb Fragment	This study
	AV cbb3 1Kb Dwn F	cattggaagcCATTCTAATAACAGCCCC	pKAS cbb3 Deletion Construct Downstream 1Kb Fragment	This study
	AV cbb3 1Kb Dwn R	tgcgcatgctagctatagttTTGAGCTAATACATGGCTTAG	pKAS cbb3 Deletion Construct Downstream 1Kb Fragment	This study
	AV cbb3 Seq F 1Kb Up	GACTGGAATTCCGTCGAAC	pKAS cbb3 Deletion Construct Sequencing Primer F	This study
	AV cbb3 Seq R 1Kb Dwn	CGTTGGAGAAGAGGGGAAG	pKAS cbb3 Deletion Construct Sequencing Primer R	This study
	AV cbb3 >1Kb Up F (2)	GCATGCAAAAGCACAAGAC	pKAS cbb3 Genome Deletion Verification Primer F	This study
	AV cbb3 >1Kb Dwn R (2)	CAAGTATGTTTTCATGGCATCG	pKAS cbb3 Genome Deletion Verification Primer R	This study
	pKAS32 Multiple Cloning Site Se	GCCTCTAAGGTTTTAAGTTT	pKAS32 specific sequencing primer	Lab Collection
	pKAS32 Multiple Cloning Site Se	CTTTCAAGGTAGCGGTTACC	pKAS32 specific sequencing primer	Lab Collection
RT-qPCR Primer Sets				
recA VC0543	*recA* qPCR F	GGGTAACCTCAAGCAATCCA	qPCR Primer	PMID: 32873763
	recA qPCR R	CCACTCTTCGCCTTCTTTG	qPCR Primer	PMID: 32873763
cbb3 VC1442	cbb3 qPCR F	ACAAGTGCCCTGTTTGCAAC	qPCR Primer	This study
	cbb3 qPCR F	AAGGTGATTGCAGCGGAAAC	qPCR Primer	This study
bd I VC1844	bd I qPCR F	AGTTTGTTCACACCGTTGCG	qPCR Primer	This study
	bd I qPCR F	TGATGCCGCAATCGCAAATG	qPCR Primer	This study
bd II VCA0872	bd II qPCR F	TGGTCACGCTTGTCAAAACG	qPCR Primer	This study
	bd II qPCR F	TGCATCCAACCGTTTGCAAC	qPCR Primer	This study
bd III VC1571	bd III qPCR F	TTGGTGTGATGCTGTTTGGC	qPCR Primer	This study
	bd III qPCR F	AGCACCAGAATCCAAAACGC	qPCR Primer	This study

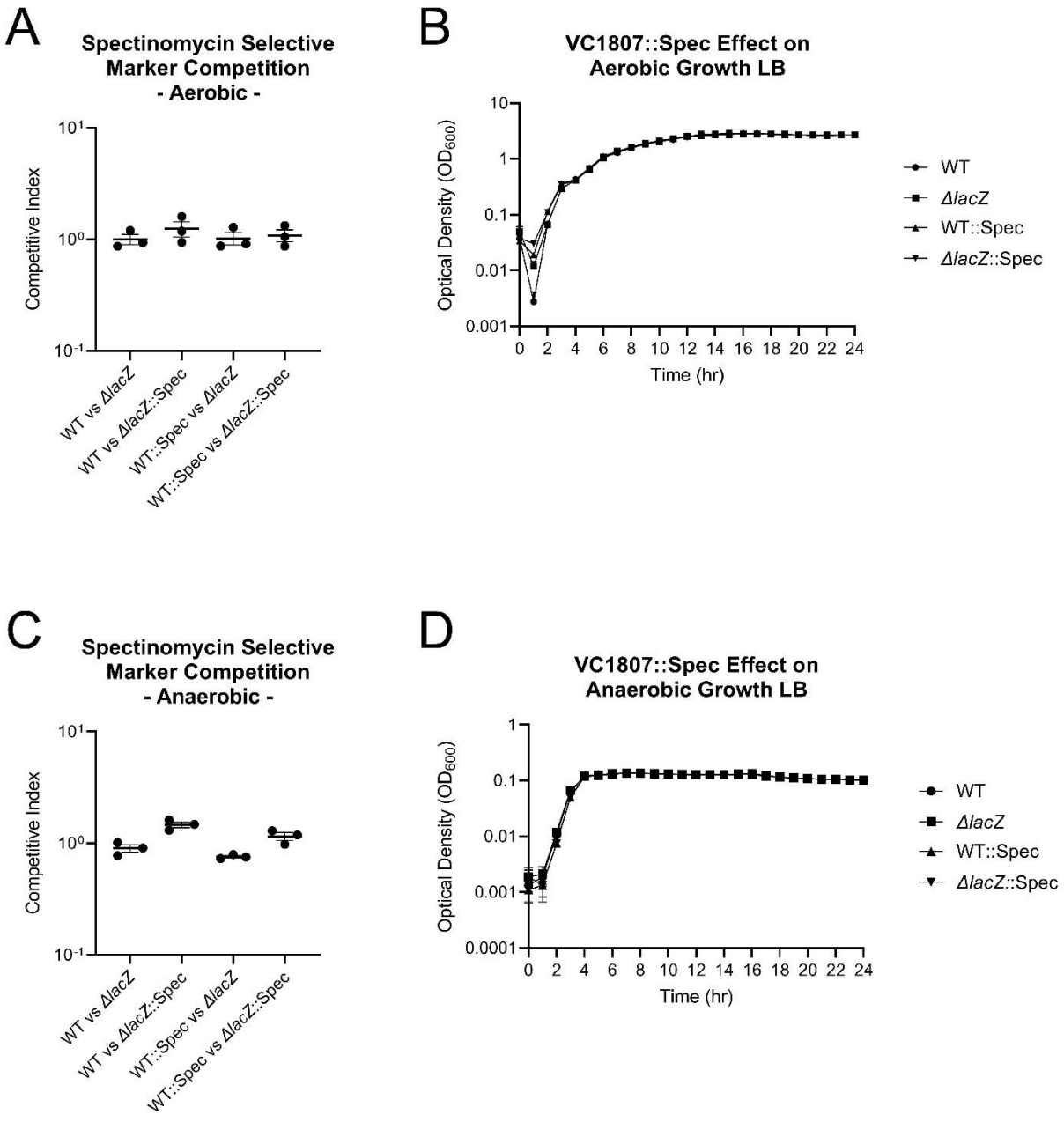

Figure B.1. MuGENT spectinomycin selective marker shows no fitness defect in vitro. Comparison of wild type and Δ*lacZ* C6706 *V. cholerae* strains with and without MuGENT spectinomycin selective marker in pseudogene VC1807. (A) Aerobic in vitro competition assay after 20h. (B) Aerobic growth curve assay. (C) Anaerobic in vitro competition assay after 20h. (D) Anaerobic growth curve assay. All assays were performed in LB media. Bars in in vitro competitions represent the arithmetic mean where error bars represent the standard error of the mean. Growth curves are an average of three biological replicates where error bars represent the standard error of the mean.

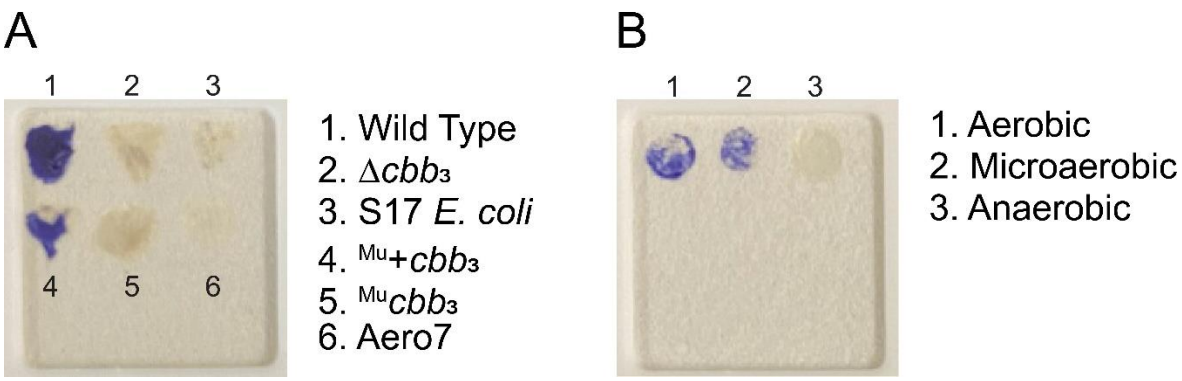

Figure B.2. *cbb*$_3$ deficient strains and wild type grown anaerobically do not maintain a functional *cbb*$_3$ oxidase complex. *V. cholerae* cultures were grown on LB agar plates and spotted onto a rapid test DrySlide containing $N_1N_1N'_1N'$-tetramethyl-*p*-phenylene-diamine dihydrochloride (Wurster's blue; TMPD) that turns blue when reduced by cytochrome c oxidases. (A) *V. cholerae cbb*$_3$ mutant strain spots and *E. coli* (cytochrome c deficient) control. (B) Wild type *V. cholerae* grown in aerobic, microaerobic, and anaerobic conditions.

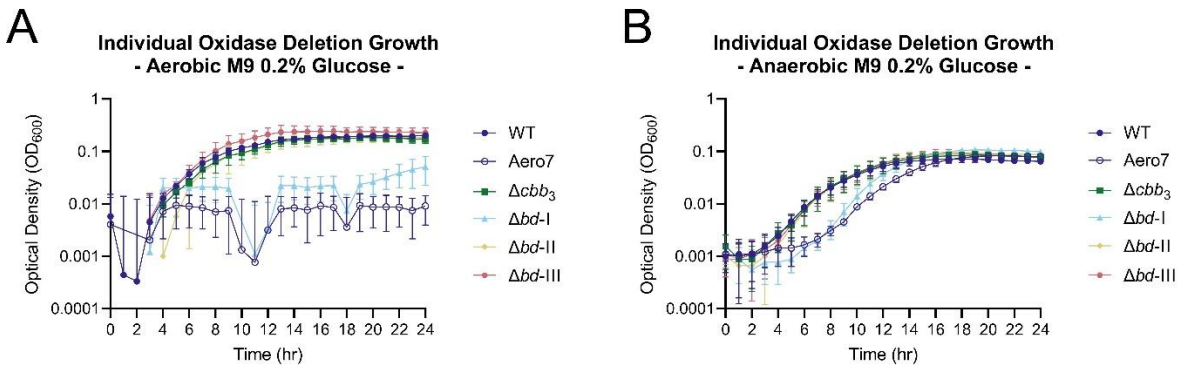

Figure B.3. *V. cholerae* oxidases generally support the same pattern of growth in minimal M9 0.2% D-glucose media as seen in LB. (A-B) Single terminal oxidase deletion mutants grown in M9 0.2% D-glucose, aerobically and anaerobically, respectively. Inoculums for all growth experiments were prepared in anaerobic conditions. Growth curves are an average of three biological replicates where error bars represent the standard error of the mean.

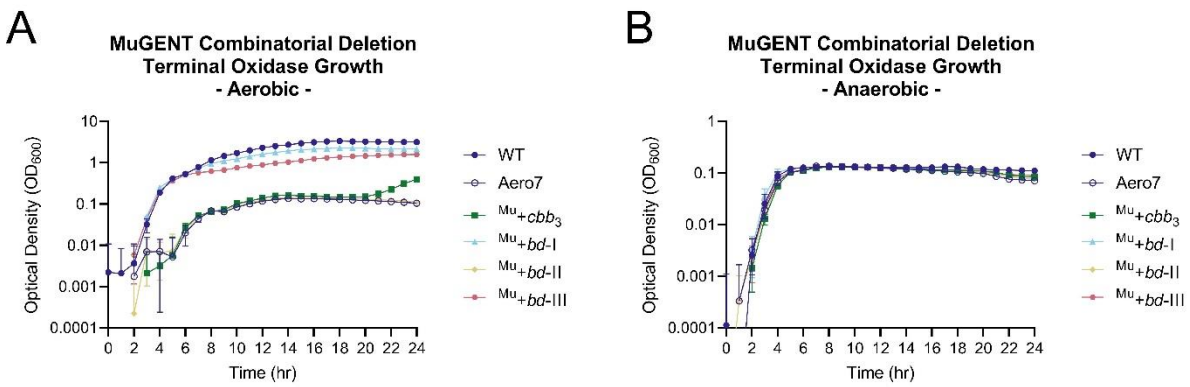

Figure B.4. *V. cholerae* oxidases generally support the same pattern of growth in combinatorial MuGENT knockout strains. (A-B) Combinatorial terminal oxidase deletion mutant growth in LB. Inoculums were prepared anaerobically and subsequently grown in aerobic and anaerobic conditions, respectively. Triple deletion mutant strains have a '+' with an oxidase name (e.g. +*cbb*$_3$), indicating the sole remaining oxidase, with the other three oxidases disrupted by mutation. Growth curves are an average of three biological replicates where error bars represent the standard error of the mean.

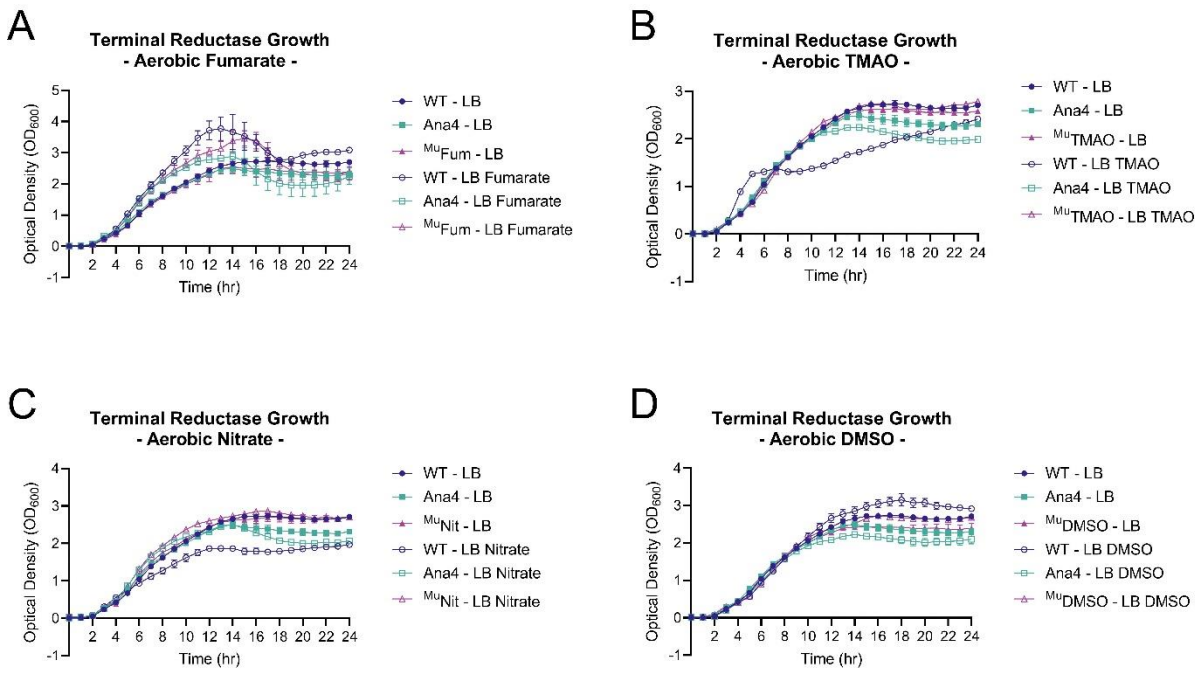

Figure B.5. Terminal reductase mutants are variable for aerobic growth in the presence of cognate electron acceptor molecules. *V. cholerae* terminal reductase aerobic growth characteristics in LB in the presence and absence of alternative electron acceptors (A) 50mM fumarate, (B) 50mM trimethylamine-N-oxide (TMAO), (C) 50mM nitrate, and (D) 50mM dimethyl sulfoxide (DMSO). Inoculums were prepared aerobically. Closed symbols indicate LB growth media lacked an alternative electron acceptor whereas open symbols indicate LB growth media was supplemented with a given alternative electron acceptor. Growth curves are an average of three biological replicates where error bars represent the standard error of the mean.

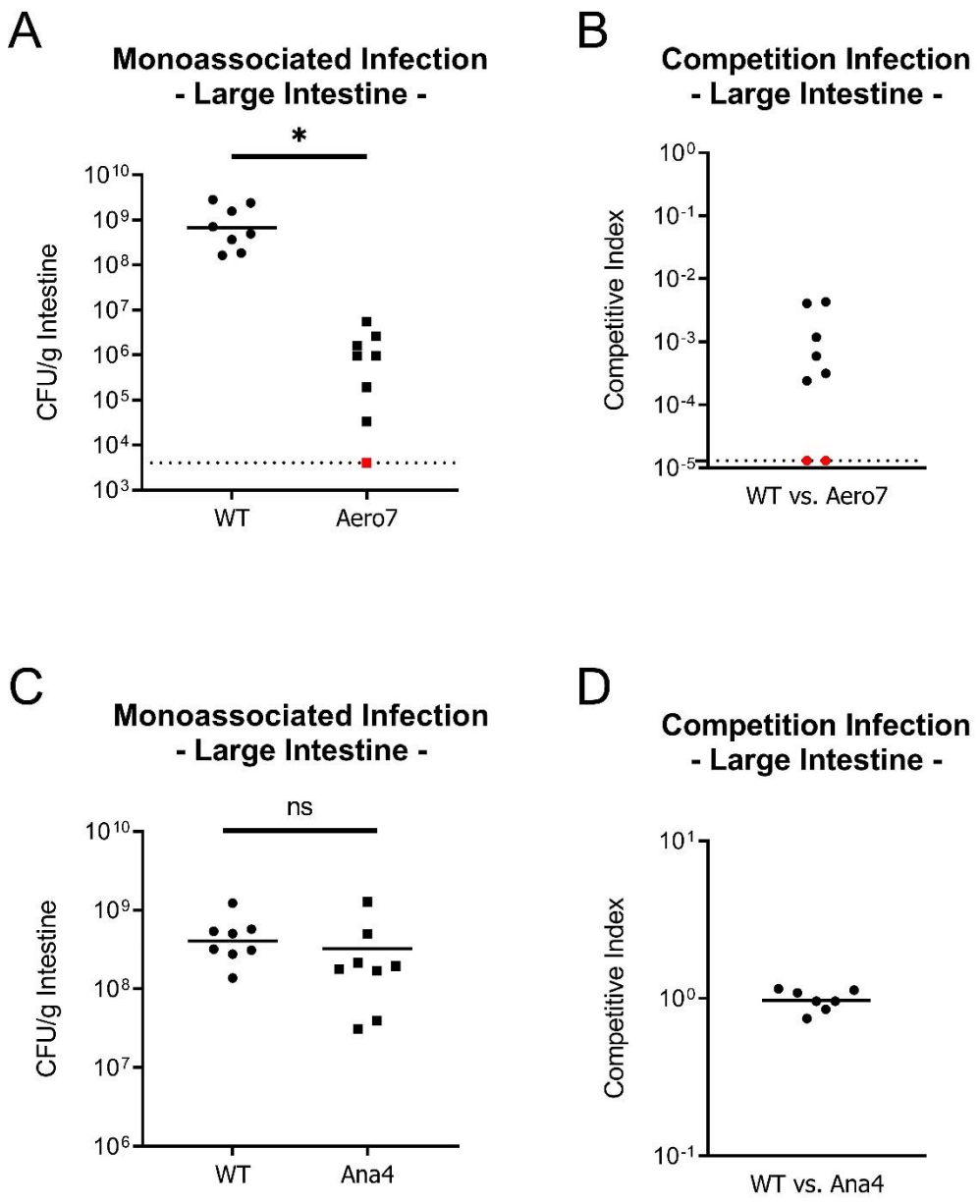

Figure B.6. Functional terminal oxidases, but not alternative terminal reductases, are required for optimal colonization of the large intestine. Aero7 and Ana4 colonization of the large intestine in both monoassociated and competition infections. (A) Monoassociated infection of strain Aero7. (B) Competition infection of strain Aero7. (C) Monoassociated infection of strain Ana4. (D) Competition infection of strain Ana4. Bars represent the geometric mean. Horizontal dashed lines indicate the limit of detection (LOD) and red dots indicate recovered CFUs were below the LOD. Competitive index scores were calculated as [($Mutant_{Output}/WT_{Output}$) / ($Mutant_{Input}/WT_{Input}$)]. Statistical analysis was performed using GraphPad PRISM. *, $P < 0.05$. A Mann-Whitney U-test was used in the determination of significance between WT and Aero7. A Student's T-test was performed on log transformed data in the determination of signifance between WT and Ana4.

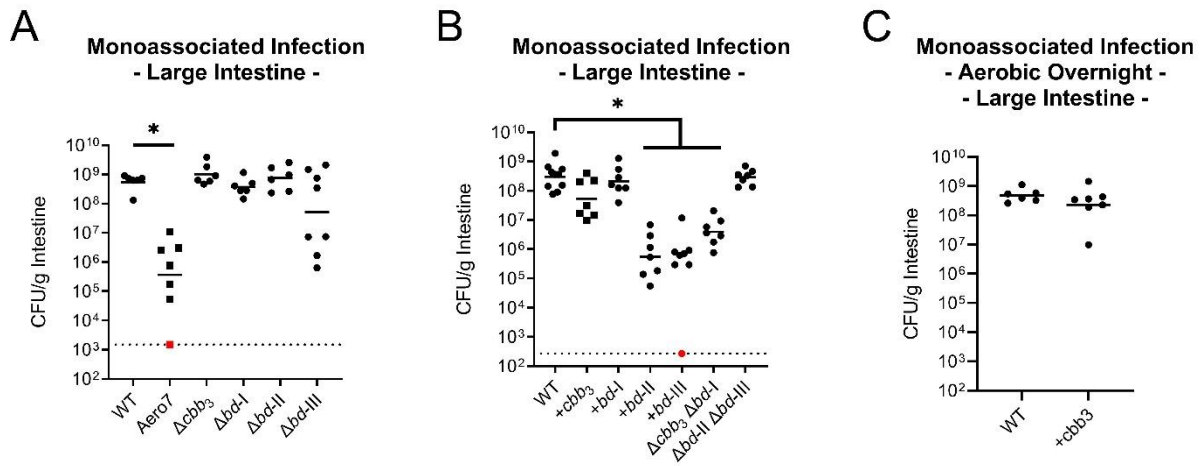

Figure B.7. Individual and combinatorial oxidase mutants colonize the large intestine more efficiently than the small intestine but reflect overall colonization patterns present in the small intestine. Monoassociated *in vivo* colonization assays in the large intestine for (A) single and (B) combinatorial oxidase deletion strains. Triple deletion mutant strains have a '+' with an oxidase name (e.g. +*cbb*$_3$), indicating the sole remaining oxidase, with the other three oxidases disrupted by mutation. Bars represent the geometric mean. Horizontal dashed lines indicate the limit of detection (LOD) and red dots indicate recovered CFUs were below the LOD. Statistical analysis was performed using GraphPad PRISM. *, $P < 0.05$. A Mann-Whitney U-test was used in the determination of significance between WT and Aero7 and WT and +*bd*-III whereas an Analysis of Variance with post-hoc Dunnett's multiple comparisons test was conducted on log transformed CFU/g intestine for all other strain comparisons.

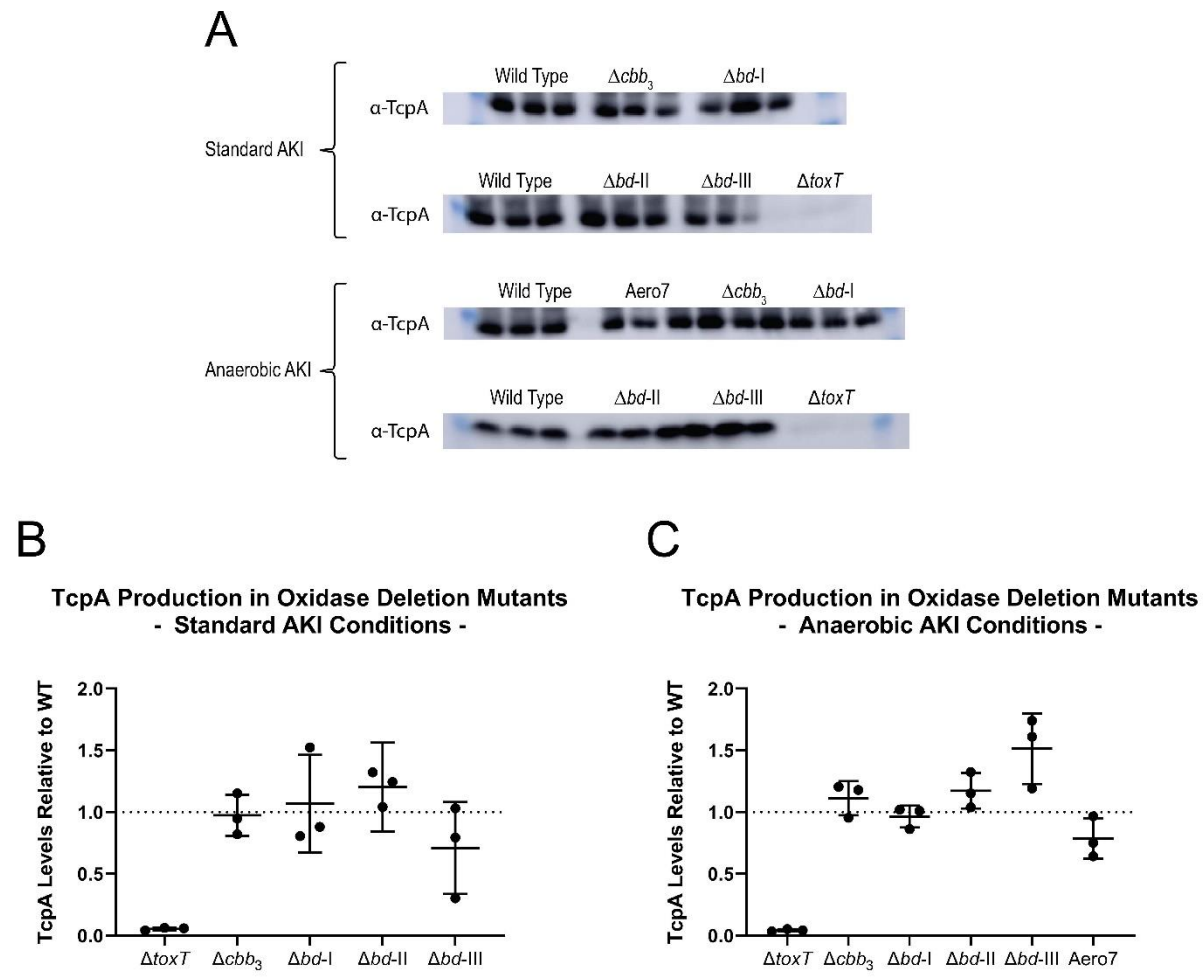

Figure B.8. TcpA production is functional in individual oxidase deletion mutants. (A) Western blot visualization of TcpA, a required virulence factor in *V. cholerae* pathogenesis, in both standard and anaerobic AKI conditions. (B) Densitometry analysis of TcpA production in standard AKI conditions. (C) Densitometry analysis of TcpP production in anaerobic AKI conditions. TcpA levels are displayed as relative to TcpA production in wild type cells. ImageJ was used to perform the densitometry analysis across three biological replicates. Horizontal bars represent the arithmetic mean where error bars represent the standard deviation of the mean.

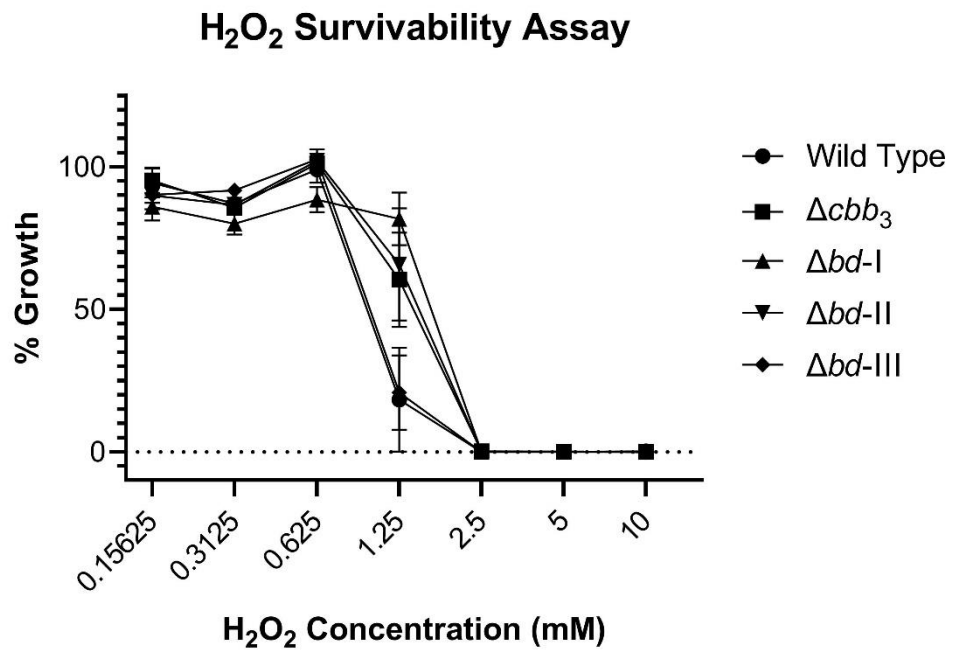

Figure B.9. Terminal oxidase complexes are not required for cell survival under hydrogen peroxide stress. Minimum inhibitory concentration determination of individual oxidase deletion strains. Growth percentage was calculated as a function of optical density for test strains in various concentrations of H_2O_2 (0.15625mM, 0.3125mM, 0.625mM, 1.25mM, 2.5mM, 5mM, and 10mM) divided by the optical density for wild type *V. cholerae* grown in LB media without H_2O_2. All strains showed signs of growth reduction at 1.25mM H_2O_2 and were all entirely inhibited for growth at 2.5mM H_2O_2. Data points represent the arithmetic mean of three biological replicates with error bars representing the standard error of the mean.

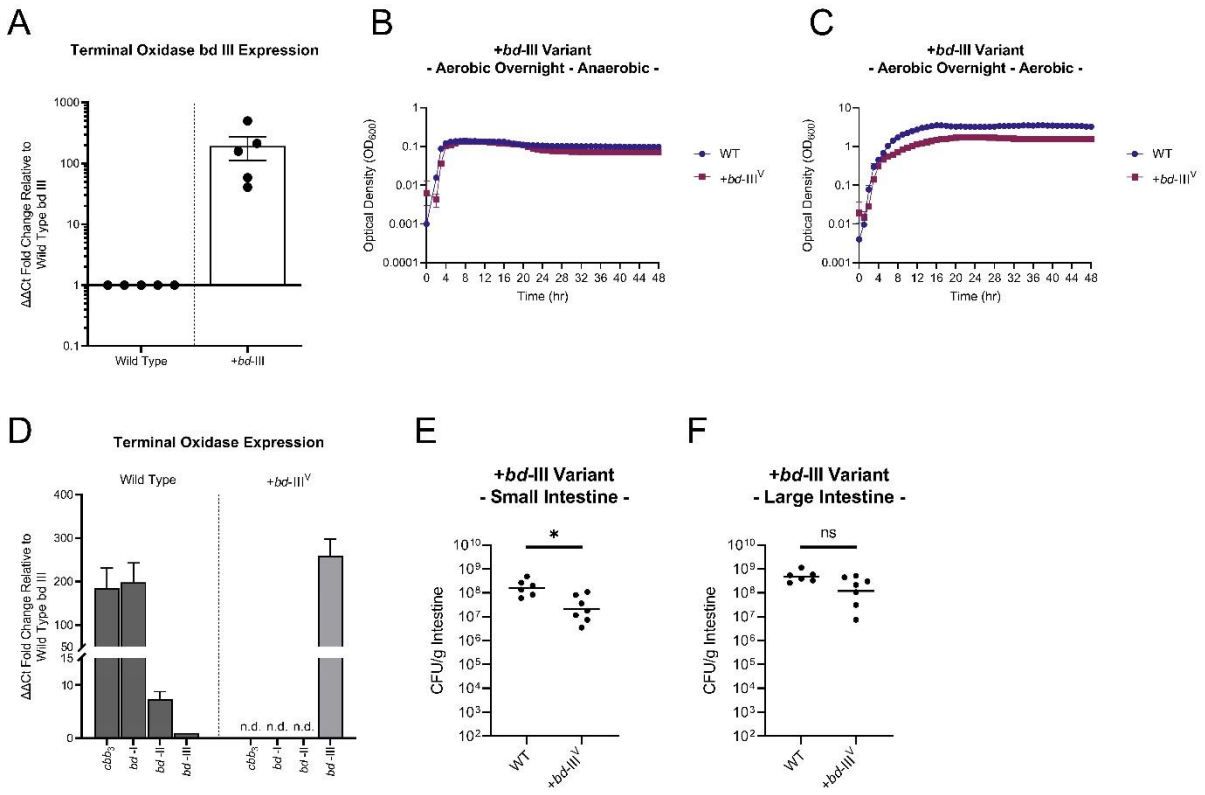

Figure B.10. Variant +*bd*-III strain (+*bd*-III^V) indicates that the *bd*-III oxidase, when expressed, is capable of supporting aerobic respiration in *V. cholerae* and colonization of the infant mouse. (A) Wild type and +*bd*-III strain (Δ*cbb*$_3$ Δ*bd*-I Δ*bd*-II) *bd*-III expression. Expression was determined for the primary subunit of the *bd*-III oxidase VC1571. Dots represent biological replicates of relative *bd*-III expression between +*bd*-III and wild type strains. Bars represent arithmetic mean with error bars representing the standard error of the mean. (B-C) Wild type and +*bd*-III^V growth in LB. Inoculums were prepared aerobically and subsequently grown in aerobic and anaerobic conditions, respectively. Data points represent the mean of triplicate growth curves with error bars representing the standard error of the mean. (D) *In vitro* expression of terminal oxidases in +*bd*-III^V strain. Expression was determined for the primary subunit of each oxidase complex (VC1442, VC1844, VCA0872, VC1571). Bars represent the arithemtic mean with error bars representing the standard error of the mean. (E) Monoassociated infection of +*bd*-III^V in the small intestine. (F) Monoassociated infection of +*bd*-III^V in the large intestine. Bars in monoassociated infections represent the geometric mean.

APPENDIX C

Investigating the Mucin Response Network of Shiga-toxin Producing *Escherichia coli* (STEC)

C.1 – Introduction

STEC causes disease in the large intestine of infected human hosts (290). Virulence factors encoded on the Locus of Enterocyte Effacement (LEE) of STEC stimulate the remodeling of actin filaments, forming a pedestal on host epithelial cells (291). STEC produces Shiga toxin (Stx), an AB_5 class toxin that binds to the vascular epithelium. Stx kills host cells which leads to bloody diarrhea among other disease symptoms (292). Translocation of Stx to the kidney can cause hemolytic uremic syndrome, the most severe complication associated with STEC infection (293).

Within the human intestine, the mucosal barrier functions as a barrier to infection and is composed of a loose and dense mucus layer in the large intestine (294). To be successful in causing disease, STEC has evolved mechanisms to bypass both layers of mucus and gain access to the host epithelium. Through a literature review, a collection of gene targets that comprise the STEC “mucin response network” has been generated (Table C.1). Genes part of this list are involved in mucin sugar metabolism, mucin cell signaling, and mucin degradation (mucinases). Previous work has shown sugar constituents of mucin to contribute to pathogenesis of STEC (295, 296). The LEE1 operon which encodes the LEE regulator *ler* has been shown to be controlled by sugar signaling (297). NagC and FusR act as transcriptional repressors of the LEE1 operon in the presence of *N*-acetylglucosamine (GlcNAc) and fucose, respectively, both constituents of host mucin (295, 296). This interaction leads to spatial control over the activation of virulence factor production in STEC within the intestinal tract to activate virulence factors nearer the host epithelium. The outer loose mucus layer contains

many free mucin constituents, such as GlcNAc and fucose, whereas the inner dense mucus layer contains fewer free sugars, leading to the de-repression of the LEE1 operon near the site of infection (295, 296).

Table C.1. Shiga toxin-producing *E. coli* mucin response network.

Shiga toxin-producing *Escherichia coli* O157:H7 str. EDL933			
Mucin Response Protein	**Gene Name**	**Function/Pathway**	**Reference**
Mucinase	stcE (pO157)	Mucinase	(298)
	sulfatase (Z2210)	Mucinase	(295)
Transcriptional Regulators	fusK (Z0462)	Fucose	(296)
	fusR (Z0463)	Fucose	(296)
	galR (Z4155)	Galactose	(299)
	galK (Z0927)	Galactose	(300)
	agaR (Z4483)	N-acetylgalactosamine, N-galactosamine	(301)
	nagC (Z0823)	N-acetylglucosamine	(295)
	mlc (Z2587)	Mannose	(302)
	nanR (Z4584)	Neuraminic acid	(303)
Metabolic Pathways	agaS (Z4490)	N-acetylgalactosamine, Galactosamine	(301)
	nagE (Z0826)	N-acetylglucosamine	(300)
	fucA (Z4117)	Fucose	(300)
	manA (Z2616)	Mannose	(300)
	manX (Z2860)	Mannose	(302)
	nanA (Z4583)	Neuraminic acid	(300)

The purpose of this research was to primarily identify variations in the sequence profiles among STEC isolates. We hypothesized that changes in the mucin response network may be important for disease onset and disease outcome as mucin signaling has shown to be important for pathogen virulence (295, 296). Genotypic variation in STEC isolates may provide a deeper understanding of specific bacterial response pathways that are influential in causing disease and may be useful indicators for disease severity.

C.2 – Results

A subset of published NCBI STEC genomes were analyzed for the presence of mucin response genes and for sequence variation among isolates. This collection included both O157 and non-O157 STEC isolates. Sequences for each mucin response gene listed in Table C.1 were aligned between isolates using *E. coli* K-12 as an outgroup comparison. Each gene sequence was aligned with MUSCLE in MEGA7 and phylogenetic maximum likelihood trees were constructed using 500 bootstrap replications. Maximum likelihood trees for each mucin response gene are depicted in Figures C.1-C.14. Initial analysis indicates STEC serogroups group together for all mucin response genes tested. In a number of genomic sequences, target genes exhibited sequence variation which may become targets of future investigation to determine changes to protein function and eventual disease outcome.

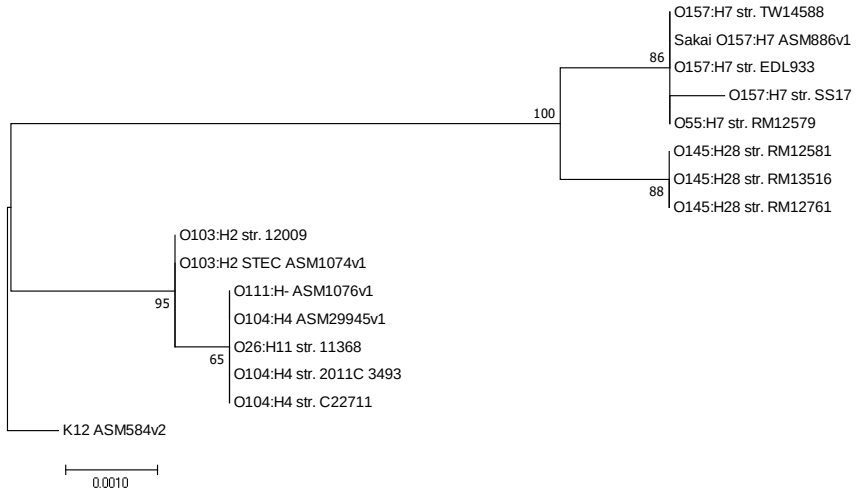

Figure C.1. Maximum likelihood tree of the STEC sulfatase Z2210 mucin response gene. The evolutionary history was inferred using Maximum Likelihood method based on the Tamura-Nei model. The highest likelihood tree is shown. The tree was constructed using a 500 bootstrap replication.

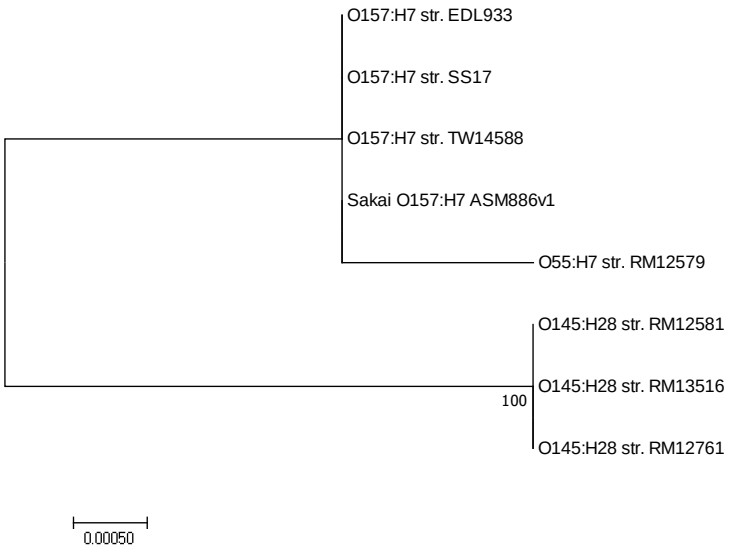

Figure C.2. Maximum likelihood tree of STEC mucin response gene *fusK*. The evolutionary history was inferred using Maximum Likelihood method based on the Tamura-Nei model. The highest likelihood tree is shown. The tree was constructed using a 500 bootstrap replication.

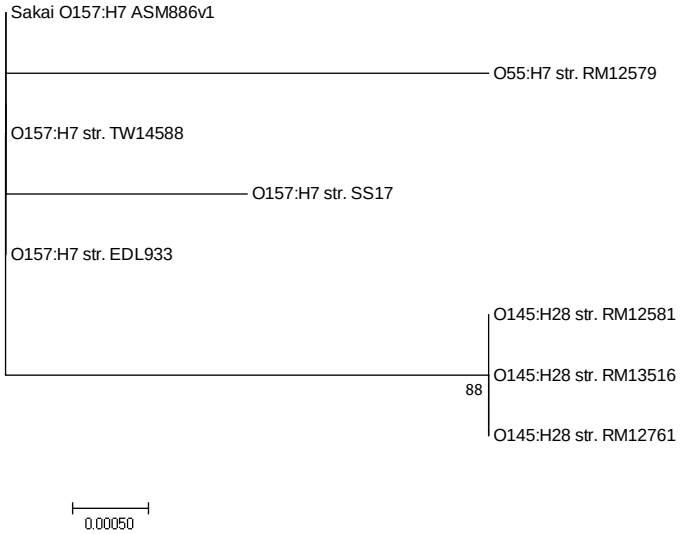

Figure C.3. Maximum likelihood tree of STEC mucin response gene *fusR*. The evolutionary history was inferred using Maximum Likelihood method based on the Tamura-Nei model. The highest likelihood tree is shown. The tree was constructed using a 500 bootstrap replication.

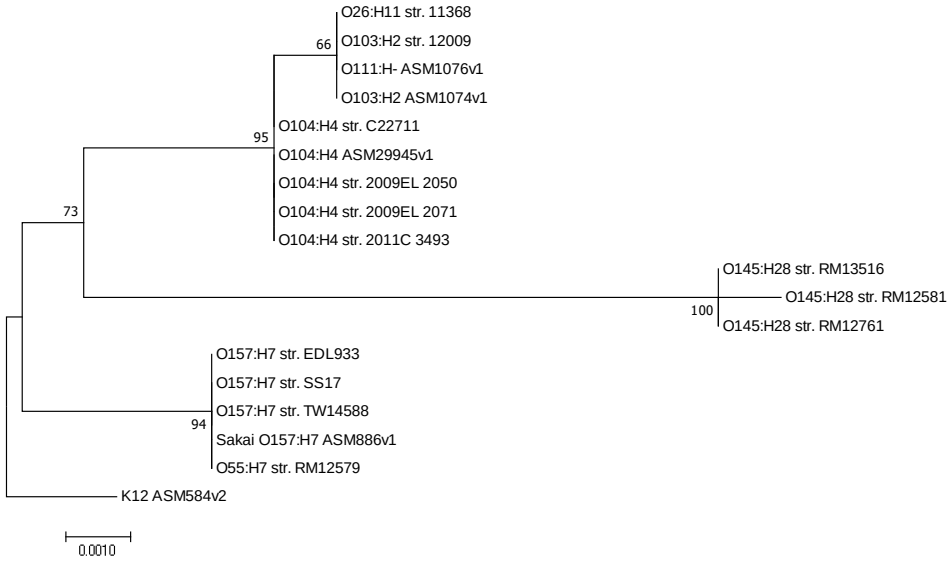

Figure C.4. Maximum likelihood tree of STEC mucin response gene *galR*. The evolutionary history was inferred using Maximum Likelihood method based on the Tamura-Nei model. The highest likelihood tree is shown. The tree was constructed using a 500 bootstrap replication.

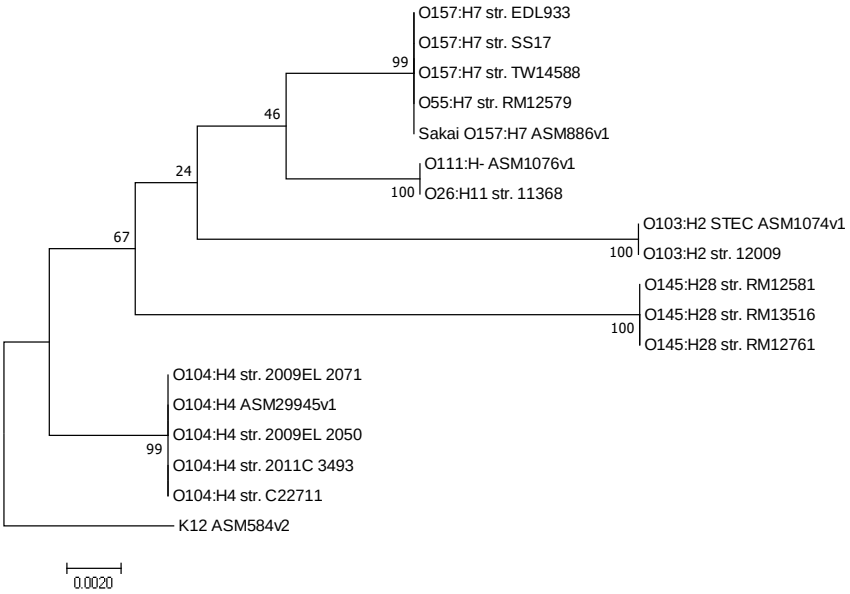

Figure C.5. Maximum likelihood tree of STEC mucin response gene *galK*. The evolutionary history was inferred using Maximum Likelihood method based on the Tamura-Nei model. The highest likelihood tree is shown. The tree was constructed using a 500 bootstrap replication.

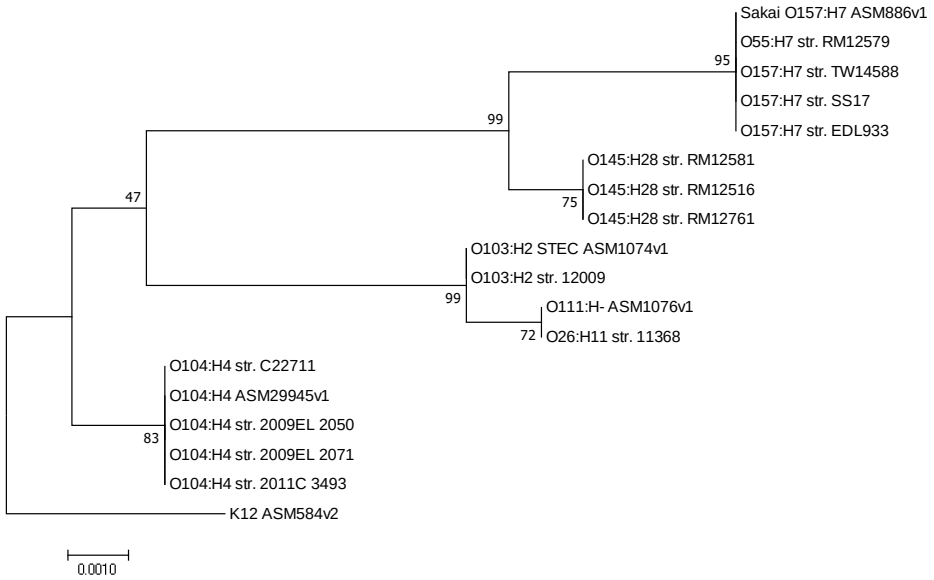

Figure C.6. Maximum likelihood tree of STEC mucin response gene *agaR*. The evolutionary history was inferred using Maximum Likelihood method based on the Tamura-Nei model. The highest likelihood tree is shown. The tree was constructed using a 500 bootstrap replication.

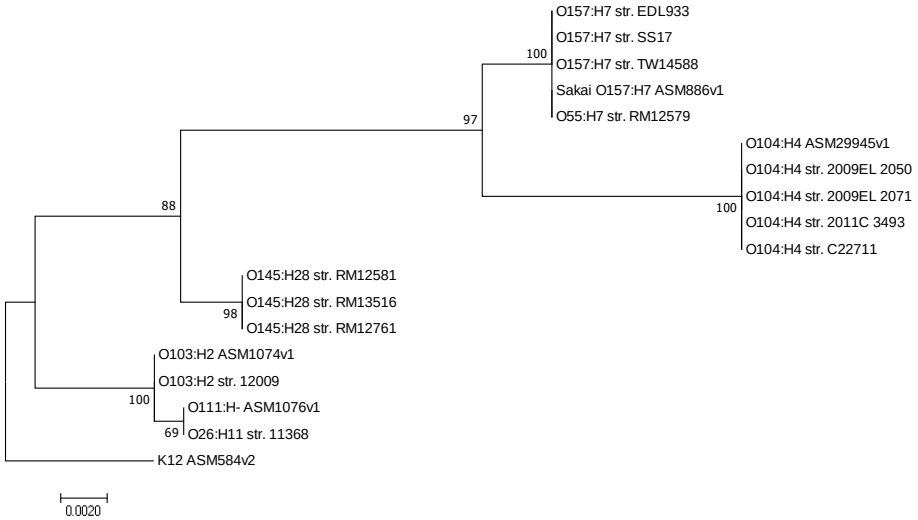

Figure C.7. Maximum likelihood tree of STEC mucin response gene *nagC*. The evolutionary history was inferred using Maximum Likelihood method based on the Tamura-Nei model. The highest likelihood tree is shown. The tree was constructed using a 500 bootstrap replication.

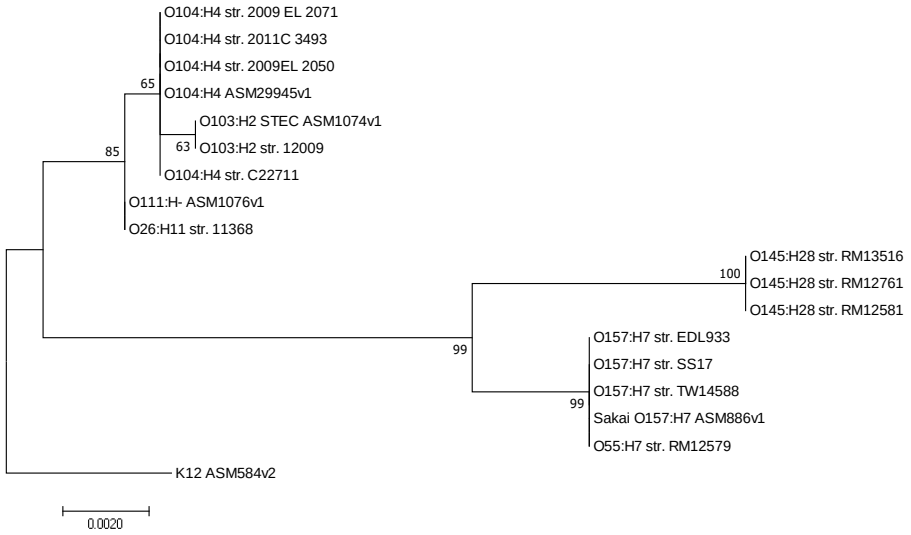

Figure C.8. Maximum likelihood tree of STEC mucin response gene *mlc*. The evolutionary history was inferred using Maximum Likelihood method based on the Tamura-Nei model. The highest likelihood tree is shown. The tree was constructed using a 500 bootstrap replication.

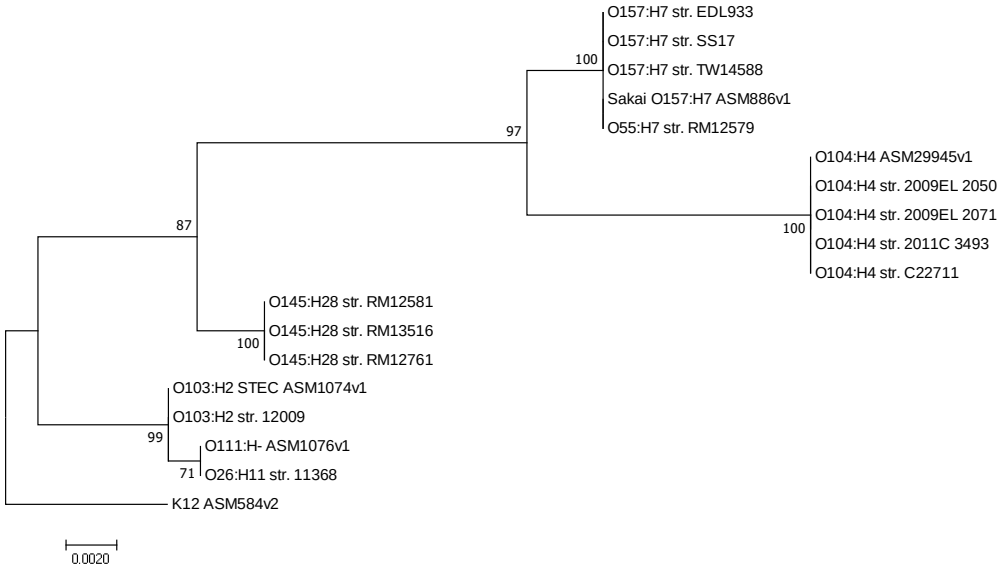

Figure C.9. Maximum likelihood tree of STEC mucin response gene *nanR*. The evolutionary history was inferred using Maximum Likelihood method based on the Tamura-Nei model. The highest likelihood tree is shown. The tree was constructed using a 500 bootstrap replication.

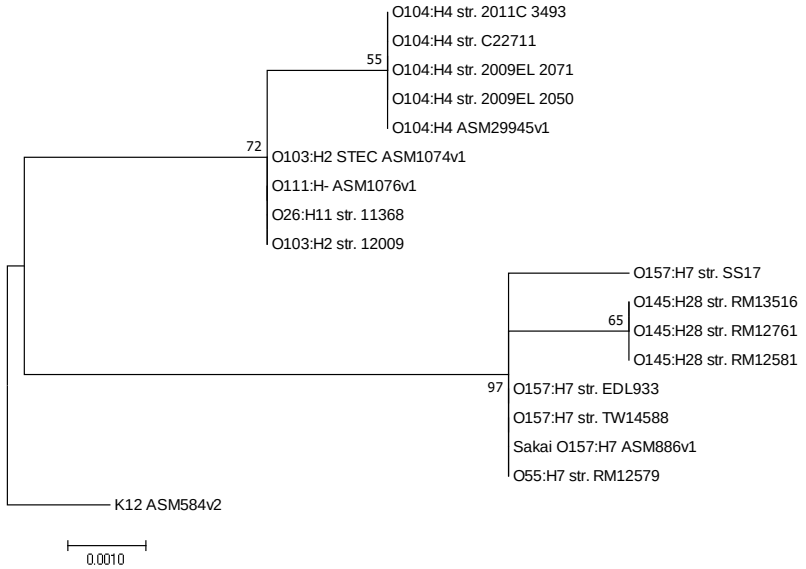

Figure C.10. Maximum likelihood tree of STEC mucin response gene *fucA*. The evolutionary history was inferred using Maximum Likelihood method based on the Tamura-Nei model. The highest likelihood tree is shown. The tree was constructed using a 500 bootstrap replication.

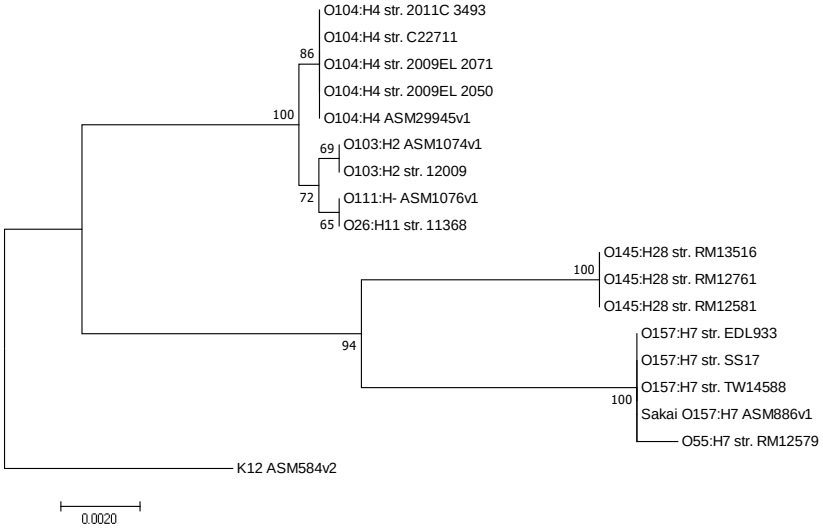

Figure C.11. Maximum likelihood tree of STEC mucin response gene *nagE*. The evolutionary history was inferred using Maximum Likelihood method based on the Tamura-Nei model. The highest likelihood tree is shown. The tree was constructed using a 500 bootstrap replication.

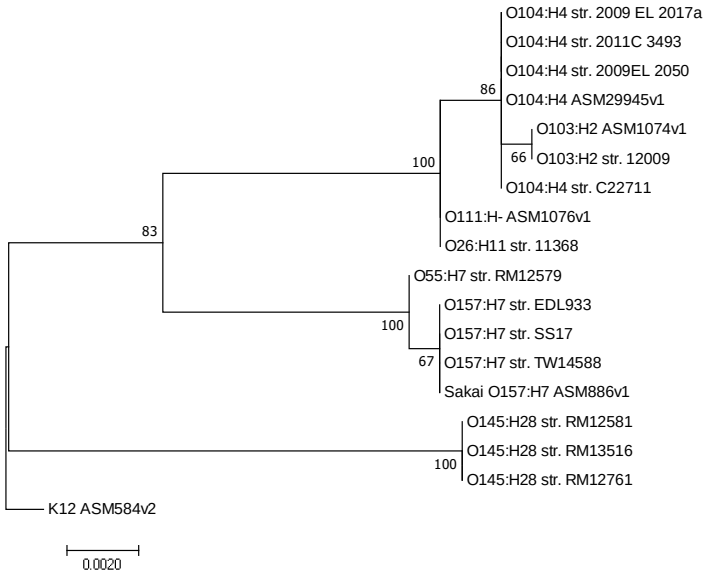

Figure C.12. Maximum likelihood tree of STEC mucin response gene *manA*. The evolutionary history was inferred using Maximum Likelihood method based on the Tamura-Nei model. The highest likelihood tree is shown. The tree was constructed using a 500 bootstrap replication.

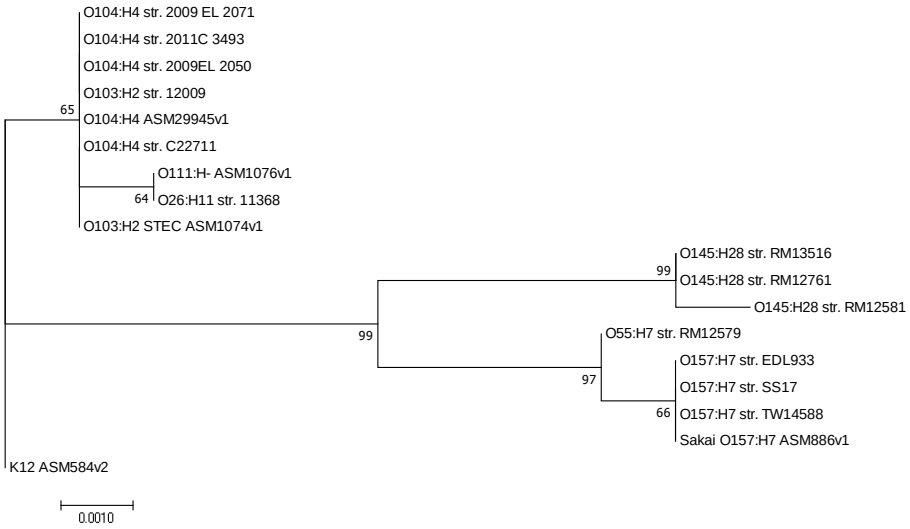

Figure C.13. Maximum likelihood tree of STEC mucin response gene *manX*. The evolutionary history was inferred using Maximum Likelihood method based on the Tamura-Nei model. The highest likelihood tree is shown. The tree was constructed using a 500 bootstrap replication.

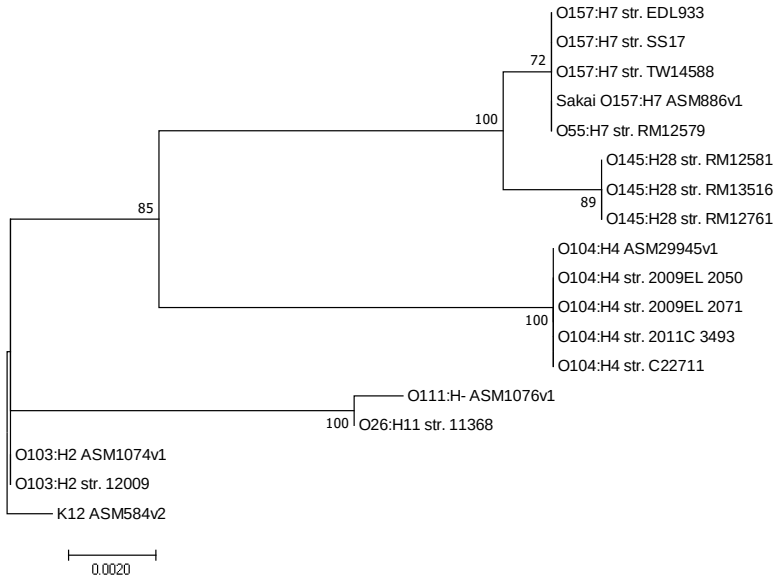

Figure C.14. Maximum likelihood tree of STEC mucin response gene *nanA*. The evolutionary history was inferred using Maximum Likelihood method based on the Tamura-Nei model. The highest likelihood tree is shown. The tree was constructed using a 500 bootstrap replication.

C.3 – Future Directions

Through partnership with the Manning lab at Michigan State University, which has collected an extensive library of STEC genomes in partnership with the Michigan Department of Health and Humans Services (MDHHS), we would look to perform a similar genome analysis among isolates. To strengthen our analysis, target gene sequences would be aligned with MUSCLE in MEGA7 and phylogenetic trees constructed by maximum likelihood with 1000 bootstrap replications and neighbor joining as a secondary tree building method. From this analysis, genes of interest can be determined and assessed through genetic manipulation of STEC to compare mucin response capacity.

As isolates were obtained in partnership with the MDHHS, epidemiological data concerning patients and clinical disease presentation are available to link to individual STEC genomes. To do this, univariate analysis of the mucin response genes in STEC will investigate potential associations with clinical outcomes listed in Table C.2 (304). A Chi-squared analysis with be performed to determine the Odds Ratio with a 95% confidence interval and associated p-value, which will be calculated and reported for each analysis; with a value $P < 0.05$ considered as significant (305). Drawing these associations allows for a better understanding of mucin response pathways that contribute to disease outcome (306). By correlating disease outcome to the mucin response network, we may be able to identify specific genome patterns that affect disease presentation in infected individuals as a result of mucin interactions.

Table C.2. Clinical outcomes of STEC infection.

	Shiga toxin-producing *Escherichia coli*
Clinical Outcomes	Cramps, Vomiting, Abdominal pain, Body aches, Diarrhea, Bloody diarrhea, Hemolytic uremic syndrome, Hospitalization, Death

REFERENCES

REFERENCES

1. Jabłońska J, Tawfik DS. 2021. The evolution of oxygen-utilizing enzymes suggests early biosphere oxygenation. Nat Ecol Evol 5:442–448.

2. Lyons TW, Reinhard CT, Planavsky NJ. 2014. The rise of oxygen in Earth's early ocean and atmosphere. Nature. Nature Publishing Group.

3. Albenberg L, Esipova T V., Judge CP, Bittinger K, Chen J, Laughlin A, Grunberg S, Baldassano RN, Lewis JD, Li H, Thom SR, Bushman FD, Vinogradov SA, Wu GD. 2014. Correlation between intraluminal oxygen gradient and radial partitioning of intestinal microbiota. Gastroenterology 147:1055-1063.e8.

4. Martín R, Miquel S, Ulmer J, Langella P, Bermúdez-Humarán LG. 2014. Gut ecosystem: How microbes help us. Benef Microbes. Wageningen Academic Publishers.

5. Friedman ES, Bittinger K, Esipova T V, Hou L, Chau L, Jiang J, Mesaros C, Lund PJ, Liang X, FitzGerald GA, Goulian M, Lee D, Garcia BA, Blair IA, Vinogradov SA, Wu GD. 2018. Microbes vs. chemistry in the origin of the anaerobic gut lumen. Proc Natl Acad Sci U S A 115:4170–4175.

6. Roediger WEW. 1980. Role of anaerobic bacteria in the metabolic welfare of the colonic mucosa in man. Gut 21:793–798.

7. Rivera-Chávez F, Zhang LF, Faber F, Lopez CA, Byndloss MX, Olsan EE, Xu G, Velazquez EM, Lebrilla CB, Winter SE, Bäumler AJ. 2016. Depletion of butyrate-producing Clostridia from the gut microbiota drives an aerobic luminal expansion of Salmonella. Cell Host Microbe 19:443–454.

8. Zheng L, Kelly CJ, Colgan SP. 2015. Physiologic hypoxia and oxygen homeostasis in the healthy intestine. A review in the theme: cellular responses to hypoxia. Am J Physiol Cell Physiol 309:350–360.

9. Ward JBJ, Keely SJ, Keely SJ. 2014. Oxygen in the regulation of intestinal epithelial transport. J Physiol. Blackwell Publishing Ltd.

10. JM A, SM C, HT L, SY C, HJ K, BA V. 2018. The intestinal epithelium: central coordinator of mucosal immunity. Trends Immunol 39:677–696.

11. Rivera-Chávez F, Lopez CA, Bäumler AJ. 2017. Oxygen as a driver of gut dysbiosis. Free Radic Biol Med 105:93–101.

12. Ravcheev DA, Thiele I. 2014. Systematic genomic analysis reveals the complementary aerobic and anaerobic respiration capacities of the human gut microbiota. Front Microbiol 5:674.

13. Pryde SE, Duncan SH, Hold GL, Stewart CS, Flint HJ. 2002. The microbiology of butyrate formation in the human colon. FEMS Microbiol Lett 217:133–139.

14. Byndloss MX, Olsan EE, Rivera-Chávez F, Tiffany CR, Cevallos SA, Lokken KL, Torres TP, Byndloss AJ, Faber F, Gao Y, Litvak Y, Lopez CA, Xu G, Napoli E, Giulivi C, Tsolis RM, Revzin A, Lebrilla CB, Bäumler AJ. 2017. Microbiota-activated PPAR-γ signaling inhibits dysbiotic Enterobacteriaceae expansion. Science (80-) 357:570–575.

15. Kelly CJ, Zheng L, Campbell EL, Saeedi B, Scholz CC, Bayless AJ, Wilson KE, Glover LE, Kominsky DJ, Magnuson A, Weir TL, Ehrentraut SF, Pickel C, Kuhn KA, Lanis JM, Nguyen V, Taylor CT, Colgan SP. 2015. Crosstalk between microbiota-derived short-chain fatty acids and intestinal epithelial HIF augments tissue barrier function. Cell Host Microbe 17:662–671.

16. Kastl AJ, Terry NA, Wu GD, Albenberg LG. 2020. The structure and function of the human small intestinal microbiota: current understanding and future directions. CMGH. Elsevier Inc.

17. Wang M, Ahrné S, Jeppsson B, Molin G. 2005. Comparison of bacterial diversity along the human intestinal tract by direct cloning and sequencing of 16S rRNA genes. FEMS Microbiol Ecol 54:219–231.

18. Pearce SC, Weber GJ, Van Sambeek DM, Soares JW, Racicot K, Breault DT. 2020. Intestinal enteroids recapitulate the effects of short-chain fatty acids on the intestinal epithelium. PLoS One 15:e0230231.

19. Booijink CCGM, El-Aidy S, Rajilić-Stojanović M, Heilig HGHJ, Troost FJ, Smidt H, Kleerebezem M, De Vos WM, Zoetendal EG. 2010. High temporal and inter-individual variation detected in the human ileal microbiota. Environ Microbiol 12:3213–3227.

20. Francino MP. 2016. Antibiotics and the human gut microbiome: Dysbioses and accumulation of resistances. Front Microbiol. Frontiers Media S.A.

21. Iacob S, Iacob DG. 2019. Infectious threats, the intestinal barrier, and its trojan horse: dysbiosis. Front Microbiol 10:1676.

22. Degruttola AK, Low D, Mizoguchi A, Mizoguchi E. 2016. Current understanding of dysbiosis in disease in human and animal models. Inflamm Bowel Dis 22:1137–1150.

23. Zeng MY, Inohara N, Nuñez G. 2017. Mechanisms of inflammation-driven bacterial dysbiosis in the gut. Mucosal Immunol. Nature Publishing Group.

24. Rinninella E, Raoul P, Cintoni M, Franceschi F, Miggiano GAD, Gasbarrini A, Mele MC. 2019. What is the healthy gut microbiota composition? A changing ecosystem across age, environment, diet, and diseases. Microorganisms 7:14.

25. Huttenhower C, Gevers D, Knight R, Abubucker S, Badger JH, Chinwalla AT, Creasy HH, Earl AM, Fitzgerald MG, Fulton RS, Giglio MG, Hallsworth-Pepin K, Lobos EA, Madupu R, Magrini V, Martin JC, Mitreva M, Muzny DM, Sodergren EJ, Versalovic J, Wollam AM, Worley KC, Wortman JR, Young SK, Zeng Q, Aagaard KM, Abolude OO, Allen-Vercoe E, Alm EJ, Alvarado L, Andersen GL, Anderson S, Appelbaum E, Arachchi HM, Armitage G, Arze CA, Ayyaz T, Baker CC, Begg L, Belachew T, Bhonagiri V, Bihan M, Blaser MJ, Bloom T, Bonazzi V, Paul Brooks J, Buck GA, Buhay CJ, Busam DA, Campbell JL, Canon SR, Cantarel BL, Chain PSG, Chen IMA, Chen L, Chhibba S, Chu K, Ciulla DM, Clemente JC, Clifton SW, Conlan S, Crabtree J, Cutting MA, Davidovics NJ, Davis CC, Desantis TZ, Deal C, Delehaunty KD, Dewhirst FE, Deych E, Ding Y, Dooling DJ, Dugan SP, Michael Dunne W, Scott Durkin A, Edgar RC, Erlich RL, Farmer CN, Farrell RM, Faust K, Feldgarden M, Felix VM, Fisher S, Fodor AA, Forney LJ, Foster L, Di Francesco V, Friedman J, Friedrich DC, Fronick CC, Fulton LL, Gao H, Garcia N, Giannoukos G, Giblin C, Giovanni MY, Goldberg JM, Goll J, Gonzalez A, Griggs A, Gujja S, Kinder Haake S, Haas BJ, Hamilton HA, Harris EL, Hepburn TA, Herter B, Hoffmann DE, Holder ME, Howarth C, Huang KH, Huse SM, Izard J, Jansson JK, Jiang H, Jordan C, Joshi V, Katancik JA, Keitel WA, Kelley ST, Kells C, King NB, Knights D, Kong HH, Koren O, Koren S, Kota KC, Kovar CL, Kyrpides NC, La Rosa PS, Lee SL, Lemon KP, Lennon N, Lewis CM, Lewis L, Ley RE, Li K, Liolios K, Liu B, Liu Y, Lo CC, Lozupone CA, Dwayne Lunsford R, Madden T, Mahurkar AA, Mannon PJ, Mardis ER, Markowitz VM, Mavromatis K, McCorrison JM, McDonald D, McEwen J, McGuire AL, McInnes P, Mehta T, Mihindukulasuriya KA, Miller JR, Minx PJ, Newsham I, Nusbaum C, Oglaughlin M, Orvis J, Pagani I, Palaniappan K, Patel SM, Pearson M, Peterson J, Podar M, Pohl C, Pollard KS, Pop M, Priest ME, Proctor LM, Qin X, Raes J, Ravel J, Reid JG, Rho M, Rhodes R, Riehle KP, Rivera MC, Rodriguez-Mueller B, Rogers YH, Ross MC, Russ C, Sanka RK, Sankar P, Fah Sathirapongsasuti J, Schloss JA, Schloss PD, Schmidt TM, Scholz M, Schriml L, Schubert AM, Segata N, Segre JA, Shannon WD, Sharp RR, Sharpton TJ, Shenoy N, Sheth NU, Simone GA, Singh I, Smillie CS, Sobel JD, Sommer DD, Spicer P, Sutton GG, Sykes SM, Tabbaa DG, Thiagarajan M, Tomlinson CM, Torralba M, Treangen TJ, Truty RM, Vishnivetskaya TA, Walker J, Wang L, Wang Z, Ward D V., Warren W, Watson MA, Wellington C, Wetterstrand KA, White JR, Wilczek-Boney K, Wu Y, Wylie KM, Wylie T, Yandava C, Ye L, Ye Y, Yooseph S, Youmans BP, Zhang L, Zhou Y, Zhu Y, Zoloth L, Zucker JD, Birren BW, Gibbs RA, Highlander SK, Methé BA, Nelson KE, Petrosino JF, Weinstock GM, Wilson RK, White O. 2012. Structure, function and diversity of the healthy human microbiome. Nature 486:207–214.

26. Faust K, Sathirapongsasuti JF, Izard J, Segata N, Gevers D, Raes J, Huttenhower C. 2012. Microbial co-occurrence relationships in the Human Microbiome. PLoS Comput Biol 8.

27. Hartman AL, Lough DM, Barupal DK, Fiehn O, Fishbein T, Zasloff M, Eisen JA. 2009. Human gut microbiome adopts an alternative state following small bowel transplantation. Proc Natl Acad Sci U S A 106:17187–17192.

28. Donohoe DR, Wali A, Brylawski BP, Bultman SJ. 2012. Microbial regulation of glucose metabolism and cell-cycle progression in mammalian colonocytes. PLoS One 7:46589.

29. Reese AT, Cho EH, Klitzman B, Nichols SP, Wisniewski NA, Villa MM, Durand HK, Jiang S, Midani FS, Nimmagadda SN, O'connell TM, Wright JP, Deshusses MA, David LA. 2018. Antibiotic-induced changes in the microbiota disrupt redox dynamics in the gut. Elife 7.

30. Dethlefsen L, Huse S, Sogin ML, Relman DA. 2008. The pervasive effects of an antibiotic on the human gut microbiota, as revealed by deep 16s rRNA sequencing. PLoS Biol 6:2383–2400.

31. Young VB, Schmidt TM. 2004. Antibiotic-associated diarrhea accompanied by large-scale slterations in the composition of the fecal microbiota. J Clin Microbiol 42:1203–1206.

32. Duncan SH, Louis P, Flint HJ. 2004. Lactate-utilizing bacteria, isolated from human feces, that produce butyrate as a major fermentation product. Appl Environ Microbiol 70:5810–7.

33. Fachi JL, Felipe J de S, Pral LP, da Silva BK, Corrêa RO, de Andrade MCP, da Fonseca DM, Basso PJ, Câmara NOS, de Sales e Souza ÉL, dos Santos Martins F, Guima SES, Thomas AM, Setubal JC, Magalhães YT, Forti FL, Candreva T, Rodrigues HG, de Jesus MB, Consonni SR, Farias A dos S, Varga-Weisz P, Vinolo MAR. 2019. Butyrate protects mice from Clostridium difficile-induced colitis through an HIF-1-dependent mechanism. Cell Rep 27:750-761.e7.

34. Elvers KT, Wilson VJ, Hammond A, Duncan L, Huntley AL, Hay AD, van der Werf ET. 2020. Antibiotic-induced changes in the human gut microbiota for the most commonly prescribed antibiotics in primary care in the UK: a systematic review. BMJ Open 10:e035677.

35. Brown SP, Inglis RF, Taddei F. 2009. Evolutionary ecology of microbial wars: Within-host competition and (incidental) virulence. Evol Appl 2:32–39.

36. Singh P, Teal TK, Marsh TL, Tiedje JM, Mosci R, Jernigan K, Zell A, Newton DW, Salimnia H, Lephart P, Sundin D, Khalife W, Britton RA, Rudrik JT, Manning SD. 2015. Intestinal microbial communities associated with acute enteric infections and disease recovery. Microbiome 3:45.

37. Bratburd JR, Keller C, Vivas E, Gemperline E, Li L, Rey FE, Currie CR. 2018. Gut microbial and metabolic responses to Salmonella enterica serovar Typhimurium and Candida albicans. MBio 9.

38. Gillis CC, Hughes ER, Spiga L, Winter MG, Zhu W, Furtado de Carvalho T, Chanin RB, Behrendt CL, Hooper L V, Santos RL, Winter SE. 2018. Dysbiosis-associated change in host metabolism generates lactate to support Salmonella

growth. Cell Host Microbe 23:54-64.e6.

39. Westerman TL, Bogomolnaya L, Andrews-Polymenis HL, Katherine Sheats M, Elfenbein JR. 2018. The Salmonella type-3 secretion system-1 and flagellar motility influence the neutrophil respiratory burst. PLoS One 13:e0203698.

40. Gill N, Ferreira RBR, Antunes LCM, Willing BP, Sekirov I, Al-Zahrani F, Hartmann M, Finlay BB. 2012. Neutrophil elastase alters the murine gut microbiota resulting in enhanced Salmonella colonization. PLoS One 7:49646.

41. Gantois I, Ducatelle R, Pasmans F, Haesebrouck F, Hautefort I, Thompson A, Hinton JC, Van Immerseel F. 2006. Butyrate specifically down-regulates Salmonella pathogenicity island 1 gene expression. Appl Environ Microbiol 72:946–949.

42. Lopez CA, Miller BM, Rivera-Chávez F, Velazquez EM, Byndloss MX, Chávez-Arroyo A, Lokken KL, Tsolis RM, Winter SE, Bäumler AJ. 2016. Virulence factors enhance Citrobacter rodentium expansion through aerobic respiration. Science 353:1249–53.

43. Rivera-Chávez F, Mekalanos JJ. 2019. Cholera toxin promotes pathogen acquisition of host-derived nutrients. Nature 572:244–248.

44. MacIntyre DL, Miyata ST, Kitaoka M, Pukatzki S. 2010. The Vibrio cholerae type VI secretion system displays antimicrobial properties. Proc Natl Acad Sci U S A 107:19520–19524.

45. Zhao W, Caro F, Robins W, Mekalanos JJ. 2018. Antagonism toward the intestinal microbiota and its effect on Vibrio cholerae virulence. Science (80-) 359:210–213.

46. Fu Y, Ho BT, Mekalanos JJ. 2018. Tracking Vibrio cholerae cell-cell interactions during infection reveals bacterial population dynamics within intestinal microenvironments. Cell Host Microbe 23:274-281.e2.

47. Sana TG, Lugo KA, Monack DM. 2017. T6SS: The bacterial “fight club” in the host gut. PLoS Pathog. Public Library of Science.

48. Das S, Chaudhuri K. 2003. Identification of a unique IAHP (IcmF Associated Homologous Proteins) cluster in Vibrio cholerae and other Proteobacteria through in silico analysis. In Silico Biol 3:287–300.

49. Navarro-Garcia F, Ruiz-Perez F, Cataldi Á, Larzábal M. 2019. Type VI secretion system in pathogenic escherichia coli: Structure, role in virulence, and acquisition. Front Microbiol. Frontiers Media S.A.

50. Silberger DJ, Zindl CL, Weaver CT. 2017. Citrobacter rodentium: A model enteropathogen for understanding the interplay of innate and adaptive

components of type 3 immunity. Mucosal Immunol. Nature Publishing Group.

51. Gueguen E, Cascales E. 2013. Promoter swapping unveils the role of the citrobacter rodentium CTS1 type VI secretion system in interbacterial competition. Appl Environ Microbiol 79:32–38.

52. Sana TG, Flaugnatti N, Lugo KA, Lam LH, Jacobson A, Baylot V, Durand E, Journet L, Cascales E, Monack DM. 2016. Salmonella Typhimurium utilizes a T6SS-mediated antibacterial weapon to establish in the host gut. Proc Natl Acad Sci U S A 113:E5044–E5051.

53. Lupp C, Robertson ML, Wickham ME, Sekirov I, Champion OL, Gaynor EC, Finlay BB. 2007. Host-mediated inflammation disrupts the intestinal microbiota and promotes the overgrowth of Enterobacteriaceae. Cell Host Microbe 2:119–129.

54. Hughes ER, Winter MG, Duerkop BA, Spiga L, Furtado de Carvalho T, Zhu W, Gillis CC, Büttner L, Smoot MP, Behrendt CL, Cherry S, Santos RL, Hooper L V., Winter SE. 2017. Microbial respiration and formate oxidation as metabolic signatures of inflammation-associated dysbiosis. Cell Host Microbe 21:208–219.

55. Takahashi K, Nishida A, Fujimoto T, Fujii M, Shioya M, Imaeda H, Inatomi O, Bamba S, Andoh A, Sugimoto M. 2016. Reduced abundance of butyrate-producing bacteria species in the fecal microbial community in Crohn's disease, p. 59–65. *In* Digestion. S. Karger AG.

56. Walujkar SA, Dhotre DP, Marathe NP, Lawate PS, Bharadwaj RS, Shouche YS. 2014. Characterization of bacterial community shift in human Ulcerative Colitis patients revealed by Illumina based 16S rRNA gene amplicon sequencing. Gut Pathog 6:22.

57. Seksik P, Rigottier-Gois L, Gramet G, Sutren M, Pochart P, Marteau P, Jian R, Doré J. 2003. Alterations of the dominant faecal bacterial groups in patients with Crohn's disease of the colon. Gut 52:237–242.

58. Sokol H, Seksik P, Rigottier-Gois L, Lay C, Lepage P, Podglajen I, Marteau P, Doré J. 2006. Specificities of the fecal microbiota in inflammatory bowel disease. Inflamm Bowel Dis 12:106–111.

59. Rigottier-Gois L. 2013. Dysbiosis in inflammatory bowel diseases: The oxygen hypothesis. ISME J. Nature Publishing Group.

60. Quinn RA, Comstock W, Zhang T, Morton JT, Da Silva R, Tran A, Aksenov A, Nothias LF, Wangpraseurt D, Melnik A V., Ackermann G, Conrad D, Klapper I, Knight R, Dorrestein PC. 2018. Niche partitioning of a pathogenic microbiome driven by chemical gradients. Sci Adv 4:eaau1908.

61. Unden G, Becker S, Bongaerts -G Holighaus Schirawski JJ, Six S. 1995. O2-

Sensing and O2-dependent gene regulation in facultatively anaerobic bacteriaArch Microbiol.

62. Kiley PJ, Beinert H. 2003. The role of Fe-S proteins in sensing and regulation in bacteria. Curr Opin Microbiol. Elsevier Ltd.

63. Beinert H. 2000. Iron-sulfur proteins: Ancient structures, still full of surprises. J Biol Inorg Chem. Springer Verlag.

64. Fontecave M. 2006. Iron-sulfur clusters: Ever-expanding roles. Nat Chem Biol 2:171–174.

65. Spiro S, Guest JR. 1990. FNR and its role in oxygen-regulated gene expression in Escherichia coli . FEMS Microbiol Lett 75:399–428.

66. Outten FW. 2007. Iron-sulfur clusters as oxygen-responsive molecular switches. Nat Chem Biol. Nature Publishing Group.

67. Crack JC, Green J, Cheesman MR, Le Brun NE, Thomson AJ. 2007. Superoxide-mediated amplification of the oxygen-induced switch from [4Fe-4S] to [2Fe-2S] clusters in the transcriptional regulator FNR. Proc Natl Acad Sci U S A 104:2092–2097.

68. Fink RC, Evans MR, Porwollik S, Vazquez-Torres A, Jones-Carson J, Troxell B, Libby SJ, McClelland M, Hassan HM. 2007. FNR is a global regulator of virulence and anaerobic metabolism in Salmonella enterica serovar Typhimurium (ATCC 14028s). J Bacteriol 189:2262–2273.

69. Green J, Rolfe MD, Smith LJ. 2014. Transcriptional regulation of bacterial virulence gene expression by molecular oxygenand nitric oxide. Virulence 5:794–809.

70. Marteyn B, West NP, Browning DF, Cole JA, Shaw JG, Palm F, Mounier J, Prévost MC, Sansonetti P, Tang CM. 2010. Modulation of Shigella virulence in response to available oxygen in vivo. Nature 465:355–358.

71. Way SS, Sallustio S, Magliozzo RS, Goldberg MB. 1999. Impact of either elevated or decreased levels of cytochrome bd expression on Shigella flexneri virulence. J Bacteriol 181:1229–1237.

72. Tinevez J-Y, Arena ET, Anderson M, Nigro G, Injarabian L, André A, Ferrari M, Campbell-Valois F-X, Devin A, Shorte SL, Sansonetti PJ, Marteyn BS. 2019. Shigella-mediated oxygen depletion is essential for intestinal mucosa colonization. Nat Microbiol 1–9.

73. K E, N H, S I, EC L, ST C. 1989. Molecular genetic analysis of FNR-dependent promoters. Mol Microbiol 3:869–878.

74. Antelmann H, Helmann JD. 2011. Thiol-based redox switches and gene regulation. Antioxidants Redox Signal. Mary Ann Liebert, Inc.

75. Hillion M, Antelmann H. 2015. Thiol-based redox switches in prokaryotes. Biol Chem. Walter de Gruyter GmbH.

76. Sang Ho L, Hava DL, Waldor MK, Camilli A. 1999. Regulation and temporal expression patterns of Vibrio cholerae virulence genes during infection. Cell 99:625–634.

77. Marrero K, Sánchez A, Rodríguez-Ulloa A, González LJ, Castellanos-Serra L, Paz-Lago D, Campos J, Rodríguez BL, Suzarte E, Ledón T, Padrón G, Fando R. 2009. Anaerobic growth promotes synthesis of colonization factors encoded at the Vibrio pathogenicity island in Vibrio cholerae El Tor. Res Microbiol 160:48–56.

78. Liu Z, Yang M, Peterfreund GL, Tsou AM, Selamoglu N, Daldal F, Zhong Z, Kan B, Zhu J. 2011. Vibrio cholerae anaerobic induction of virulence gene expression is controlled by thiol-based switches of virulence regulator AphB. Proc Natl Acad Sci 108:810–815.

79. Liu Z, Wang H, Zhou Z, Naseer N, Xiang F, Kan B, Goulian M, Zhu J. 2016. Differential thiol-based switches jump-start Vibrio cholerae pathogenesis. Cell Rep 14:347–354.

80. Bekker M, Alexeeva S, Laan W, Sawers G, De Mattos JT, Hellingwerf K. 2010. The ArcBA two-component system of Escherichia coli is regulated by the redox state of both the ubiquinone and the menaquinone pool. J Bacteriol 192:746–754.

81. Evans MR, Fink RC, Vazquez-Torres A, Porwollik S, Jones-Carson J, McClelland M, Hassan HM. 2011. Analysis of the ArcA regulon in anaerobically grown Salmonella enterica sv. Typhimurium. BMC Microbiol 11:1–16.

82. Malpica R, Franco B, Rodriguez C, Kwon O, Georgellis D. 2004. Identification of a quinone-sensitive redox switch in the ArcB sensor kinase. Proc Natl Acad Sci U S A 101:13318–13323.

83. Loui C, Chang AC, Lu S. 2009. Role of the ArcAB two-component system in the resistance of Escherichia coli to reactive oxygen stress. BMC Microbiol 9:183.

84. Pardo-Esté C, Hidalgo AA, Aguirre C, Briones AC, Cabezas CE, Castro-Severyn J, Fuentes JA, Opazo CM, Riedel CA, Otero C, Pacheco R, Valvano MA, Saavedra CP. 2018. The ArcAB two-component regulatory system promotes resistance to reactive oxygen species and systemic infection by Salmonella Typhimurium. PLoS One 13:e0203497.

85. Sengupta N, Paul K, Chowdhury R. 2003. The global regulator ArcA modulates expression of virulence factors in Vibrio cholerae. Infect Immun 71:5583–5589.

86. Lu S, Killoran PB, Fang FC, Riley LW. 2002. The global regulator ArcA controls resistance to reactive nitrogen and oxygen intermediates in Salmonella enterica serovar enteritidis. Infect Immun 70:451–461.

87. van der Stel AX, van Mourik A, Heijmen-van Dijk L, Parker CT, Kelly DJ, van de Lest CHA, van Putten JPM, Wösten MMSM. 2015. The Campylobacter jejuni RacRS system regulates fumarate utilization in a low oxygen environment. Environ Microbiol 17:1049–1064.

88. Taylor BL. 1983. How do bacteria find the optimal concentration of oxygen? Trends Biochem Sci. Elsevier Current Trends.

89. Rebbapragada A, Johnson MS, Harding GP, Zuccarelli AJ, Fletcher HM, Zhulin IB, Taylor BL. 1997. The Aer protein and the serine chemoreceptor Tsr independently sense intracellular energy levels and transduce oxygen, redox, and energy signals for Escherichia coli behavior. Proc Natl Acad Sci U S A 94:10541–10546.

90. Edwards JC, Johnson MS, Taylor BL. 2006. Differentiation between electron transport sensing and proton motive force sensing by the Aer and Tsr receptors for aerotaxis. Mol Microbiol 62:823–837.

91. Murphy SG, Johnson BA, Ledoux CM, Dörr T. 2021. Vibrio cholerae's mysterious Seventh Pandemic island (VSP-II) encodes novel Zur-regulated zinc starvation genes involved in chemotaxis and cell congregation. PLOS Genet 17:e1009624.

92. Boin MA, Häse CC. 2007. Characterization of Vibrio cholerae aerotaxis. FEMS Microbiol Lett 276:193–201.

93. Butler SM, Camilli A. 2004. Both chemotaxis and net motility greatly influence the infectivity of Vibrio cholerae. Proc Natl Acad Sci U S A 101:5018–5023.

94. Laszlo DJ, Taylor BL. 1981. Aerotaxis in Salmonella typhimurium: Role of electron transport. J Bacteriol 145:990–1001.

95. Rivera-Chávez F, Winter SE, Lopez CA, Xavier MN, Winter MG, Nuccio SP, Russell JM, Laughlin RC, Lawhon SD, Sterzenbach T, Bevins CL, Tsolis RM, Harshey R, Adams LG, Bäumler AJ. 2013. Salmonella uses energy taxis to benefit from intestinal inflammation. PLoS Pathog 9:1003267.

96. KT E, IB Z, JA S, VJ D. 2009. Conserved residues in the HAMP domain define a new family of proposed bipartite energy taxis receptors. J Bacteriol 191:375–387.

97. KT E, VJ D. 2008. Characterization of CetA and CetB, a bipartite energy taxis system in Campylobacter jejuni. Mol Microbiol 69:1091–1103.

98. Schüller S, Phillips AD. 2010. Microaerobic conditions enhance type III secretion and adherence of enterohaemorrhagic Escherichia coli to polarized human

intestinal epithelial cells. Environ Microbiol 12:2426–2435.

99. Melson EM, Kendall MM. 2019. The sRNA DicF integrates oxygen sensing to enhance enterohemorrhagic Escherichia coli virulence via distinctive RNA control mechanisms. Proc Natl Acad Sci U S A 116:14210–14215.

100. Tran SL, Billoud L, Lewis SB, Phillips AD, Schüller S. 2014. Shiga toxin production and translocation during microaerobic human colonic infection with Shiga toxin-producing E.coliO157: H7 and O104: H4. Cell Microbiol 16:1255–1266.

101. Ellis SJ, Yasir M, Browning DF, Busby SJW, Schüller S. 2019. Oxygen and contact with human intestinal epithelium independently stimulate virulence gene expression in enteroaggregative Escherichia coli. Cell Microbiol 21.

102. Krishnan HH, Ghosh A, Paul K, Chowdhury R. 2004. Effect of anaerobiosis on expression of virulence factors in Vibrio cholerae. Infect Immun 72:3961–3967.

103. Van Alst AJ, DiRita VJ. 2020. Aerobic metabolism in Vibrio cholerae is required for population expansion during Infection. MBio 11.

104. Barbuddhe SB, Chakraborty T. 2009. Listeria as an enteroinvasive gastrointestinal pathogen. Curr Top Microbiol Immunol. Springer Verlag.

105. Burkholder KM, Kim KP, Mishra KK, Medina S, Hahm BK, Kim H, Bhunia AK. 2009. Expression of LAP, a SecA2-dependent secretory protein, is induced under anaerobic environment. Microbes Infect 11:859–867.

106. Wallace N, Newton E, Abrams E, Zani A, Sun Y. 2017. Metabolic determinants in Listeria monocytogenes anaerobic listeriolysin O production. Arch Microbiol 199:827–837.

107. Rinehart E, Chapman J, Sun Y. 2020. The production of listeriolysin O and subsequent intracellular infections by Listeria monocytogenes are regulated by exogenous short chain fatty acid mixtures. Toxins (Basel) 12.

108. Vadia S, Seveau S. 2014. Fluxes of Ca2+ and K+ are required for the listeriolysin O-dependent internalization pathway of Listeria monocytogenes. Infect Immun 82:1084–1091.

109. Schnupf P, Portnoy DA. 2007. Listeriolysin O: a phagosome-specific lysin. Microbes Infect.

110. Bueno E, Sit B, Waldor MK, Cava F. 2018. Anaerobic nitrate reduction divergently governs population expansion of the enteropathogen Vibrio cholerae. Nat Microbiol 3:1346–1353.

111. Bueno E, Sit B, Waldor MK, Cava F. 2020. Genetic dissection of the fermentative

and respiratory contributions supporting Vibrio cholerae hypoxic growth. J Bacteriol 202.

112. Jones SA, Gibson T, Maltby RC, Chowdhury FZ, Stewart V, Cohen PS, Conway T. 2011. Anaerobic respiration of Escherichia coli in the mouse intestine. Infect Immun 79:4218–4226.

113. Jones SA, Chowdhury FZ, Fabich AJ, Anderson A, Schreiner DM, House AL, Autieri SM, Leatham MP, Lins JJ, Jorgensen M, Cohen PS, Conway T. 2007. Respiration of Escherichia coli in the mouse intestine. Infect Immun 75:4891–4899.

114. Winter SE, Thiennimitr P, Winter MG, Butler BP, Huseby DL, Crawford RW, Russell JM, Bevins CL, Adams LG, Tsolis RM, Roth JR, Bäumler AJ. 2010. Gut inflammation provides a respiratory electron acceptor for Salmonella. Nature 467:426–429.

115. Thiennimitr P, Winter SE, Winter MG, Xavier MN, Tolstikov V, Huseby DL, Sterzenbach T, Tsolis RM, Roth JR, Bäumler AJ. 2011. Intestinal inflammation allows Salmonella to use ethanolamine to compete with the microbiota. Proc Natl Acad Sci U S A 108:17480–17485.

116. Berger CN, Crepin VF, Roumeliotis TI, Wright JC, Serafini N, Pevsner-Fischer M, Yu L, Elinav E, Di Santo JP, Choudhary JS, Frankel G. 2018. The Citrobacter rodentium type III secretion system effector EspO affects mucosal damage repair and antimicrobial responses. PLoS Pathog 14.

117. Carson D, Barry R, Hopkins EGD, Roumeliotis TI, García-Weber D, Mullineaux-Sanders C, Elinav E, Arrieumerlou C, Choudhary JS, Frankel G. 2020. Citrobacter rodentium induces rapid and unique metabolic and inflammatory responses in mice suffering from severe disease. Cell Microbiol 22:e13126.

118. Sellars MJ, Hall SJ, Kelly DJ. 2002. Growth of Campylobacter jejuni supported by respiration of fumarate, nitrate, nitrite, trimethylamine-N-oxide, or dimethyl sulfoxide requires oxygen. J Bacteriol 184:4187–4196.

119. Kassem II, Candelero-Rueda RA, Esseili KA, Rajashekara G. 2017. Formate simultaneously reduces oxidase activity and enhances respiration in Campylobacter jejuni. Sci Rep 7:1–11.

120. Imlay JA. 2002. How oxygen damages microbes: Oxygen tolerance and obligate anaerobiosis. Adv Microb Physiol. Academic Press.

121. Giordano N, Hastie JL, Smith AD, Foss ED, Gutierrez-Munoz DF, Carlson PE. 2018. Cysteine desulfurase IscS2 plays a role in oxygen resistance in Clostridium difficile. Infect Immun 86.

122. Folgosa F, Martins MC, Teixeira M. 2018. The multidomain flavodiiron protein

from Clostridium difficile 630 is an NADH:oxygen oxidoreductase. Sci Rep 8.

123. Kint N, Feliciano CA, Martins MC, Morvan C, Fernandes SF, Folgosa F, Dupuy B, Texeira M, Martin-Verstraete I. 2020. How the anaerobic enteropathogen Clostridioides difficile tolerates low O2 tensions. MBio 11:1–17.

124. Knippel RJ, Wexler AG, Miller JM, Beavers WN, Weiss A, de Crécy-Lagard V, Edmonds KA, Giedroc DP, Skaar EP. 2020. Clostridioides difficile senses and hijacks host heme for incorporation into an oxidative stress defense system. Cell Host Microbe 28:411-421.e6.

125. Li H, Zhou X, Huang Y, Liao B, Cheng L, Ren B. 2021. Reactive oxygen species in pathogen clearance: the killing mechanisms, the adaption response, and the side effects. Front Microbiol. Frontiers Media S.A.

126. Nguyen GT, Green ER, Mecsas J. 2017. Neutrophils to the ROScue: Mechanisms of NADPH oxidase activation and bacterial resistance. Front Cell Infect Microbiol. Frontiers Media S.A.

127. Zhao X, Drlica K. 2014. Reactive oxygen species and the bacterial response to lethal stress. Curr Opin Microbiol. Elsevier Ltd.

128. Dukan S, Touati D. 1996. Hypochlorous acid stress in Escherichia coli: Resistance, DNA damage, and comparison with hydrogen peroxide stress. J Bacteriol 178:6145–6150.

129. Borisov VB, Siletsky SA, Nastasi MR, Forte E. 2021. ROS defense systems and terminal oxidases in bacteria. Antioxidants 10:839.

130. De Groote MA, Ochsner UA, Shiloh MU, Nathan C, McCord JM, Dinauer MC, Libby SJ, Vazquez-Torres A, Xu Y, Fang FC. 1997. Periplasmic superoxide dismutase protects Salmonella from products of phagocyte NADPH-oxidase and nitric oxide synthase. Proc Natl Acad Sci U S A 94:13997–14001.

131. Myers KS, Yan H, Ong IM, Chung D, Liang K, Tran F, Keleş S, Landick R, Kiley PJ. 2013. Genome-scale analysis of Escherichia coli FNR reveals complex features of transcription factor binding. PLoS Genet 9:1003565.

132. Gebendorfer KM, Drazic A, Le Y, Gundlach J, Bepperling A, Kastenmüller A, Ganzinger KA, Braun N, Franzmann TM, Winter J. 2012. Identification of a hypochlorite-specific transcription factor from Escherichia coli. J Biol Chem 287:6892–6903.

133. Schwartz CE, Krall J, Norton L, McKay K, Kay D, Lynch RE. 1983. Catalase and superoxide dismutase in Escherichia coli. J Biol Chem 258:6277–6281.

134. Hong Y, Zeng J, Wang X, Drlica K, Zhao X. 2019. Post-stress bacterial cell death mediated by reactive oxygen species. Proc Natl Acad Sci U S A 116:10064–

10071.

135. Chanin RB, Winter MG, Spiga L, Hughes ER, Zhu W, Taylor SJ, Arenales A, Gillis CC, Büttner L, Jimenez AG, Smoot MP, Santos RL, Winter SE. 2020. Epithelial-derived reactive oxygen species enable AppBCX-mediated aerobic respiration of Escherichia coli during intestinal inflammation. Cell Host Microbe 28.

136. Sousa FL, Alves RJ, Ribeiro MA, Pereira-Leal JB, Teixeira M, Pereira MM. 2012. The superfamily of heme-copper oxygen reductases: Types and evolutionary considerations. Biochim Biophys Acta - Bioenerg 1817:629–637.

137. Borisov VB, Gennis RB, Hemp J, Verkhovsky MI. 2011. The cytochrome bd respiratory oxygen reductases. Biochim Biophys Acta 1398–1413.

138. Kaila VRI, Wikström M. 2021. Architecture of bacterial respiratory chains. Nat Rev Microbiol 19:319–330.

139. Nakamoto RK, Baylis Scanlon JA, Al-Shawi MK. 2008. The rotary mechanism of the ATP synthase. Arch Biochem Biophys. NIH Public Access.

140. Poole RK, Cook GM. 2000. Redundancy of aerobic respiratory chains in bacteria? Routes, reasons and regulation. Adv Microb Physiol. Academic Press.

141. Tseng CP, Albrecht J, Gunsalus RP. 1996. Effect of microaerophilic cell growth conditions on expression of the aerobic (cyoABCDE and cydAB) and anaerobic (narGHJI, frdABCD, and dmsABC) respiratory pathway genes in Escherichia coli. J Bacteriol 178:1094–1098.

142. Bai H, Rolfe MD, Jia W, Coakley S, Poole RK, Green J, Holcombe M. 2014. Agent-based modeling of oxygen-responsive transcription factors in Escherichia coli. PLoS Comput Biol 10:1003595.

143. D'Mello R, Hill S, Poole RK. 1995. The oxygen affinity of cytochrome bo' in Escherichia coli determined by the deoxygenation of oxyleghemoglobin and oxymyoglobin: K(m) values for oxygen are in the submicromolar range. J Bacteriol. American Society for Microbiology.

144. D'Mello R, Hill S, Poole RK. 1996. The cytochrome bd quinol oxidase in Escherichia coli has an extremely high oxygen affinity and two oxygen-binding haems: Implications for regulation of activity in vivo by oxygen inhibition. Microbiology 142:755–763.

145. Cotter PA, Chepuri V, Gennis RB, Gunsalus RP. 1990. Cytochrome o (cyoABCDE) and d (cydAB) oxidase gene expression in Escherichia coli is regulated by oxygen, pH and the fnr gene product. J Bacteriol 172:6333–6338.

146. Dassa J, Fsihi H, Marck C, Dion M, Kieffer-Bontemps M, Boquet P. 1991. A new oxygen-regulated operon in Escherichia coli comprises the genes for a putative

third cytochrome oxidase and for pH 2.5 acid phosphatase (appA). Mol Gen Genet 229:341–352.

147. Heidelberg JF, Eisen JA, Nelson WC, Clayton RA, Gwinn ML, Dodson RJ, Haft DH, Hickey EK, Peterson JD, Umayam L, Gill SR, Nelson KE, Read TD, Tettelin H, Richardson D, Ermolaeva MD, Vamathevan J, Bass S, Qin H, Dragoi I, Sellers P, McDonald L, Utterback T, Fleishmann RD, Nierman WC, White O, Salzberg SL, Smith HO, Colwell RR, Mekalanos JJ, Craig Venter J, Fraser CM. 2000. DNA sequence of both chromosomes of the cholera pathogen Vibrio cholerae. Nature 406:477–483.

148. Corbett D, Goldrick M, Fernandes VE, Davidge K, Poole RK, Andrew PW, Cavet J, Roberts IS. 2017. Listeria monocytogenes has both cytochrome bd-type and cytochrome aa 3 -type terminal oxidases, which allow growth at different oxygen levels, and both are important in infection. Infect Immun 85.

149. Jackson RJ, Elvers KT, Lee LJ, Gidley MD, Wainwright LM, Lightfoot J, Park SF, Poole RK. 2007. Oxygen reactivity of both respiratory oxidases in Campylobacter jejuni: The cydAB genes encode a cyanide-resistant, low-affinity oxidase that is not of the cytochrome bd type. J Bacteriol 189:1604–1615.

150. Borisov VB, Forte E, Davletshin A, Mastronicola D, Sarti P, Giuffrè A. 2013. Cytochrome bd oxidase from Escherichia coli displays high catalase activity: An additional defense against oxidative stress. FEBS Lett 587:2214–2218.

151. Mason MG, Shepherd M, Nicholls P, Dobbin PS, Dodsworth KS, Poole RK, Cooper CE. 2009. Cytochrome bd confers nitric oxide resistance to Escherichia coli. Nat Chem Biol 5:94–96.

152. Forte E, Borisov VB, Falabella M, Colaço HG, Tinajero-Trejo M, Poole RK, Vicente JB, Sarti P, Giuffre A. 2016. The terminal oxidase Cytochrome bd promotes sulfide-resistant bacterial respiration and growth. Sci Rep 6:1–8.

153. Stintzi A, Marlow D, Palyada K, Naikare H, Panciera R, Whitworth L, Clarke C. 2005. Use of genome-wide expression profiling and mutagenesis to study the intestinal lifestyle of Campylobacter jejuni. Infect Immun 73:1797–1810.

154. Weingarten RA, Grimes JL, Olson JW. 2008. Role of Campylobacter jejuni respiratory oxidases and reductases in host colonization. Appl Environ Microbiol 74:1367–1375.

155. Raleigh JA, Chou SC, Arteel GE, Horsman MR. 1999. Comparisons among pimonidazole binding, oxygen electrode measurements, and radiation response in C3H mouse tumors. Radiat Res 151:580–589.

156. Kizaka-Kondoh S, Konse-Nagasawa H. 2009. Significance of nitroimidazole compounds and hypoxia-inducible factor-1 for imaging tumor hypoxia. Cancer Sci. John Wiley & Sons, Ltd.

157. Harris NR, Carter PR, Yadav AS, Watts MN, Zhang S, Kosloski-Davidson M, Grisham MB. 2011. Relationship between inflammation and tissue hypoxia in a mouse model of chronic colitis. Inflamm Bowel Dis 17:742–746.

158. Werth N, Beerlage C, Rosenberger C, Yazdi AS, Edelmann M, Amr A, Bernhardt W, von Eiff C, Becker K, Schäfer A, Peschel A, Kempf VAJ. 2010. Activation of hypoxia inducible factor 1 is a general phenomenon in infections with human pathogens. PLoS One 5:1–12.

159. Esipova T V., Karagodov A, Miller J, Wilson DF, Busch TM, Vinogradov SA. 2011. Two new “protected” oxyphors for biological oximetry: Properties and application in tumor imaging. Anal Chem 83:8756–8765.

160. Grist SM, Chrostowski L, Cheung KC. 2010. Optical oxygen sensors for applications in microfluidic cell culture. Sensors (Switzerland). Molecular Diversity Preservation International.

161. Bunge F, van den Driesche S, Waespy M, Radtke A, Belge G, Kelm S, Waite AM, Mirastschijski U, Vellekoop MJ. 2019. Microfluidic oxygen sensor system as a tool to monitor the metabolism of mammalian cells. Sensors Actuators, B Chem 289:24–31.

162. Thomas PC, Halter M, Tona A, Raghavan SR, Plant AL, Forry SP. 2009. A noninvasive thin film sensor for monitoring oxygen tension during in vitro cell culture. Anal Chem 81:9239–9246.

163. Wang C, Dang T, Baste J, Anil Joshi A, Bhushan A. 2021. A novel standalone microfluidic device for local control of oxygen tension for intestinal-bacteria interactions. FASEB J 35:e21291.

164. Potzkei J, Kunze M, Drepper T, Gensch T, Jaeger KE, Büchs J. 2012. Real-time determination of intracellular oxygen in bacteria using a genetically encoded FRET-based biosensor. BMC Biol 10:1–13.

165. Nomata J, Hisabori T. 2018. Development of heme protein based oxygen sensing indicators. Sci Rep 8:1–12.

166. Safran M, Kim WY, O’Connell F, Flippin L, Günzler V, Horner JW, DePinho RA, Kaelin WG. 2006. Mouse model for noninvasive imaging of HIF prolyl hydroxylase activity: Assessment of an oral agent that stimulates erythropoietin production. Proc Natl Acad Sci U S A 103:105–110.

167. Suntharasamai P, Migasena S, Vongsthongsri U, Supanaranond W, Pitisuttitham P, Supeeranan L, Chantra A, Naksrisook S. 1992. Clinical and bacteriological studies of El Tor cholera after ingestion of known inocula in Thai volunteers. Vaccine 10:502–505.

168. Tailford LE, Crost EH, Kavanaugh D, Juge N. 2015. Mucin glycan foraging in the

human gut microbiome. Front Genet 6:81.

169. Derrien M, Vaughan EE, Plugge CM, de Vos WM. 2004. Akkermansia municiphila gen. nov., sp. nov., a human intestinal mucin-degrading bacterium. Int J Syst Evol Microbiol 54:1469–1476.

170. Prizont R. 1982. Degradation of intestinal glycoproteins by pathogenic Shigella flexneri. Infect Immun 36:615–20.

171. Slomiany BL, Murty VL, Piotrowski J, Liau YH, Sundaram P, Slomiany A. 1992. Glycosulfatase activity of Helicobacter pylori toward gastric mucin. Biochem Biophys Res Commun 183:506–13.

172. Hews CL, Tran S-L, Wegmann U, Brett B, Walsham ADS, Kavanaugh D, Ward NJ, Juge N, Schüller S. 2017. The StcE metalloprotease of enterohaemorrhagic Escherichia coli reduces the inner mucus layer and promotes adherence to human colonic epithelium ex vivo. Cell Microbiol 19:e12717.

173. Carlson-Banning KM, Sperandio V. 2016. Catabolite and oxygen regulation of enterohemorrhagic Escherichia coli virulence. MBio 7:e01852-16.

174. Cantarel BI, Coutinho PM, Rancurel C, Bernard T, Lombard V, Henrissat B. 2009. The Carbohydrate-Active EnZymes database (CAZy): An expert resource for glycogenomics. Nucleic Acids Res 37:D233-8.

175. Mondal M, Nag D, Koley H, Saha DR, Chatterjee NS. 2014. The Vibrio cholerae extracellular chitinase ChiA2 is important for survival and pathogenesis in the host intestine. PLoS One 9:e103119.

176. Almagro-Moreno S, Boyd EF. 2009. Sialic acid catabolism confers a competitive advantage to pathogenic Vibrio cholerae in the mouse intestine. Infect Immun 77:3807–16.

177. Ghosh S, Rao KH, Sengupta M, Bhattacharya SK, Datta A. 2011. Two gene clusters co-ordinate for a functional N-acetylglucosamine catabolic pathway in Vibrio cholerae. Mol Microbiol 80:1549–1560.

178. Hayes CA, Dalia TN, Dalia AB. 2017. Systematic genetic dissection of PTS in *Vibrio cholerae* uncovers a novel glucose transporter and a limited role for PTS during infection of a mammalian host. Mol Microbiol 104:568–579.

179. Millet YA, Alvarez D, Ringgaard S, von Andrian UH, Davis BM, Waldor MK. 2014. Insights into Vibrio cholerae intestinal colonization from monitoring fluorescently labeled bacteria. PLoS Pathog 10:e1004405.

180. Shi J, Romero PR, Schoolnik GK, Spormann AM, Karp PD. 2006. Evidence supporting predicted metabolic pathways for Vibrio cholerae: gene expression data and clinical tests. Nucleic Acids Res 34:2438–44.

181. Patra T, Koley H, Ramamurthy T, Ghose AC, Nandy RK. 2012. The Entner-Doudoroff pathway is obligatory for gluconate utilization and contributes to the pathogenicity of Vibrio cholerae. J Bacteriol 194:3377–85.

182. Kühn J, Finger F, Bertuzzo E, Borgeaud S, Gatto M, Rinaldo A, Blokesch M. 2014. Glucose- but not rice-based oral rehydration therapy enhances the production of virulence determinants in the human pathogen Vibrio cholerae. PLoS Negl Trop Dis 8:e3347.

183. Wang J, Xing X, Yang X, Jung I-J, Hao G, Chen Y, Liu M, Wang H, Zhu J. 2018. Gluconeogenic growth of Vibrio cholerae is important for competing with host gut microbiota. J Med Microbiol 67:1628–1637.

184. De Kok A, Hengeveld AF, Martin A, Westphal AH. 1998. The pyruvate dehydrogenase multi-enzyme complex from Gram-negative bacteria. Biochim Biophys Acta - Protein Struct 1385:353–366.

185. Knappe J, Sawers G. 1990. A radical-chemical route to acetyl-CoA: the anaerobically induced pyruvate formate-lyase system of Escherichia coli. FEMS Microbiol Rev 75:383–398.

186. Minato Y, Fassio SR, Wolfe AJ, Häse CC. 2013. Central metabolism controls transcription of a virulence gene regulator in Vibrio cholerae. Microbiology 159:792–802.

187. Hu D, Liu B, Feng L, Ding P, Guo X, Wang M, Cao B, Reeves PR, Wang L. 2016. Origins of the current seventh cholera pandemic. Proc Natl Acad Sci U S A 113:E7730–E7739.

188. DiRita VJ, Neely M, Taylor RK, Bruss PM. 1996. Differential expression of the ToxR regulon in classical and El Tor biotypes of Vibrio cholerae is due to biotype-specific control over toxT expression. Proc Natl Acad Sci U S A 93:7991–7995.

189. Brumfield KD, Carignan BM, Son MS. 2018. Genotypic and phenotypic assays to distinguish Vibrio cholerae biotype, p. 11–28. *In* Methods in molecular biology (Clifton, N.J.).

190. Beyhan S, Tischler AD, Camilli A, Yildiz FH. 2006. Differences in gene expression between the classical and El Tor biotypes of Vibrio cholerae O1. Infect Immun 74:3633–42.

191. Yoon SS, Mekalanos JJ. 2006. 2,3-Butanediol synthesis and the emergence of the Vibrio cholerae El Tor biotype. Infect Immun 74:6547–6556.

192. Severin GB, Ramliden MS, Hawver LA, Wang K, Pell ME, Kieninger A-K, Khataokar A, O'Hara BJ, Behrmann L V., Neiditch MB, Benning C, Waters CM, Ng W-L. 2018. Direct activation of a phospholipase by cyclic GMP-AMP in El Tor *Vibrio cholerae*. Proc Natl Acad Sci 115:E6048–E6055.

193. Cohen D, Melamed S, Millman A, Shulman G, Oppenheimer-Shaanan Y, Kacen A, Doron S, Amitai G, Sorek R. 2019. Cyclic GMP–AMP signalling protects bacteria against viral infection. Nature 574:691–695.

194. Cameron DE, Urbach JM, Mekalanos JJ. 2008. A defined transposon mutant library and its use in identifying motility genes in Vibrio cholerae. Proc Natl Acad Sci U S A 105:8736–8741.

195. Alazzam B, Bonnassie-Rouxin S, Dufour V, Ermel G. 2011. MCLMAN, a new minimal medium for Campylobacter jejuni NCTC 11168. Res Microbiol 162:173–179.

196. Holmén Larsson JM, Thomsson KA, Rodríguez-Piñeiro AM, Karlsson H, Hansson GC. 2013. Studies of mucus in mouse stomach, small intestine, and colon. III. Gastrointestinal Muc5ac and Muc2 mucin O-glycan patterns reveal a regiospecific distribution. Am J Physiol Gastrointest Liver Physiol 305:G357-63.

197. 2016. LB solid or liquid medium: Cold Spring Harb Protoc 2016:pdb.rec088203.

198. Skorupski K, Taylor RK. 1996. Positive selection vectors for allelic exchange. Gene 169:47–52.

199. Iwanaga M, Yamamoto K, Higa N, Ichinose Y, Nakasone N, Tanabe M. 1986. Culture conditions for stimulating cholera toxin production by Vibrio cholerae O1 El Tor. Microbiol Immunol 30:1075–1083.

200. Sloup RE, Konal AE, Severin GB, Korir ML, Bagdasarian MM, Bagdasarian M, Waters CM. 2017. Cyclic di-GMP and VpsR induce the expression of type II secretion in Vibrio cholerae. J Bacteriol 199:e00106-17.

201. Svennerholm AM, Holmgren J. 1978. Identification of Escherichia coli heat-labile enterotoxin by means of a ganglioside immunosorbent assay (GM1-ELISA) procedure. Curr Microbiol 1:19–23.

202. Amin Marashi SM, Rajabnia R, Imani Fooladi AA, Hojati Z, Moghim S, Nasr Esfahani B. 2013. Determination of ctxAB expression in Vibrio cholerae Classical and El Tor strains using Real-Time PCR. Int J Mol Cell Med 2:9–13.

203. Anthouard R, DiRita VJ. 2013. Small-molecule inhibitors of toxT expression in Vibrio cholerae. MBio 4:e00403-13.

204. Li M, Ho PY, Yao S, Shimizu K. 2006. Effect of lpdA gene knockout on the metabolism in Escherichia coli based on enzyme activities, intracellular metabolite concentrations and metabolic flux analysis by 13C-labeling experiments. J Biotechnol 122:254–266.

205. Bergstrom KSB, Xia L. 2013. Mucin-type O-glycans and their roles in intestinal homeostasis. Glycobiology 23:1026–1037.

206. Schömig VJ, Käsdorf BT, Scholz C, Bidmon K, Lieleg O, Berensmeier S. 2016. An optimized purification process for porcine gastric mucin with preservation of its native functional properties. RSC Adv 6:44932–44943.

207. Zhang Z, Khan NM, Nunez KM, Chess EK, Szabo CM. 2012. Complete monosaccharide analysis by high-performance anion-exchange chromatography with pulsed amperometric detection. Anal Chem 84:4104–4110.

208. Looft T, Cai G, Choudhury B, Lai LX, Lippolis JD, Reinhardt TA, Sylte MJ, Casey TA. 2019. Avian intestinal mucus modulates Campylobacter jejuni gene expression in a host-specific manner. Front Microbiol 9:3215.

209. Lee K-M, Park Y, Bari W, Yoon MY, Go J, Kim SC, Lee H-I, Yoon SS. 2012. Activation of cholera toxin production by anaerobic respiration of trimethylamine N-oxide in Vibrio cholerae. J Biol Chem 287:39742–52.

210. Wang Q, Ou MS, Kim Y, Ingram LO, Shanmugam KT. 2010. Metabolic flux control at the pyruvate node in an anaerobic escherichia coli strain with an active pyruvate dehydrogenase. Appl Environ Microbiol 76:2107–2114.

211. Sezonov G, Joseleau-Petit D, D'Ari R. 2007. Escherichia coli physiology in Luria-Bertani broth. J Bacteriol 189:8746–9.

212. DiRita VJ, Parsot C, Jander G, Mekalanos JJ. 1991. Regulatory cascade controls virulence in Vibrio cholerae. Proc Natl Acad Sci U S A 88:5403–7.

213. Medrano AI, DiRita VJ, Castillo G, Sanchez J. 1999. Transient transcriptional activation of the Vibrio cholerae El Tor virulence regulator toxT in response to culture conditions. Infect Immun 67:2178–83.

214. Klose KE. 2000. The suckling mouse model of cholera. Trends Microbiol 8:189–191.

215. Nygren E, Li BL, Holmgren J, Attridge SR. 2009. Establishment of an adult mouse model for direct evaluation of the efficacy of vaccines against Vibrio cholerae. Infect Immun 77:3475–3484.

216. Spiga L, Winter MG, Furtado de Carvalho T, Zhu W, Hughes ER, Gillis CC, Behrendt CL, Kim J, Chessa D, Andrews-Polymenis HL, Beiting DP, Santos RL, Hooper L V., Winter SE. 2017. An oxidative central metabolism enables Salmonella to utilize microbiota-derived succinate. Cell Host Microbe 22:1–11.

217. Robbe C, Capon C, Coddeville B, Michalski J-C. 2004. Structural diversity and specific distribution of O-glycans in normal human mucins along the intestinal tract. Biochem J 384:307–316.

218. Glover LE, Lee JS, Colgan SP. 2016. Oxygen metabolism and barrier regulation in the intestinal mucosa. J Clin Invest 126:3680–3688.

219. Wolfe AJ. 2005. The acetate switch. Microbiol Mol Biol Rev 69:12–50.

220. Hang S, Purdy AE, Robins WP, Wang Z, Mandal M, Chang S, Mekalanos JJ, Watnick PI. 2014. The acetate switch of an intestinal pathogen disrupts host insulin signaling and lipid metabolism. Cell Host Microbe 16:592–604.

221. Bishop AL, Patimalla B, Camilli A. 2014. Vibrio cholerae-induced inflammation in the neonatal mouse cholera model. Infect Immun 82:2434–47.

222. Qadri F, Bhuiyan TR, Dutta KK, Raqib R, Alam MS, Alam NH, Svennerholm AM, Mathan MM. 2004. Acute dehydrating disease caused by Vibrio cholerae serogroups O1 and O139 induce increases in innate cells and inflammatory mediators at the mucosal surface of the gut. Gut 53:62–69.

223. Ma AT, Mekalanos JJ. 2010. In vivo actin cross-linking induced by Vibrio cholerae type VI secretion system is associated with intestinal inflammation. Proc Natl Acad Sci U S A 107:4365–4370.

224. Ghosh P, Sinha R, Samanta P, Saha DR, Koley H, Dutta S, Okamoto K, Ghosh A, Ramamurthy T, Mukhopadhyay AK. 2019. Haitian variant Vibrio cholerae O1 strains manifest higher virulence in animal models. Front Microbiol 10:110.

225. Fan F, Liu Z, Jabeen N, Birdwell LD, Zhu J, Kan B. 2014. Enhanced interaction of Vibrio cholerae virulence regulators TcpP and ToxR under oxygen-limiting conditions. Infect Immun 82:1676–82.

226. Pelaseyed T, Bergström JH, Gustafsson JK, Ermund A, Birchenough GMH, Schütte A, van der Post S, Svensson F, Rodríguez-Piñeiro AM, Nyström EEL, Wising C, Johansson MEV, Hansson GC. 2014. The mucus and mucins of the goblet cells and enterocytes provide the first defense line of the gastrointestinal tract and interact with the immune system. Immunol Rev 260:8–20.

227. Nhu NT, Wang HJ, Dufour YS. 2019. Acidic pH reduces Vibrio cholerae motility in mucus by weakening flagellar motor torque. bioRxiv

228. Hansson GC, Johansson ME V. 2010. The inner of the two Muc2 mucin-dependent mucus layers in colon is devoid of bacteria. Gut Microbes 1:51–54.

229. Bergstrom KSB, Kissoon-Singh V, Gibson DL, Ma C, Montero M, Sham HP, Ryz N, Huang T, Velcich A, Finlay BB, Chadee K, Vallance BA. 2010. Muc2 protects against lethal infectious colitis by disassociating pathogenic and commensal bacteria from the colonic mucosa. PLoS Pathog 6:e1000902.

230. Zarepour M, Bhullar K, Montero M, Ma C, Huang T, Velcich A, Xia L, Vallance BA. 2013. The mucin muc2 limits pathogen burdens and epithelial barrier dysfunction during Salmonella enterica serovar Typhimurium colitis. Infect Immun 81:3672–3683.

231. Wong E, Vaaje-Kolstad G, Ghosh A, Hurtado-Guerrero R, Konarev P V., Ibrahim AFM, Svergun DI, Eijsink VGH, Chatterjee NS, van Aalten DMF. 2012. The Vibrio cholerae colonization factor GbpA possesses a modular structure that governs binding to different host surfaces. PLoS Pathog 8:e1002373.

232. Krebs SJ, Taylor RK. 2011. Protection and attachment of Vibrio cholerae mediated by the toxin-coregulated pilus in the infant mouse model. J Bacteriol 193:5260–5270.

233. Epple HJ, Kreusel KM, Hanski C, Schulzke JD, Riecken EO, Fromm M. 1997. Differential stimulation of intestinal mucin secretion by cholera toxin and carbachol. Pflugers Arch Eur J Physiol 433:638–647.

234. Reddi G, Pruss K, Cottingham KL, Taylor RK, Almagro-Moreno S. 2018. Catabolism of mucus components influences motility of Vibrio cholerae in the presence of environmental reservoirs. PLoS One 13:e0201383.

235. Spagnuolo AM, Dirita V, Kirschner D. 2011. A model for Vibrio cholerae colonization of the human intestine. J Theor Biol 289:247–58.

236. Abel S, Abel zur Wiesch P, Chang H-H, Davis BM, Lipsitch M, Waldor MK. 2015. STAMP: Sequence tag-based analysis of microbial population dynamics. Nat Methods 12:223–6, 3 p following 226.

237. Finkelstein RA, Boesman-Finkelstein M, Chang Y, Hase CC. 1991. Vibrio cholerae hemagglutinin/protease, colonial variation, virulence, and detachment. Infect Immun 60:472–8.

238. Silva AJ, Leitch GJ, Camilli A, Benitez JA. 2006. Contribution of hemagglutinin/protease and motility to the pathogenesis of El Tor biotype cholera. Infect Immun 74:2072–2079.

239. Silva AJ, Pham K, Benitez JA. 2003. Haemagglutinin/protease expression and mucin gel penetration in El Tor biotype Vibrio cholerae. Microbiology 149:1883–91.

240. Nelson EJ, Chowdhury A, Harris JB, Begum YA, Chowdhury F, Khan AI, Larocque RC, Bishop AL, Ryan ET, Camilli A, Qadri F, Calderwood SB. 2007. Complexity of rice-water stool from patients with Vibrio cholerae plays a role in the transmission of infectious diarrhea. Proc Natl Acad Sci U S A 104:19091–6.

241. Merrell DS, Butler SM, Qadri F, Dolganov NA, Alam A, Cohen MB, Calderwood SB, Schoolnik GK, Camilli A. 2002. Host-induced epidemic spread of the cholera bacterium. Nature 417:642–645.

242. Sawers G, Suppmann B. 1992. Anaerobic induction of pyruvate formate-lyase gene expression is mediated by the ArcA and FNR proteins. J Bacteriol 174:3474–8.

243. Kaiser M, Sawers G. 1994. Pyruvate formate-lyase is not essential for nitrate respiration by *Escherichia coli*. FEMS Microbiol Lett 117:163–168.

244. Fu Y, Waldor MK, Mekalanos JJ. 2013. Tn-seq analysis of vibrio cholerae intestinal colonization reveals a role for T6SS-mediated antibacterial activity in the host. Cell Host Microbe 14:652–663.

245. Kamp HD, Patimalla-Dipali B, Lazinski DW, Wallace-Gadsden F, Camilli A. 2013. Gene Fitness Landscapes of Vibrio cholerae at Important Stages of Its Life Cycle. PLoS Pathog 9:1–11.

246. Harris JB, LaRocque RC, Qadri F, Ryan ET, Calderwood SB. 2012. Cholera, p. 2466–2476. *In* The Lancet. Lancet Publishing Group.

247. Reen FJ, Almagro-Moreno S, Ussery D, Boyd EF. 2006. The genomic code: inferring Vibrionaceae niche specialization. Nat Rev Microbiol 4:697–704.

248. Bueno E, Pinedo V, Cava F. 2020. Adaptation of Vibrio cholerae to hypoxic environments. Front Microbiol. Frontiers Media S.A.

249. Hemp J, Christian C, Barquera B, Gennis RB, Martínez TJ. 2005. Helix switching of a key active-site residue in the cytochrome cbb 3 oxidases. Biochemistry 44:10766–10775.

250. Ahn YO, Lee HJ, Kaluka D, Yeh SR, Rousseau DL, Ädelroth P, Gennis RB. 2015. The two transmembrane helices of CcoP are sufficient for assembly of the cbb3-type heme-copper oxygen reductase from Vibrio cholerae. Biochim Biophys Acta - Bioenerg 1847:1231–1239.

251. Durand A, Bourbon ML, Steunou AS, Khalfaoui-Hassani B, Legrand C, Legrand A, Astier C, Ouchane S. 2018. Biogenesis of the bacterial cbb3 cytochrome c oxidase: Active subcomplexes support a sequential assembly model. J Biol Chem 293:808–818.

252. Preisig O, Zufferey R, Thöny-Meyer L, Appleby CA, Hennecke H. 1996. A high-affinity cbb3-type cytochrome oxidase terminates the symbiosis-specific respiratory chain of Bradyrhizobium japonicum. J Bacteriol 178:1532–1538.

253. Rice CW, Hempfling WP. 1978. Oxygen limited continuous culture and respiratory energy conservation in Escherichia coli. J Bacteriol 134:115–124.

254. Cotter PA, Melville SB, Albrecht JA, Gunsalus RP. 1997. Aerobic regulation of cytochrome d oxidase (cydAB) operon expression in Escherichia coli : roles of Fnr and ArcA in repression and activation. Mol Microbiol 25:605–615.

255. Smith A, Hill S, Anthony C. 1990. The purification, characterization and role of the d-type cytochrome oxidase of Klebsiella pneumoniae during nitrogen fixation. J Gen Microbiol 136:171–180.

256. Pitcher RS, Watmough NJ. 2004. The bacterial cytochrome cbb3 oxidases. Biochim Biophys Acta - Bioenerg. Elsevier.

257. Ito T, Gallegos R, Matano LM, Butler NL, Hantman N, Kaili M, Coyne MJ, Comstock LE, Malamy MH, Barquera B. 2020. Genetic and biochemical analysis of anaerobic respiration in Bacteroides fragilis and its importance in vivo. MBio 11.

258. Oh YT, Park Y, Yoon MY, Bari W, Go J, Min KB, Raskin DM, Lee K-M, Yoon SS. 2014. Cholera toxin production during anaerobic trimethylamine N-oxide respiration is mediated by stringent response in Vibrio cholerae. J Biol Chem 289:13232–42.

259. Dalia TN, Yoon SH, Galli E, Barre F-X, Waters CM, Dalia AB. 2017. Enhancing multiplex genome editing by natural transformation (MuGENT) via inactivation of ssDNA exonucleases. Nucleic Acids Res 45:7527–7537.

260. Dalia AB, Mcdonough E, Camilli A. 2014. Multiplex genome editing by natural transformation. Proc Natl Acad Sci U S A 111:8937–8942.

261. Ahn YO, Albertsson I, Gennis RB, Ädelroth P. 2018. Mechanism of proton transfer through the KC proton pathway in the Vibrio cholerae cbb3 terminal oxidase. Biochim Biophys Acta - Bioenerg 1859:1191–1198.

262. Thöny-Meyer L. 1997. Biogenesis of respiratory cytochromes in bacteria. Microbiol Mol Biol Rev 61:337–376.

263. Xia D, Esser L, Tang WK, Zhou F, Zhou Y, Yu L, Yu CA. 2013. Structural analysis of cytochrome bc1 complexes: Implications to the mechanism of function. Biochim Biophys Acta - Bioenerg. Elsevier.

264. Blomberg MRA. 2020. The mechanism for oxygen reduction in the C family cbb3 cytochrome c oxidases - Implications for the proton pumping stoichiometry. J Inorg Biochem 203:110866.

265. Jasaitis A, Borisov VB, Belevich NP, Morgan JE, Konstantinov AA, Verkhovsky MI. 2000. Electrogenic reactions of cytochrome bd. Biochemistry 39:13800–13809.

266. Arai H, Kawakami T, Osamura T, Hirai T, Sakai Y, Ishii M. 2014. Enzymatic characterization and in vivo function of five terminal oxidases in Pseudomonas aeruginosa. J Bacteriol 196:4206.

267. MA S, M F, V K, GL M. 2000. Characteristics of the aerobic respiratory chains of the microaerophiles Campylobacter jejuni and Helicobacter pylori. Arch Microbiol 174:1–10.

268. Hammer ND, Reniere ML, Cassat JE, Zhang Y, Hirsch AO, Hood MI, Skaar EP. 2013. Two heme-dependent terminal oxidases power Staphylococcus aureus

organ-specific colonization of the vertebrate host. MBio 4.

269. Hayashi H, Takahashi R, Nishi T, Sakamoto M, Benno Y. 2005. Molecular analysis of jejunal, ileal, caecal and rectosigmoidal human colonic microbiota using 16S rRNA gene libraries and terminal restriction fragment length polymorphism. J Med Microbiol 54:1093–1101.

270. Spees AM, Wangdi T, Lopez CA, Kingsbury DD, Xavier MN, Winter SE, Tsolis RM, Bäumler AJ. 2013. Streptomycin-induced inflammation enhances Escherichia coli gut colonization through nitrate respiration. MBio 4:430–443.

271. Tardu M, Bulut S, Kavakli IH. 2017. MerR and ChrR mediate blue light induced photo-oxidative stress response at the transcriptional level in Vibrio cholerae. Sci Rep 7.

272. Arjona D, Wikström M, Ädelroth P. 2015. Nitric oxide is a potent inhibitor of the *cbb* $_3$ -type heme-copper oxidases. FEBS Lett 589:1214–1218.

273. Jiménez de Bagüés MP, Loisel-Meyer S, Liautard J-P, Jubier-Maurin V. 2007. Different roles of the two high-oxygen-affinity terminal oxidases of Brucella suis: cytochrome c oxidase, but not ubiquinol oxidase, is required for persistence in mice. Infect Immun 75:531–535.

274. Jünemann S. 1997. Cytochrome bd terminal oxidase. Biochim Biophys Acta - Bioenerg. Elsevier.

275. Martinez RM, Megli CJ, Taylor RK. 2010. Growth and laboratory maintenance of Vibrio cholerae. Curr Protoc Microbiol 0 6:Unit.

276. Herrington D, Hall R, Losonsky G, Mekalanos J, Taylor R, Levine M. 1988. Toxin, toxin-coregulated pili, and the toxR regulon are essential for Vibrio cholerae pathogenesis in humans. J Exp Med 168:1487–1492.

277. Ritchie JM, Rui H, Bronson RT, Waldor MK. 2010. Back to the future: Studying cholera pathogenesis using infant Rabbits. MBio 1.

278. Guinée PAM, Jansen WH, Peters PWJ. 1985. Vibrio cholerae infection and acquired immunity in an adult rabbit model. Zentralblatt für Bakteriol Mikrobiol und Hyg Ser A Med Microbiol Infect Dis Virol Parasitol 259:118–131.

279. Wernick NLB, Chinnapen DJ-F, Cho JA, Lencer WI. 2010. Cholera toxin: An intracellular journey into the cytosol by way of the endoplasmic reticulum. Toxins (Basel) 2:310.

280. Amarasingham CR, Davis BD. 1965. Regulation of α-Ketoglutarate dehydrogenase formation in Escherichia coli. J Biol Chem 240:3664–3668.

281. Guichard A, Cruz-Moreno B, Aguilar B, Van Sorge NM, Kuang J, Kurkciyan AA,

Wang Z, Hang S, Pineton De Chambrun GP, Mccole DF, Watnick P, Nizet V, Bier E. 2013. Cholera toxin disrupts barrier function by inhibiting exocyst-mediated trafficking of host proteins to intestinal cell junctions. CHOM 14:294–305.

282. Fullner KJ, Lencer WI, Mekalanos JJ. 2001. Vibrio cholerae-induced cellular responses of polarized T84 intestinal epithelial cells are dependent on production of cholera toxin and the RTX toxin. Infect Immun 69:6310–6317.

283. Zhang J, Huang Y-J, Yoon JY, Kemmitt J, Wright C, Schneider K, Sphabmixay P, Hernandez-Gordillo V, Holcomb SJ, Bhushan B, Rohatgi G, Benton K, Carpenter D, Kester JC, Eng G, Breault DT, Yilmaz O, Taketani M, Voigt CA, Carrier RL, Trumper DL, Griffith LG. 2021. Primary human colonic mucosal barrier crosstalk with super oxygen-sensitive Faecalibacterium prausnitzii in continuous culture. Med 2:74-98.e9.

284. Queen J, Satchell KJF. 2012. Neutrophils are essential for containment of Vibrio cholerae to the intestine during the proinflammatory phase of infection. Infect Immun 80:2905.

285. Antoniou E, Margonis GA, Angelou A, Pikouli A, Argiri P, Karavokyros I, Papalois A, Pikoulis E. 2016. The TNBS-induced colitis animal model: An overview. Ann Med Surg 11:9.

286. Eichele DD, Kharbanda KK. 2017. Dextran sodium sulfate colitis murine model: An indispensable tool for advancing our understanding of inflammatory bowel diseases pathogenesis. World J Gastroenterol 23:6016.

287. Kumar KM, Namachivayam K, Cheng F, Jiang RHY, Flores-Torres J, Torres BA, Maheshwari A. 2017. Trinitrobenzene sulfonic acid-induced intestinal injury in neonatal mice activates transcriptional networks similar to those seen in human necrotizing enterocolitis. Pediatr Res 81:99–112.

288. Satchell KJF, Jones CJ, Wong J, Queen J, Agarwal S, Yildiz FH. 2016. Phenotypic analysis reveals that the 2010 haiti cholera epidemic is linked to a hypervirulent strain. Infect Immun 84:2473–2481.

289. Breen P, Winters AD, Theis KR, Withey JH. 2021. Vibrio cholerae infection induces strain specific modulation of the zebrafish intestinal microbiome. Infect Immun.

290. Nguyen Y, Sperandio V. 2012. Enterohemorrhagic E. coli (EHEC) pathogenesis. Front Cell Infect Microbiol 2:90.

291. Battle SE, Brady MJ, Vanaja SK, Leong JM, Hecht GA. 2014. Actin pedestal formation by enterohemorrhagic Escherichia coli enhances bacterial host cell attachment and concomitant type III translocation. Infect Immun 82:3713–22.

292. Melton-Celsa AR. 2014. Shiga toxin (Stx) classification, structure, and function.

Microbiol Spectr 2:EHEC-0024-2013.

293. Obrig TG, Karpman D. 2012. Shiga toxin pathogenesis: kidney complications and renal failure. Curr Top Microbiol Immunol 357:105–36.

294. Atuma C, Strugala V, Allen A, Holm L. 2001. The adherent gastrointestinal mucus gel layer: thickness and physical state in vivo. Am J Physiol Liver Physiol 280:G922–G929.

295. Le Bihan G, Sicard J-F, Garneau P, Bernalier-Donadille A, Gobert AP, Garrivier A, Martin C, Hay AG, Beaudry F, Harel J, Jubelin G. 2017. The NAG sensor NagC regulates LEE gene expression and contributes to gut colonization by Escherichia coli O157:H7. Front Cell Infect Microbiol 7:134.

296. Pacheco AR, Curtis MM, Ritchie JM, Munera D, Waldor MK, Moreira CG, Sperandio V. 2012. Fucose sensing regulates bacterial intestinal colonization. Nature 492:113–117.

297. Franzin FM, Sircili MP. 2015. Locus of enterocyte effacement: A pathogenicity island involved in the virulence of enteropathogenic and enterohemorragic Escherichia coli subjected to a complex network of gene regulation. Biomed Res Int 2015:1–10.

298. Lathem WW, Grys TE, Witowski SE, Torres AG, Kaper JB, Tarr PI, Welch RA. 2002. StcE, a metalloprotease secreted by Escherichia coli O157:H7, specifically cleaves C1 esterase inhibitor. Mol Microbiol 45:277–88.

299. Qian Z, Trostel A, Lewis DEA, Lee SJ, He X, Stringer AM, Wade JT, Schneider TD, Durfee T, Adhya S. 2016. Genome-wide transcriptional regulation and chromosome structural arrangement by GalR in E. coli. Front Mol Biosci 3:74.

300. Bertin Y, Chaucheyras-Durand F, Robbe-Masselot C, Durand A, de la Foye A, Harel J, Cohen PS, Conway T, Forano E, Martin C. 2013. Carbohydrate utilization by enterohaemorrhagic Escherichia coli O157:H7 in bovine intestinal content. Environ Microbiol 15:610–22.

301. Leyn SA, Gao F, Yang C, Rodionov DA. 2012. N-acetylgalactosamine utilization pathway and regulon in proteobacteria: genomic reconstruction and experimental characterization in Shewanella. J Biol Chem 287:28047–56.

302. Plumbridge J. 1998. Control of the expression of the manXYZ operon in Escherichia coli: Mlc is a negative regulator of the mannose PTS. Mol Microbiol 27:369–80.

303. Kalivoda KA, Steenbergen SM, Vimr ER. 2013. Control of the Escherichia coli sialoregulon by transcriptional repressor NanR. J Bacteriol 195:4689–4701.

304. Djomassi LD, Gessner BD, Andze GO, Mballa GAE. 2013. National surveillance

data on the epidemiology of cholera in Cameroon. J Infect Dis 208:S92–S97.

305. Szumilas M. 2010. Explaining odds ratios. J Can Acad Child Adolesc Psychiatry 19:227–9.

306. Preußel K, Höhle M, Stark K, Werber D. 2013. Shiga toxin-producing Escherichia coli O157 is more likely to lead to hospitalization and death than non-O157 serogroups – except O104. PLoS One 8:e78180.